# THE UNIVERSITY OF MICHIGAN

## STUDIES IN RADAR CROSS SECTIONS XXVII

## CALCULATED FAR FIELD PATTERNS FROM SLOT ARRAYS ON CONICAL SHAPES

R. E. Doll, R. F. Goodrich, R. E. Kleinman, A. L. Maffett,
C. E. Schensted and K. M. Siegel

Approved _Keeve M. Siegel_
Keeve M. Siegel
Project Supervisor

**2713-1-F = RL-2064**

# THE UNIVERSITY OF MICHIGAN
2713-1-F

## STUDIES IN RADAR CROSS SECTIONS

I    "Scattering by a Prolate Spheroid", F. V. Schultz (UMM-42, March 1950), W-33(038)-ac-14222. UNCLASSIFIED.

II    "The Zeros of the Associated Legendre Functions $P_n^m(\mu')$ of Non-Integral Degree", K. M. Siegel, D. M. Brown, H. E. Hunter, H. A. Alperin and C. W. Quillen (UMM-82, April 1951), W-33(038)-ac-14222. UNCLASSIFIED.

III    "Scattering by a Cone", K. M. Siegel and H. A. Alperin (UMM-87, January 1952), AF-30(602)-9. UNCLASSIFIED.

IV    "Comparison Between Theory and Experiment of the Cross Section of a Cone", K. M. Siegel, H. A. Alperin, J. W. Crispin, Jr. , H. E. Hunter, R. E. Kleinman, W. C. Orthwein and C. E. Schensted (UMM-92, February 1953), AF-30(602)-9. UNCLASSIFIED.

V    "An Examination of Bistatic Early Warning Radars", K. M. Siegel (UMM-98, August 1952), W-33(038)-ac-14222. SECRET.

VI    "Cross Sections of Corner Reflectors and Other Multiple Scatterers at Microwave Frequencies", R. R. Bonkowski, C. R. Lubitz and C. E. Schensted (UMM-106, October 1953), AF-30(602)-9. SECRET - Unclassified when Appendix is removed.

VII    "Summary of Radar Cross Section Studies Under Project Wizard", K. M. Siegel, J. W. Crispin, Jr. , and R. E. Kleinman (UMM-108, November 1952), W-33(038)-ac-14222. SECRET.

VIII    "Theoretical Cross Section as a Function of Separation Angle Between Transmitter and Receiver at Small Wavelengths", K. M. Siegel, H. A. Alperin, R. R. Bonkowski, J. W. Crispin, Jr. , A. L. Maffett, C. E. Schensted and I. V. Schensted (UMM-115, October 1953), W-33(038)-ac-14222. UNCLASSIFIED.

IX    "Electromagnetic Scattering by an Oblate Spheroid", L. M. Rauch (UMM-116, October 1953), AF-30(602)-9. UNCLASSIFIED.

X    "Scattering of Electromagnetic Waves by Spheres", H. Weil, M. L. Barasch and T. A. Kaplan (2255-20-T, July 1956), AF-30(602)-1070. UNCLASSIFIED.

XI    "The Numerical Determination of the Radar Cross Section of a Prolate Spheroid", K. M. Siegel, B. H. Gere, I. Marx and F. B. Sleator (UMM-126, December 1953), AF-30(602)-9. UNCLASSIFIED.

XII    "Summary of Radar Cross Section Studies Under Project MIRO", K. M. Siegel, M. E. Anderson, R. R. Bonkowski and W. C. Orthwein (UMM-127, December 1953), AF-30(602)-9, SECRET.

XIII    "Description of a Dynamic Measurement Program", K. M. Siegel and J. M. Wolf, (UMM-128, May 1954), W-33(038)-ac-14222. CONFIDENTIAL.

XIV    "Radar Cross Section of a Ballistic Missile", K. M. Siegel, M. L. Barasch, J. W. Crispin, Jr. , W. C. Orthwein, I. V. Schensted and H. Weil (UMM-134, September 1954), W-33(038)-ac-14222. SECRET.

XV    "Radar Cross Sections of B-47 and B-52 Aircraft", C. E. Schensted, J. W. Crispin, and K. M. Siegel (2260-1-T, August 1954), AF-33(616)-2531. CONFIDENTIAL.

XVI    "Microwave Reflection Characteristics of Buildings", H. Weil, R. R. Bonkowski, T. A. Kaplan and M. Leichter (2255-12-T, May 1955), AF-30(602)-1070. SECRET.

XVII    Complete Scattering Matrices and Circular Polarization Cross Sections for the B-47 Aircraft at S-band", A. L. Maffett, M. L. Barasch, W. E. Burdick, R. F. Goodrich, W. C. Orthwein, C. E. Schensted and K. M. Siegel (2260-6-T, June 1955), AF-33(616)-2531. CONFIDENTIAL.

XVIII    "Airborne Passive Measures and Countermeasures", K. M. Siegel, M. L. Barasch, J. W. Crispin Jr. , R. F. Goodrich, A. H. Halpin, A. L. Maffett, W. C. Orthwein, C. E. Schensted and C. J. Titus (2260-29-F, January 1956), AF-33(616)-2531. SECRET.

XIX    "Radar Cross Section of a Ballistic Missile II", K. M. Siegel, M. L. Barasch, H. Brysk, J. W. Crispin, Jr. , T. B. Curtz and T. A. Kaplan (2428-3-T, January 1956), AF-04(645)-33. SECRET.

XX    "Radar Cross Section of Aircraft and Missiles", K. M. Siegel, W. E. Burdick, J. W. Crispin, Jr. , and S. Chapman (WR-31-J, ONR-ACR-10, March 1956). SECRET.

XXI    "Radar Cross Section of a Ballistic Missile III", K. M. Siegel, H. Brysk, J. W. Crispin, Jr. , and R. E. Kleinman (2428-19-T, October 1956), AF-04(645)-33. SECRET.

XXII    "Elementary Slot Radiators", R. F. Goodrich, A. L. Maffett, N. E. Reitlinger, C. E. Schensted and K. M. Siegel (2472-13-T, November 1956), AF-33(038)-28634, HAC PO L-265165-F47. UNCLASSIFIED.

XXIII    "A Variational Solution to the Problem of Scalar Scattering by a Prolate Spheroid", F. B. Sleator (2591-1-T, March 1957), AFCRC-TN-57-586, ASTIA Document No. 133631, AF-19(604)-1949. UNCLASSIFIED.

XXIV    "Radar Cross Section of a Ballistic Missile IV", to be published. SECRET.

XXV    "Diffraction by an Imperfectly Conducting Wedge", T.B.A. Senior (2591-2-T, October 1957), AFCRC-TN-57-791, ASTIA Document No. AD 133746, AF-19(604)-1949. UNCLASSIFIED.

XXVI    "Fock Theory Applied to an Infinite Cone", R.F. Goodrich (2591-3-T, January 1958), AF-19(604)-1949. UNCLASSIFIED.

XXVII    "Calculated Far Field Patterns from Slot Arrays on Conical Shapes", R.E. Doll, R.F. Goodrich, R.E. Kleinman, A.L. Maffett, C.E. Schensted and K.M. Siegel (2713-1-F, February 1958), AF-33(038)-28634, AF-33(600)-36192. UNCLASSIFIED.

PREFACE


This paper is the twenty-seventh in a series growing out of studies of radar cross sections at the Engineering Research Institute of The University of Michigan. The primary aims of this program are:

1. To show that radar cross sections can be determined analytically.

2. A. To determine means for computing the radiation patterns from antennas by approximate techniques which determine the pattern to the accuracy required in military problems but which do not require the unique determination of exact solutions.

   B. To determine means for computing the radar cross sections of various objects of military interest.

   (Since 2A and 2B are inter-related by the reciprocity theorem it is necessary to solve only one of these problems.)

3. To demonstrate that these theoretical cross sections and theoretically determined radiation patterns are in agreement with experimentally determined ones.

Intermediate objectives are:

1. A. To compute the exact theoretical cross sections of various simple bodies by solution of the appropriate boundary-value problems arising from electromagnetic theory.

   B. Compute the exact radiation patterns from infinitesimal solutions on the surface of simple shapes by the solution of appropriate boundary-value problems arising from electromagnetic theory.

   (Since 1A and 1B are inter-related by the reciprocity theorem it is necessary to solve only one of these problems.)

2.      To examine the various approximations possible in this problem and to determine the limits of their validity and utility.

3.      To find means of combining the simple-body solutions in order to determine the cross sections of composite bodies.

4.      To tabulate various formulas and functions necessary to enable such computations to be done quickly for arbitrary objects.

5.      To collect, summarize, and evaluate existing experimental data.

Titles of the papers already published or presently in process of publication are listed on the preceding pages.

K. M. Siegel

# THE UNIVERSITY OF MICHIGAN
2713-1-F

## TABLE OF CONTENTS

# I

## INTRODUCTION AND SUMMARY

This is the final report on Purchase Order Numbers L-265165-F47; 4-500469-FC-47-D; and 4-526406-FC-89-3 entered into between The University of Michigan and the Hughes Aircraft Company on Air Force Contracts AF-33(038)-28634 and AF-33(600)-36192. The ultimate purpose of this study is to replace radome-dish combinations (postulated but not yet researched and developed) with arrays of slots on the nose cone of a high speed vehicle. Such a replacement would eliminate the many problems associated with radomes, e.g., rain erosion, thermal stress, boresight error rate, and weight and balance problems.

Theoretically, it is always possible to duplicate a pattern produced by one type of antenna using another antenna of equal or larger surface area. For example, the pattern produced by a radome and parabolic dish combination can be duplicated by using any given covering surface as an antenna by correctly distributing the current on that surface. The required current distribution can be calculated by an application of Huygen's Principle. In particular, if the surface is chosen to be a semi-infinite cone, assume that the parabolic dish lies within the conical surface and compute the "dish field" on this surface; this field, then, if induced on a real cone, would reproduce the "dish pattern". Such a calculation serves two purposes: (1) it yields the precise current necessary to duplicate the parabolic-dish pattern, and (2) it yields results which serve as design criteria for arrays of slots, indicating a possible interim slot array design.

Such a computation is presented in Appendix C. The current distribution required varies as a function of the scan angle and the problems involved in attempting to instrument this distribution on a conical surface appear to be extremely difficult; however, since more promising methods are available, e.g., optimized slot arrays, a serious attempt at instrumentation is not warranted.

The value of most theoretical studies on either radiation or scattering problems is that the theoretical analysis very often has in it the seeds of better methods of design. Experiments can only determine the characteristics of existing designs. The approach used here was to:

1. Determine the theoretical means of computing the complete pattern of a single slot on a conical surface.

2. Determine the means of computing the pattern for any given array of slots using the methods of 1.

3. Determine optimization techniques for various design criteria.

4. Given a design configuration, to compute the pattern, e.g., the 65-slot array chosen by the Hughes Aircraft Company for analysis.

5. Apply the optimization techniques of 3, to the pattern of 4.

This report gives the results of 1 through 4.

The slot location is illustrated in Figure 1-1 which also indicates the coordinate system employed in the theoretical analysis of the 65-slot problem. Figures 1-2 through 1-5 contain comparisons of results obtained in the theoretical study with results obtained in the experimental program at the Hughes Aircraft Company.* The formulas employed

---

*See Appendix A (Section A.3) for a discussion of these comparisons, and additional experimental data obtained by HAC.

2

in the theoretical analysis of this 65-slot problem together with all of the theoretical

results obtained are presented in Appendix A. This paper reports the first analysis

which theoretically determines the pattern resulting from a many slot array on a

conical surface.

| Sketch of Cone Surface Showing Location of First Few Slots | Sketch Showing Geometry Employed - In "Plane Cut" Computations $\phi=0^{\circ}$ | Sketch Showing Geometry Employed in "Conical Cut" Computations |
|---|---|---|
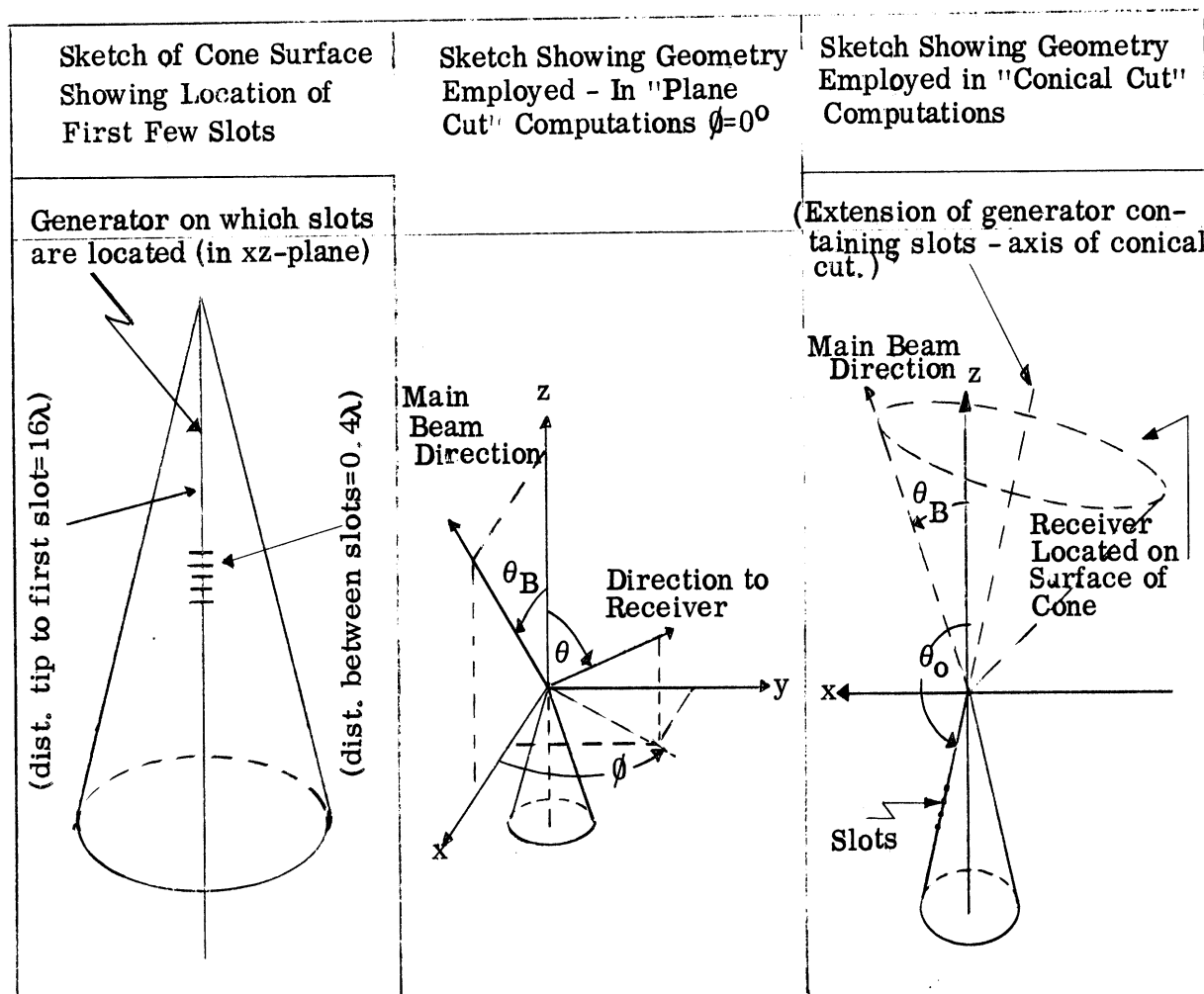


FIG. 1-1: GEOMETRY USED IN ANALYSIS OF THE 65-SLOT PROBLEM

Abscissae
of minima
(theoretical)

$$\frac{|H_\phi|^2}{|H_{max}|^2}$$

— Exp.

× Theory

$$\frac{|H_\theta|^2}{|H_{max}|^2}$$

--- Exp.

o Theory

-10db

-20db

-30db

40

0

θ

-40

FIG. 1-2  COMPARISON BETWEEN THEORY AND EXPERIMENT
FOR A PLANE CUT ($\theta_B = 10°$, $\phi = 0°$)
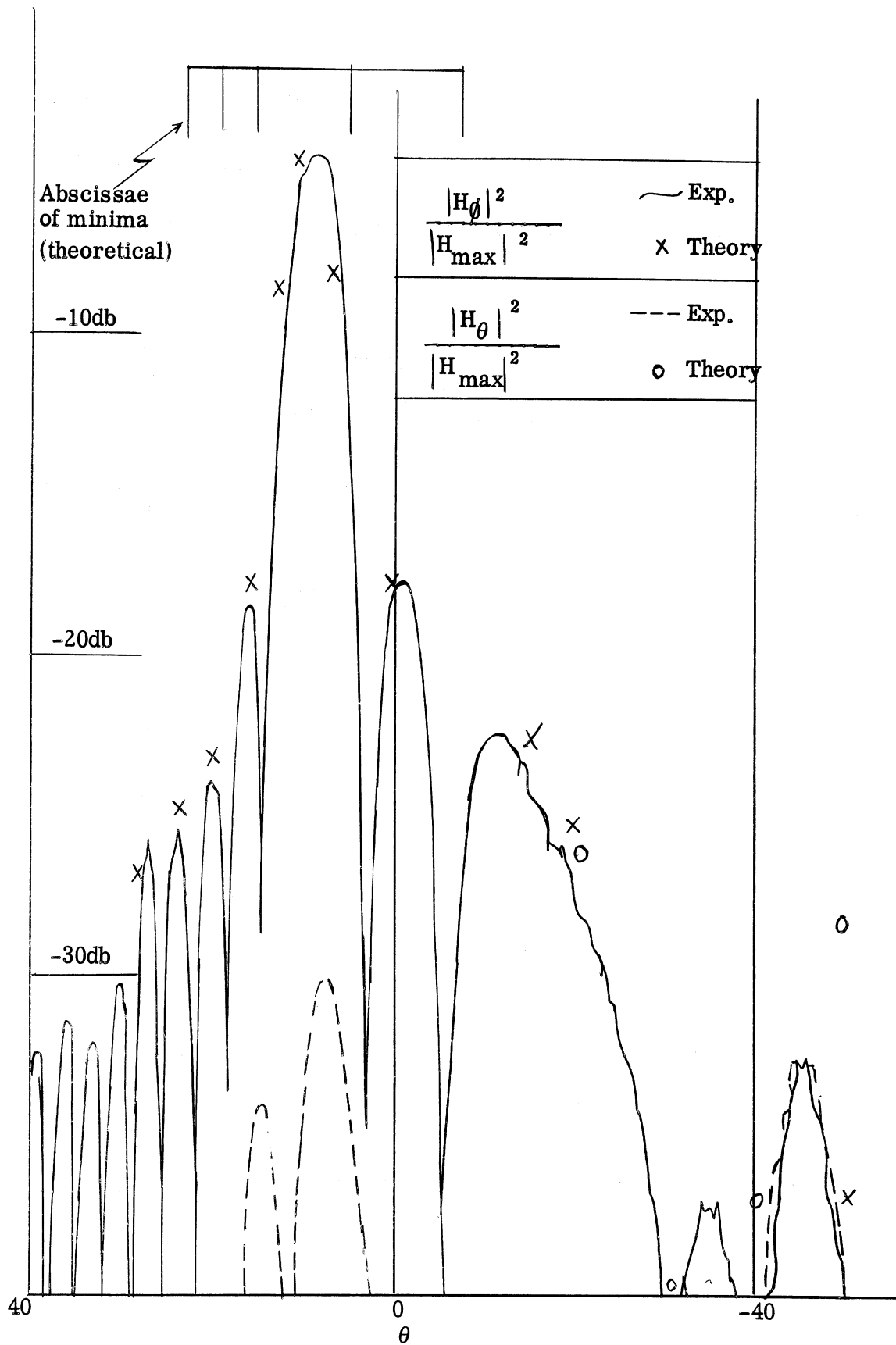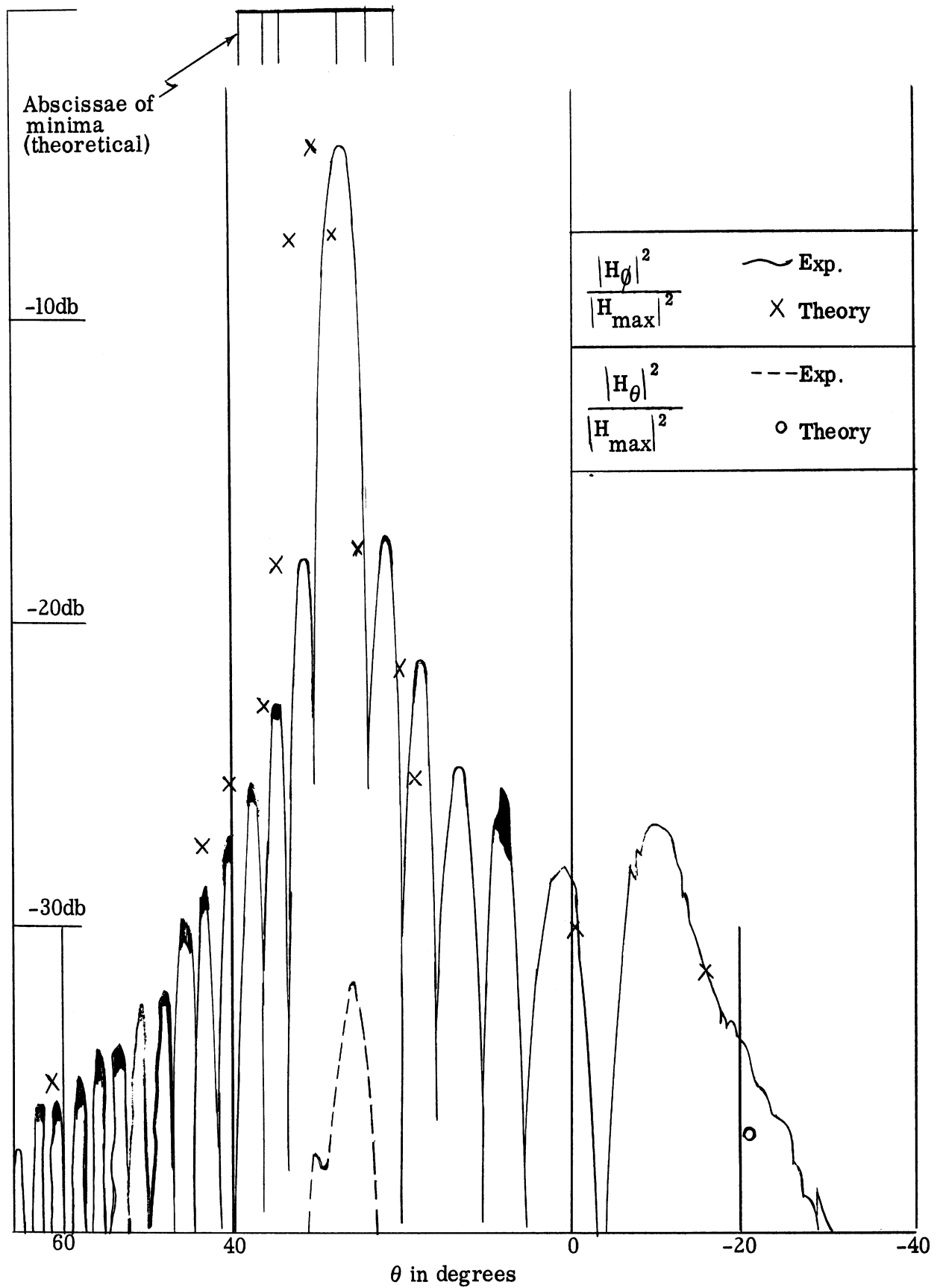
FIG. 1-3 COMPARISON BETWEEN THEORY AND EXPERIMENT FOR A
PLANE CUT ($\theta_B = 30^o$, $\phi = 0^o$)

FIG. 1-4 COMPARISON BETWEEN THEORY AND EXPERIMENT FOR A CONICAL CUT ($\theta_B = 10°$)

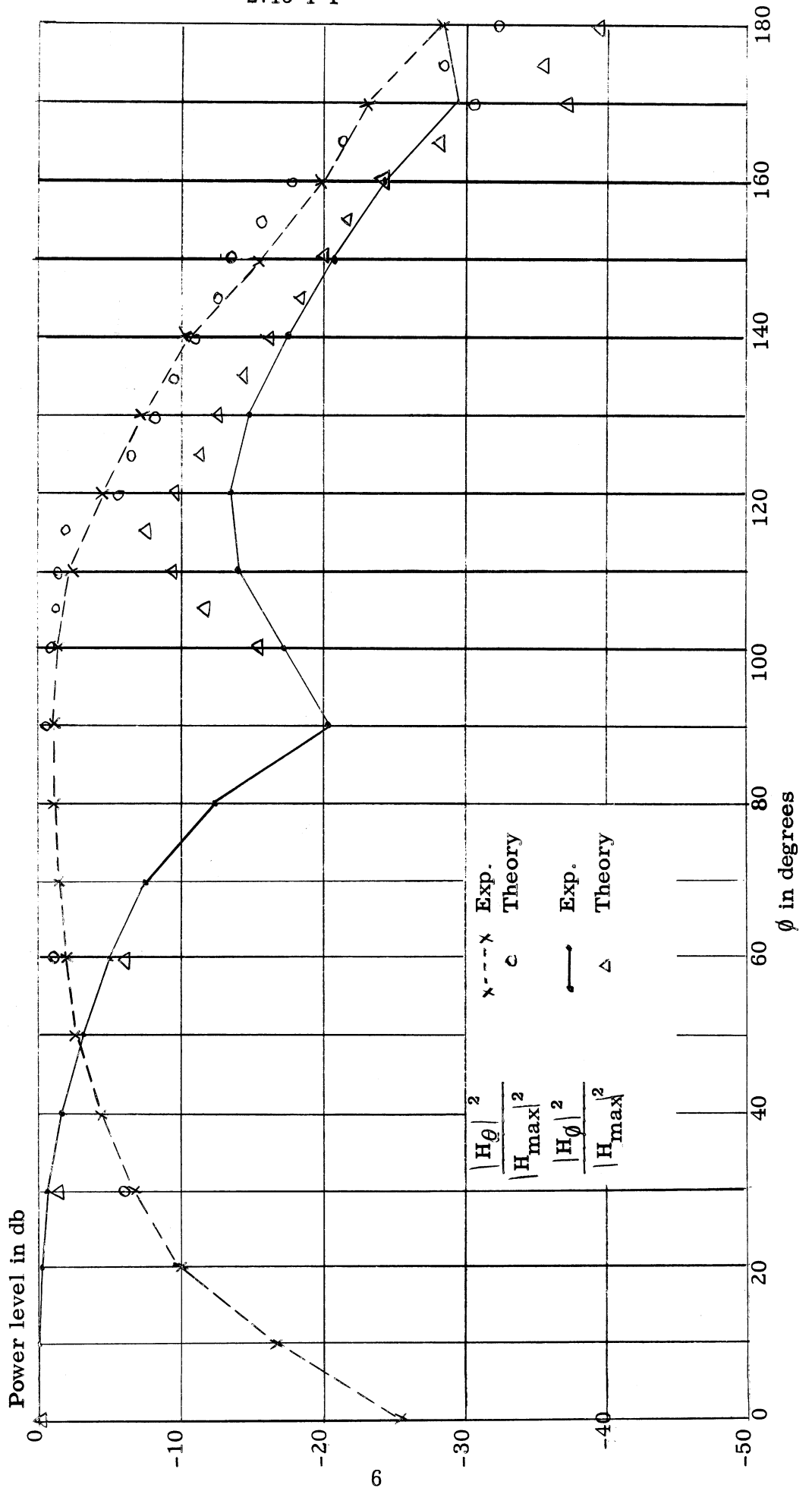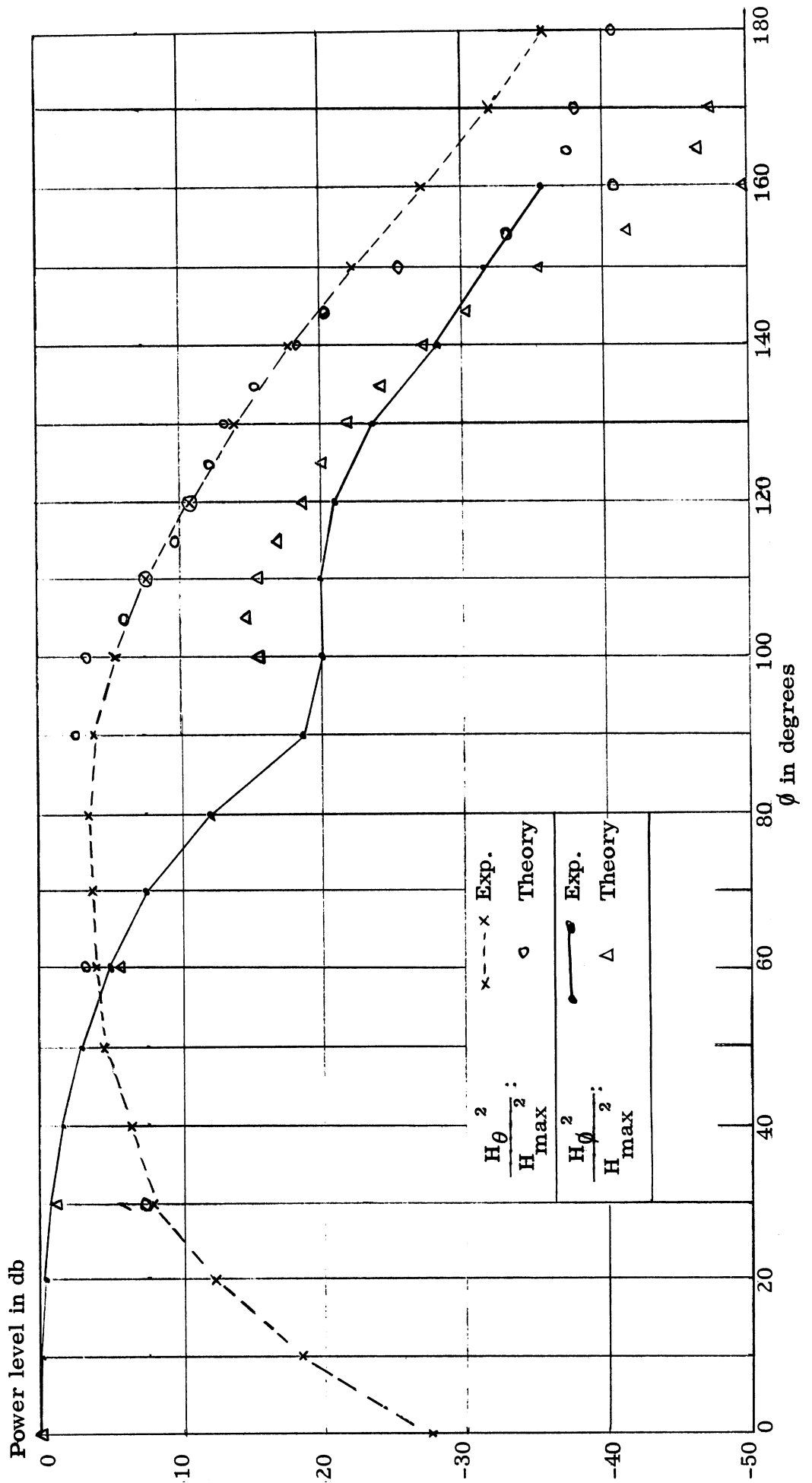FIG. 1-5 COMPARISON BETWEEN THEORY AND EXPERIMENT FOR A CONICAL CUT
($\theta_B = 30°$)

In order to obtain theoretically the far field radiated in all directions, it is necessary to employ different methods of approximation to account for different contributions to the field. Geometric Optics suffices for main beam calculations. For the receiver not in the main beam, other techniques are required to describe both the effect of the cone's tip on the radiated field and the effect of energy which appears to have crept along the body before being radiated, since these effects predominate out of the line of sight of the array. Physical Optics was used to determine the tip effect while the method available to treat the creeping waves was that due to V. A. Fock (Ref. 1) and this application used analyses of N. A. Logan (Ref. 2), J. B. Keller (Ref. 3) and one of the authors (R. F. Goodrich). The generalized arguments for Fock's universal functions were obtained for application to a conical surface; this work was performed under another Air Force Contract (AF-19(604)-1949) and is discussed in Reference 4.

In the calculation reported on in Appendix A, the Fock technique was employed only when the slots were in the cone's shadow relative to the receiver, and Geometric Optics was used in the lit region. In addition, the tip effect was examined and found (for a $15^\circ$ half angle cone with the first slot 16 wavelengths from the tip) to be of a lower order of magnitude than the other contributions to the field. These three methods for the analysis of a single slot on a cone are discussed in Section II and the regions of their applicability in the 65-slot problem are indicated graphically in Figure 1-6.

As mentioned above, although a pattern obtained from a single analysis such as the 65-slot program is, in and of itself, of extreme interest, the seeds of improvement

$\phi= \pm 180°$

$\phi= -150°$        $\phi=150°$

$\phi= -120°$        $\phi=120°$

$\phi= -90°$        $\phi=90°$

$\theta=165°$

$\theta=120°$

$\theta= 90°$

$\phi= -60°$        $\theta= 60°$        $\phi=60°$

$\theta= 30°$

$\theta= 0°$

$\phi= -30°$        $\phi=30°$

$\phi=0°$

| | points inside the cone |
|---|---|

| | region where Fock Theory was used |
|---|---|

| | region where Geometric Optics was used |
|---|---|

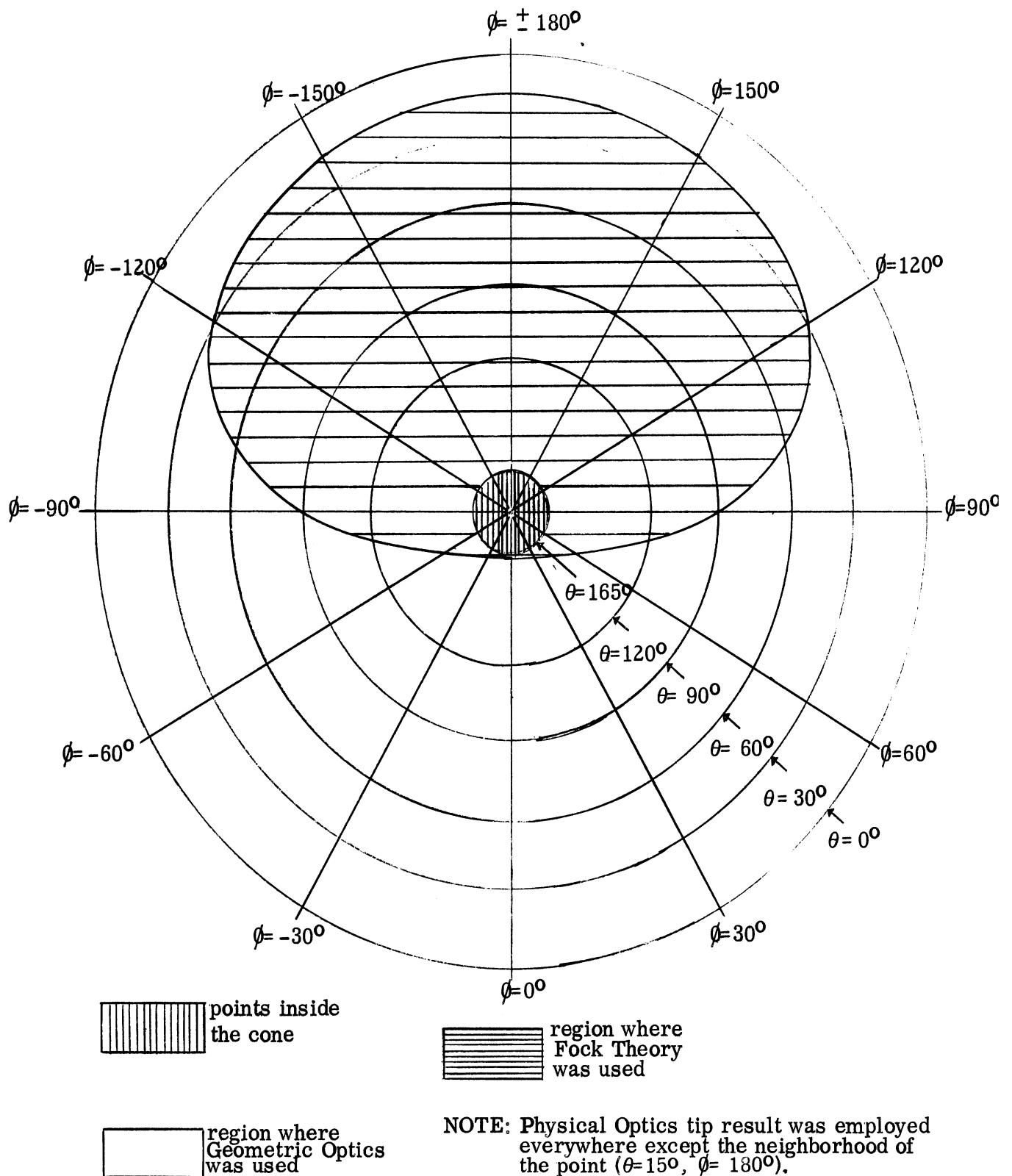NOTE: Physical Optics tip result was employed everywhere except the neighborhood of the point ($\theta=15°$, $\phi= 180°$).

FIG. 1-6    PLANAR REPRESENTATION OF
(FAR ZONE) RECEIVER POSITIONS

9

contained in the analysis are of even greater importance. That is, for many arrays of

practical interest it is possible to find a method of predicting how to alter the array to

produce a better pattern for a given purpose from the given (or computed) pattern until

we have reached a satisfactory practical solution to many particular radiation problems.

There are several methods of optimization possible and these are associated with the

particular problems present in a given system. Various systems might require as

criteria:

1. that a maximum amount of energy be in the main beam for a
   given amount of power put into the system,

2. that there be a maximum gain for a fixed amount of input
   power,

3. that the ratio of main beam power to side lobe level be a
   maximum,

4. that there be a certain spread of power in many side lobes
   as compared with the admissable power in a few side lobes, etc.

In a given application the criteria which are used will depend upon the specific system

requirements. Rather than consider a specific system we have selected two more

general criteria for analysis here. We feel that the results obtained are highly important

contributions to the optimization problem and that these optimization methods should be

applied to slot array computations. The first of these deals with obtaining a low side lobe

level for a given maximum beam power; this method of optimization is discussed in

Section III. The second method utilizes a special purpose analog computor which we feel

may yield the excitation for the maximum gain possible in surface arrays. This second optimization procedure is discussed in Section IV.

Thus, in summary, we have established the fact that radiation patterns from slots on cones can be computed, we know what current distributions are required to duplicate radome-dish patterns, and we have methods which give every indication of leading to patterns which will be an improvement over the radome-dish type. One would expect this on theoretical grounds since utilizing the entire surface of a cone as an antenna increases the area available over a radome-dish combination (thus obtaining a larger effective aperture) and also because the bias errors due to the radome would be withdrawn from the system.

Although the results reported here represent a definite breakthrough for the surface antenna problem, considerably more work is required before this program can be considered to be complete. For example, the optimization methods should be explored more fully and applied to particular cases of interest, e.g., the 65 slots on a cone generator. Further basic research is required on the nature of the radiated field in the vicinity of the transition region (that region of space which separates the "geometric optics region" from the "Fock theory region"). It is our belief that the amplitude is a slowly varying function in this transition region although the phase is a rapidly varying function. However, this belief is based upon physical principles and should be substantiated by basic mathematical analysis. In addition to the consideration of optimization from the viewpoint of a particular array, considerable attention should be given to

optimization on the basis of a variable array; such an approach (if successful) would lead to a method of optimization which would be applicable to almost any system regardless of what basic input parameter philosophy was inherent in that system.

In considering the optimization procedures, it is necessary to keep sight of the final applications. Indeed, the optimization goal is, given a certain antenna requirement, to reduce to a minimum the complexity, value, and number of the input parameters. As an illustration, it has been shown that point by point control of the field on the entire surface will permit the reproduction of a dish pattern but at the cost of a greatly complicated excitation mechanism. On the other hand, a series of linear arrays of the kind considered in this report may be quite sufficient for a given application at a much reduced cost in the complexity of the input mechanism. An understanding of this approach to optimization needs to be an aim of future study.

Under University of Michigan Purchase Order No. 154216 (under the prime Contract No. AF-33(038)-28634) the University of Illinois investigated the problem of establishing a criterion for approximating a continuous source distribution by a discrete source distribution for line sources under various conditions of excitation. A further investigation considered the approximation of the radiation pattern of an electric dipole in free space by a distribution of dipoles on the surface of a perfectly conducting sphere. This work is reported in Reference 5.

# THE  UNIVERSITY  OF  MICHIGAN
2713-1-F

II

INFINITESIMAL SLOTS

## 2.1 Introduction

We wish to find an expression for the far field radiated by a transverse infinitesi-

mal slot located on the surface of a cone at a large distance (in wavelengths) from the tip

of the cone. The infinitesimal slot can be considered as a magnetic dipole. To find its

far field we make use of the Reciprocity Theorem (see Section 2.6). This theorem

requires us then to find the field induced on the cone (at the point where we wish to

locate the slot) by a magnetic dipole. The dipole is arbitrarily oriented at an arbitrary

point in space but has to be located far from both the cone tip and the point where the

slot is to be placed.

If the dipole is located sufficiently far from the cone, the wavefronts of the

dipole field near the cone are essentially plane. Hence, we approximate the field incident

upon the cone by the field of a plane wave, whose magnitude is carefully adjusted so that

the dipole nature of the incident field is retained. Thus our problem becomes one of

determining the fields induced on the cone surface by a plane wave incident from an

arbitrary direction.

We treat this field induced on the cone surface as a quantity having two dominant

contributions. One of these contributions arises from energy which either impinges

directly upon a neighborhood of the point where the slot is to be placed or travels to

this point along a geodesic from the shadow boundary. We call the former part of this

14

contribution the "geometric optics" term and the latter the "creeping wave" term. The other of these contributions consists of energy which is scattered by the tip of the cone to the point where the slot is to be located. We call this the "tip" term. In the succeeding sections we present the methods by which these two contributions are obtained and the procedures for using them to describe the far field radiated by an infinitesimal slot on a cone. The "geometric optics" term is given implicitly in Section 2.4 and discussed more fully in Reference 16.

## 2.2 Notation

We adhere to the following notation throughout this section. Let $r, \theta, \phi$ be the usual spherical coordinates describing a field point in the radiation problem, a source point in the reciprocal problem. Primed, these variables designate a field point in the reciprocal problem; double-primed, they refer to points on the cone $\theta'' = \alpha$, $\alpha < \pi/2$.

We specify that all electromagnetic fields have a time dependence given by $e^{-ikct}$ where c is the velocity of light and $k = 2\pi/\lambda$, $\lambda$ designating wavelength. The unit vector $\hat{p}$ designates the magnetic field direction for a plane wave and is called polarization by us.

## 2.3 Fock Theory

We obtain the creeping wave contribution to the field on the surface of a cone due to an incident plane wave by suitably extending an analysis due to V. A. Fock (Ref. 1).

We can consider the Fock formulation as a modification of geometric optics

based on a local analysis of the field in the region of the shadow boundary. In particular, Fock defines two universal scalar functions, F and G, whose argument $\xi$ is a function of distance measured from the shadow boundary. The polarization of the incident radiation determines the linear vector combination of the Fock functions which is approximately proportional to the field induced on the scatterer.

The creeping wave term, i.e., the magnetic field $\vec{H}_c$ evaluated on the surface at a point $\xi$ which is a function of distance into the shadow region along a geodesic, can be given in terms of the unit vectors $\hat{\theta}''$, $\hat{T}$, and $\hat{\theta}'' \times \hat{T}$ as

$$\frac{\vec{H}_c(\xi)}{H_o} = \left\{ \hat{p} \cdot \hat{\theta}'' \bigg|_{shadow} \right\} F(\xi)\hat{T} + \left\{ \hat{p} \cdot \hat{\theta}'' \times \hat{T} \bigg|_{shadow} \right\} G(\xi)\hat{\theta}'' \times \hat{T} \qquad (2.3.1)$$

where $\hat{T}$ is the tangent to the geodesic, $\hat{\theta}''$ is the normal to the surface, $\hat{p}$ is the polarization of the incident plane wave, and $F(\xi)$ and $G(\xi)$ are Fock's functions. It is important to note that in this expression for $\vec{H}_c$, $\hat{p} \cdot \hat{\theta}''$ and $\hat{p} \cdot \hat{\theta}'' \times \hat{T}$ are evaluated at that point on the shadow boundary where the creeping wave is launched, while $F(\xi)\hat{T}$ and $G(\xi)\hat{\theta}'' \times \hat{T}$ are evaluated at the point of interest in the shadow region, i.e., at the point where the slot is to be placed.

We now need to determine the geodesics on a cone, the shadow boundary for a given incidence of a plane wave, and curvature along a geodesic (to find Fock's argument $\xi$).

We find the equation of a geodesic on the cone $\theta'' = \alpha$ to be

$$r'' = a \sin \psi \sec \left[ ( |\phi''| - \phi_s^{I''}) \sin \alpha + \frac{\pi}{2} - \psi \right] = \frac{a \sin \psi}{\sin \left[ \psi - ( |\phi''| - \phi_s'') \sin \alpha \right]} \qquad (2.3.2)$$

where

$$\phi_s'' = \arccos \frac{\tan \alpha}{\tan \theta} , \qquad 0 \leqslant \phi_s'' \leqslant \pi, \quad \alpha \leqslant \theta \leqslant \pi - \alpha, \qquad (2.3.3)$$

gives the equation of the generator forming the shadow boundary (for incidence in the xz-plane); where

$$\psi = \arccos \left( - \frac{\cos \theta}{\cos \alpha} \right), \qquad 0 \leqslant \psi \leqslant \pi, \qquad (2.3.4)$$

is the angle the incident direction forms with the shadow boundary; and where a is the distance from cone tip to point where slot is to be located. The curvature K along a geodesic is given by

$$K = \frac{a^2 \cos \alpha \sin^2 \psi}{r''^3 \sin \alpha} \qquad (2.3.5)$$

Finally, $\xi$ , the argument of the Fock functions for the creeping wave term, is

$$\xi = \left( \frac{k a \sin \psi}{2 \tan^2 \alpha} \right)^{1/3} ( |\phi''| - \phi_s'') \sin \alpha \quad . \qquad (2.3.6)$$

## 2.4. Tip-scattering

We use the expression "Physical Optics field" to denote the scattered far field, $\vec{H}_s$, obtained by using Geometric Optics (i.e., the magnetic field on the surface is given by twice the tangential component of the incident magnetic field in the lit region and zero in the shadow) in the Kirchhoff-Huygens integral representation for a scattered field.

17

$\vec{H}_s$ is, for a plane wave of magnitude $H_0$ incident from an arbitrary direction,

$$\vec{H}_s \cong \frac{H_0 \, ike^{ikr'}}{2\pi r'} \, \vec{g}, \qquad \vec{g} = (\hat{r}' \cdot \hat{p})\vec{f} - (\hat{r}' \cdot \vec{f}) \, \hat{p} \tag{2.4.1}$$

where

$$\vec{f} = \int_S \hat{n} e^{-ik\vec{r}'' \cdot (\hat{r} + \hat{r}')} \, dS \, . \tag{2.4.2}$$

S is the portion of the cone surface illuminated by the plane wave and $\hat{n}$ is the outward normal to the cone. Equation (2.4.2) may be written

$$\vec{f} = \int_0^\infty \int_A^B (\cos\alpha \cos \phi'' \hat{i}_x + \cos\alpha \sin\phi'' \hat{i}_y - \sin\alpha \, \hat{i}_z) e^{-ikr''M} r'' \sin\alpha \, d\phi'' dr''. \tag{2.4.3}$$

A and B are generator shadow boundaries cast on the cone by the incident plane wave; they are

$$A = \phi - \arccos\left(\frac{\tan\alpha}{\tan\theta}\right), \qquad\qquad B = \phi + \arccos\left(\frac{\tan\alpha}{\tan\theta}\right),$$

when no shadow exists, i.e., the cone is entirely illuminated or $\theta > \pi - \alpha$, $A = \phi - \pi$ and $B = \phi + \pi$. The quantity M is given by

$$M = q + b \cos\phi'' + c \sin\phi''$$

where

$$q = \cos\alpha \, (\cos\theta' + \cos\theta),$$

$$b = \sin\alpha \, (\cos\phi' \sin\theta' + \sin\theta \cos\phi),$$

$$c = \sin\alpha \, (\sin\phi' \sin\theta' + \sin\phi \sin\theta).$$

The $r''$ integration is accomplished by an Abelian limit argument (Ref. 11), yielding

for $\vec{f}$

$$\vec{f} \cong - \frac{\sin \alpha}{k^2} \int_A^B \frac{d\phi''}{M^2} (\cos \alpha \cos \phi'' \hat{i}_x + \cos \alpha \sin \phi'' \hat{i}_y - \sin \alpha \hat{i}_z) ; \qquad (2.4.4)$$

this integration can be expressed in finite terms (Ref. 12);

$$\vec{f} \cong - \frac{\sin \alpha}{k^2} \left\{ \cos \alpha \left[ \frac{c + q \sin \phi''}{MQ} - 2bQ^{-3/2} \arctan \frac{(q-b) \tan(\phi''/2) + c}{\sqrt{Q}} \right] \hat{i}_x \right.$$

$$- \cos \alpha \left[ \frac{b + q \cos \phi''}{MQ} + 2cQ^{-3/2} \arctan \frac{(q-b) \tan(\phi''/2) + c}{\sqrt{Q}} \right] \hat{i}_y$$

$$\left. - \sin \alpha \left[ \frac{c \cos \phi'' - b \sin \phi''}{MQ} + 2qQ^{-3/2} \arctan \frac{(q-b) \tan(\phi''/2) + c}{\sqrt{Q}} \right] \hat{i}_z \right\} \Bigg|_A^B ,$$

where

$$Q = q^2 - b^2 - c^2 .$$

Care must be taken with the value of the arctangent to note where its value has moved

from one Riemann surface to the next as the value of $\phi''$ moves from A to B.

The field $\vec{H}_s$ given by Equation (2.4.1) is called the tip-scattered field because

in the Abelian evaluation of the integral for $\vec{f}$ (Eqn. 2.4.4) the major contribution,

for M bounded away from zero, is obtained from a neighborhood of the point $r''=0$,

i.e., the tip of the cone. The cases for which $M=0$ for all values of $\phi''$ in

Equation (2.4.4), correspond to forward scattering situations and these cases are

dealt with by Geometric Optics. The cases for which $M=0$ at only one value of $|\phi''|$

in the region of integration either correspond to specular reflection where again

Geometric Optics is used or require a re-examination of the Physical Optics approximation.

Although the integral in (2.4.4) does not exist in this last case we know how to correctly

handle this situation. In Appendix B we make a closer examination of the Physical Optics

integral (Eqn. 2.4.1) for this case and find that the evaluation given above can be for-

mally extended to include it. Since the major contribution to the Physical Optics integral,

when it exists, comes from a neighborhood of the cone tip we now require only that the

field point be far from this neighborhood. In this way we obtain a representation of the

tip-scattered contribution to the field on the cone surface far from the tip.

There are substantial indications that the Physical Optics field closely approxi-

mates the exact field scattered by a cone. For example, the Physical Optics method

produces, for large and small angle cones, a result for the nose-on monostatic radar

cross section which is in excellent agreement with the result produced by an exact

expansion of the cross section in powers of the cone angle(Refs. 13,14). In addition,

the rigorous bistatic radar cross section for an electromagnetic plane wave incident

along the cone axis agrees well with the Physical Optics result (Ref. 14). We know

also that it has exactly the right wavelength dependence.

## 2.5. Plane Waves versus Dipoles

In the previous sections we dealt with an incident plane wave. The field of the

plane wave on the cone surface is given by

$$\vec{H_i} = \hat{p} \, H_o \, e^{-ik\hat{r} \cdot \vec{r}''} \, . \qquad (2.5.1)$$

Since we are really interested in an incident field due to a magnetic dipole far from the cone, we relate these fields as follows:

Let a magnetic dipole with orientation $\hat{m}$, such that $\hat{m} \cdot \hat{r}$ vanishes, be located at the point $(r, \theta, \emptyset)$. Then its far field is

$$\frac{C\, e^{ikR}}{R}\hat{R} \times (\hat{R} \times \hat{m}),$$

where C is the dipole strength coefficient and R is the distance from the point $(r, \theta, \emptyset)$ to the point of observation $(r', \theta', \emptyset')$,

$$R = \left[ r^2 + r'^2 - 2\vec{r} \cdot \vec{r'} \right]^{1/2},$$

$$\cong r - \hat{r} \cdot \vec{r'} \quad \text{for } r \gg r',$$

and

$$\hat{R} = \nabla R.$$

For large r, $\hat{R}$ may be replaced by $-\hat{r}$. Since the dipole is far from the cone its field at the cone surface is given approximately by

$$\vec{H}_i = -\hat{m}\, C\, \frac{e^{ik(r - \hat{r} \cdot \vec{r''})}}{r}. \qquad (2.5.2)$$

Thus we see from Equations (2.5.1) and (2.5.2) that, at the cone surface, we may replace the incident field of a plane wave by the incident field of a dipole placed at a very large but finite distance from the cone simply by placing $\hat{p} = -\hat{m}$ and

$$H_0 = C\, \frac{e^{ikr}}{r}.$$

## 2.6 The Reciprocity Theorem

We now present the Reciprocity Theorem in a form which, with the results of the previous sections, will enable us to obtain the far field radiated by an infinitesimal slot

on a cone.

The Lorentz Reciprocity Theorem may be stated in the form

$$\int \vec{H_1} \cdot \vec{M_2} \, dV = \int \vec{H_2} \cdot \vec{M_1} \, dV$$

where $\vec{H_1}(\vec{H_2})$ is the field due to the magnetization $\vec{M_1}(\vec{M_2})$ and the integration is over all space. If $\vec{M}_{1,2}$ are of the form $\hat{m}_{1,2} \, \delta(\vec{r} - \vec{r}_{1,2})$, that is, point sources, then we find

$$\vec{H_1}(\vec{r_2}) \cdot \hat{m}_2 = \vec{H_2}(\vec{r_1}) \cdot \hat{m}_1 \quad . \tag{2.6.1}$$

Let $\hat{m}_2$ designate the direction of some specifically oriented dipole located by the vector $\vec{r_2}$. We wish to determine its field $\vec{H_2}$ at some far point $\vec{r_1}$. Suppose

$$\vec{H_2}(\vec{r_1}) = A_1(\vec{r_1})\hat{u}_1 + A_2(\vec{r_1})\hat{v}_1,$$

where $\hat{u}_1 \cdot \hat{v}_1 = 0$. Let $\hat{u}_1$ and $\hat{v}_1$ designate in turn the orientation of $\hat{m}_1$ of a dipole located by $\vec{r_1}$. Its field at $\vec{r_2}$ is in turn $\vec{H_1}(\vec{r_2}, \hat{u}_1)$ and $\vec{H_1}(\vec{r_2}, \hat{v}_1)$.

It follows from (2.6.1) that

$$\vec{H_1}(\vec{r_2}, \hat{u}_1) \cdot \hat{m}_2 = \left[ A_1(\vec{r_1})\hat{u}_1 + A_2(\vec{r_1})\hat{v}_1 \right] \cdot \hat{u}_1,$$

from which

$$\left[ \vec{H_1}(\vec{r_2}, \hat{u}_1) \cdot \hat{m}_2 \right] = A_1(\vec{r_1}) \quad . \tag{2.6.2}$$

Similarly, from (2.6.1)

$$\vec{H_1}(\vec{r_2}, \hat{v}_1) \cdot \hat{m}_2 = \left[ A_1(\vec{r_1})\hat{u}_1 + A_2(\vec{r_1})\hat{v}_1 \right] \cdot \hat{v}_1 \quad ,$$

from which

$$\left[ \vec{H_1}(\vec{r_2}, \hat{v}_1) \cdot \hat{m}_2 \right] = A_2(\vec{r_1}) \quad . \tag{2.6.3}$$

Therefore

$$\vec{H_2}(\vec{r_1}) = \left[ \vec{H_1}(\vec{r_2}, \hat{u}_1) \cdot \hat{m}_2 \right] \hat{u}_1 + \left[ \vec{H_1}(\vec{r_2}, \hat{v}_1) \cdot \hat{m}_2 \right] \hat{v}_1 \quad . \tag{2.6.4}$$

Equation (2.6.4) gives the radiated far field of a slot on the surface of a cone if we let

$$\vec{r}_1 \to \vec{r}, \qquad \vec{r}_2 \to \vec{r}'', \qquad \hat{m}_2 \to \text{direction of slot}, \qquad \hat{u}_1, \hat{v}_1 \to \text{successive values}$$

$$\text{for polarization, } \hat{p}; \qquad \vec{H}_1 \to \vec{H}_s + \vec{H}_c, \qquad \text{and } \vec{H}_2 \to \vec{H}.$$

## 2.7 The Far Field Radiated by an Infinitesimal Slot

The final part of the preceding section explains exactly how to employ the

Reciprocity Theorem to obtain a radiated far field due to an infinitesimal slot on a cone.

In Section 2.3 we have, without loss of generality, restricted the direction of

incidence to lie in the xz-plane. We may treat the results of Section 2.4 in a similar

fashion, again without loss of generality.

Now employing the results of Section 2.6 we may express the radiated far field

at a point $(r, \theta, 0)$ due to an infinitesimal slot located at $(a, \alpha, \phi'')$ in the direction $\phi''$

on the cone as

$$\vec{H} = \left\{ \left[ \vec{H}_c(\hat{p}_1) + \vec{H}_s(\hat{p}_1) \right] \cdot \hat{\phi}'' \right\} \hat{p}_1 + \left\{ \left[ \vec{H}_c(\hat{p}_2) + \vec{H}_s(\hat{p}_2) \right] \cdot \hat{\phi}'' \right\} \hat{p}_2 \ ,$$

where the results of Section 2.5 must be used to define the quantity $H_0$ appearing in

expressions for $\vec{H}_c$ and $\vec{H}_s$ given by Equations (2.3.1) and (2.4.1), respectively. Note

that $\vec{H}_c$, for a point in the lit region, is given by geometric optics.

If the slot has a small but finite length, L, then the expression for the radiated

far field obtained above can be adjusted so as to include the length and voltage, $V_0$,

across the slot. As long as a radiating magnetic dipole is equivalent to a slot in a

plane we can relate the dipole strength coefficient, C, of Section 2.5 with the voltage

across the slot as follows

$$C = \frac{ik\, V_0 L}{4\pi}$$

(see Section A. 1. 3, p. 68 of Reference 15).

It is significant to note that the term "Geometric Optics field" is a misnomer

when applied to radiated fields obtained via reciprocity from scattered "Geometric

Optics fields", since such radiated fields are no longer wavelength independent.

III

## A THEORY OF LOW SIDE LOBE ANTENNA ARRAYS

In the problem which will be considered in this Section it is assumed that there are

a number of current distributions for the array which can be excited independently, and

for each of which the radiated field is known.  We might assume that the array consists of

a number of elements which can be separately excited, and that the field radiated when

any one of these elements is excited is known.  For example, we have shown in Section 2

how to find the radiated field of an infinitesimal slot on a cone.  The problem we set for

ourselves is that of determining the excitation coefficients for an array in such a way as

to minimize the side lobe level (compared to the main beam) for a beam of a fixed width.

To restate the above symbolically let the currents $I_n$ give the radiated fields, $F_n$.

We now want to determine coefficients $A_n$ which are related to the current, $I = \sum A_n I_n$,

and field, $F = \sum A_n F_n$, in such a way that the largest value taken on by the ratio

$\left| \dfrac{F(\theta, \phi)}{F(0, 0)} \right|$ in a given region, $R$, which excludes a neighborhood of the point $\theta = 0$, $\phi = 0$

is as small as possible ($\theta$ and $\phi$ are the polar angles of the field point).

We will consider a series of less ambitious problems which will finally lead us to

the desired problem.  Rather than minimizing the largest value taken on by $\left| \dfrac{F(\theta, \phi)}{F(0, 0)} \right|$

for all points $\theta$, $\phi$ in $R$ we will minimize the largest value taken on by $\left| \dfrac{F(\theta, \phi)}{F(0, 0)} \right|$ at a

set of points $\theta_i$, $\phi_i$ in $R$.  We will eventually let the number of points cover $R$ densely

so as to solve the original problem.  Throughout the discussion we will not insist on any

more mathematical rigor than is necessary to put forward a convincing argument for the

methods used.

As a matter of notation let

$$F_n(\theta_i, \phi_i) = F_{in}$$

$$F_n(0, 0) = F_{on} .$$

Then we seek the values of $A_1, A_2, \ldots, A_N$ which will give

$$\underset{A_1, A_2, \ldots, A_N}{\text{Min}} \quad \underset{i}{\text{Max}} \quad \left| \frac{\sum_n A_n F_{in}}{\sum_n A_n F_{on}} \right| , \qquad (3.1)$$

that is we seek the values of $A_1, A_2, \ldots, A_N$ which will minimize the largest value taken

on by $\left| \dfrac{\sum A_n F_{in}}{\sum A_n F_{on}} \right|$ . Let $M$ be the number of values taken on by $i$ (excluding zero).

First of all assume $M < N$. Then we can make $\sum A_n F_{in} = 0$ for all $i \neq 0$

while $\sum A_n F_{on} \neq 0$. This disposes of this case which will not be of interest hereafter.

Next consider the case $M = N$. This case, as it will turn out, is fundamental to

the rest of the analysis. We are assuming that the matrix $F_{in}$ is non-singular which

will ordinarily be the case. For simplicity we now let

$$B_i = \sum_n F_{in} A_n . \qquad (3.2)$$

We can solve for the $A_n$ in the form

$$A_n = \sum_i (F^{-1})_{ni} B_i . \qquad (3.3)$$

Thus we have

$$\sum_n F_{on} A_n = \sum_n \sum_i F_{on} (F^{-1})_{ni} B_i = \sum_i G_i B_i \qquad (3.4)$$

where

$$G_i = \sum_n F_{on} (F^{-1})_{ni} .$$

Now our problem is to determine the values of $B_1, B_2, \ldots, B_N$ which will give

$$\underset{B_1, B_2, \ldots, B_N}{\text{Min}} \quad \underset{i}{\text{Max}} \quad \left| \frac{B_i}{\sum G_j B_j} \right| \, . \tag{3.5}$$

It is clear that the B's are not unique to the extent that we can make the replacement $B_i \rightarrow \lambda B_i$ without affecting the value of $\underset{i}{\text{Max}} \left| \frac{B_i}{\sum G_j B_j} \right|$. We will make use of this later to simplify the form of the problem. Let us now assume that all of the B's except $B_1$ have the correct value (or rather $\underline{a}$ correct value in view of the non-uniqueness). We will now proceed to evaluate $B_1$ in terms of the other B's.

First we note that

$$\underset{i}{\text{Max}} \left| \frac{B_i}{\sum G_j B_j} \right| = \underset{i}{\text{Max}} \left| \frac{B_i}{\sum \frac{G_j}{G_1} B_j} \right| \frac{1}{|G_1|}$$

$$= \frac{1}{|G_1|} \underset{i}{\text{Max}} \left| \frac{B_i}{\sum \frac{G_j}{G_1} B_j} \right| \, . \tag{3.6}$$

Next we make use of the non-uniqueness to replace $B_j$ by $B_j e^{i\alpha}$ ($\alpha$ real) where $\alpha$ is chosen so as to make $\sum_{j \neq 1} \frac{G_j}{G_1} B_j$ a positive real number, $\gamma$. Finally we let $x = - B_1$. Now what we seek is

$$\underset{x}{\text{Min}} \quad \text{Max} \left\{ \underset{i \neq 1}{\text{Max}} \left| \frac{B_i}{\gamma - x} \right| , \left| \frac{x}{\gamma - x} \right| \right\} \, . \tag{3.7}$$

Let $i_M$ be a value of $i$ (other than 1) for which $\left| \frac{B_i}{\gamma - x} \right|$ takes on its maximum value. Thus we want

$$\underset{x}{\text{Min}} \quad \text{Max} \left\{ \left| \frac{B_{i_M}}{\gamma - x} \right| , \left| \frac{x}{\gamma - x} \right| \right\} \, . \tag{3.8}$$

27

Figure 3-1 is a contour plot of $\text{Max}\left\{ \left| \dfrac{B_{i_M}}{\gamma - x} \right| , \left| \dfrac{x}{\gamma - x} \right| \right\}$ in the x-plane

for $B_{i_M} = \gamma/2$. The contour lines are for the indicated side lobe levels. The dotted

circle divides the region $\left| B_{i_M} \right| > |x|$ from the region $\left| B_{i_M} \right| < |x|$ . It is clear that the

minimum occurs for $x = - \left| B_{i_M} \right|$ . From this we see that $|B_1| = \left| B_{i_M} \right|$ . Since we

could equally well have chosen any of the other B's in place of $B_1$ we see that the mini-

mum occurs when all of the B's are equal in magnitude. Due to the non-uniqueness we

can take the B's to all be equal to one in magnitude. Then (3.5) can be written

$$\underset{\substack{B_1, B_2, \ldots, B_N \\ |B_1| = |B_2| = \ldots = |B_N| = 1}}{\text{Max}} \left| \sum G_j B_j \right| . \tag{3.9}$$

But $\left| \sum G_j B_j \right| \leq \sum |G_j B_j| = \sum |G_j|$ $(|B_j| = 1)$, so that it is clear that the

maximum will be attained for $B_j = \dfrac{|G_j|}{G_j}$ . Thus we have

$$\underset{B_1, B_2, \ldots, B_n}{\text{Min}} \underset{i}{\text{Max}} \left| \dfrac{B_i}{\sum G_j B_j} \right| = \dfrac{1}{\sum |G_j|} \tag{3.10}$$

is attained for

$$B_j = \dfrac{|G_j|}{G_j} . \tag{3.11}$$

To get the corresponding values of the A's we use (3.3). This completes the solution of

the problem M = N.

Next we consider the case $\infty > M > N$. Suppose we had a correct set of $A_n$.

Now order the M quantities $\left| \dfrac{\sum A_n F_{in}}{\sum A_n F_{on}} \right|$ starting with the largest and ending with the
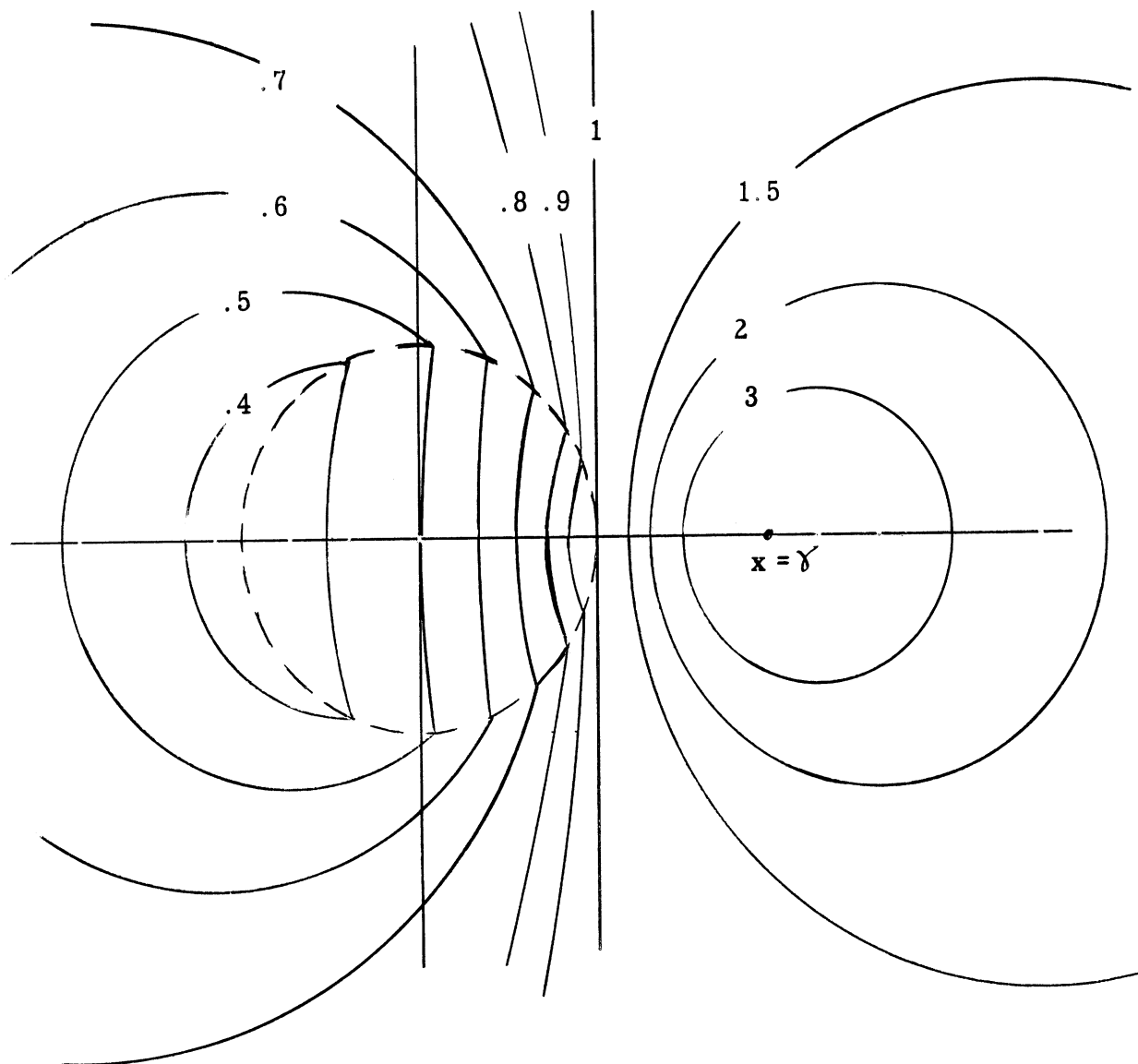
smallest. Pick out the first N of these.

FIG. 3-1: CONTOUR PLOT OF MAX $\left\{ \left| \dfrac{B_{i_M}}{\gamma - x} \right| , \left| \dfrac{x}{\gamma - x} \right| \right\}$

IN THE COMPLEX x-PLANE FOR THE CASE OF $B_{i_M} = \gamma/2$.

Suppose, in the first instance, that the N quantities are not all equal for the solution when all M are involved. Then we can make a small change in the A's in such a way as to decrease the largest of the N quantities while, if the change in the A's is small enough, none of the other M - N values will be larger than the largest of the N values. Thus the N values are equal.

Next suppose that the N chosen quantities are larger than the next largest of the M. Then unless the N A's have the values they would have if the remaining M - N quantities were ignored, we can again make small changes in the A's which will reduce the N quantities uniformly while keeping any of the remaining M - N all smaller than the chosen N.

Thus we see in this case (when the N largest quantities are larger than the remaining M - N if the A's have been correctly chosen to solve the problem) that we need to consider only N of the M quantities in order to arrive at the correct solution. The question is, which N of the M quantities must we deal with. We will now answer this question. We assert that we must choose the N quantities which yield the largest value of $\dfrac{1}{\sum |G_j|}$ (note that the $G_j$ depend on which N of the M quantities are chosen). To establish this assertion we show a contradiction in the converse assumption. Let us assume, then, that the solution is obtained for a choice which does not lead to the maximum value of $\dfrac{1}{\sum |G_j|}$. Now let us consider the N quantities which lead to the largest value of $\dfrac{1}{\sum |G_j|}$. We know that not all of these N quantities can be made smaller than the largest $\dfrac{1}{\sum |G_j|}$ and thus the assumption that none of them are larger than one of the smaller $\dfrac{1}{\sum |G_j|}$ is false. This establishes the assertion.

We are thus led to the following method of attacking our original problem.  First

we start with $N$ arbitrary points.  We then vary these points so as to maximize the value

of $\frac{1}{\sum |G_j|}$ .  We would then hope that the A's which correspond to the $N$ points which

maximize $\frac{1}{\sum |G_j|}$ would solve the problem.  We can easily test to see if they do solve

our problem by computing the field resulting from this choice of the A's.  If the side-lobe

level is nowhere greater than it is at the $N$ chosen points we have solved our problem

since the side-lobe level cannot be made any lower at the $N$ points.  However, if the

side-lobe level is higher at some other point then we have not solved our problem.

Now it turns out that in some cases the above method works, and in some cases

it does not.  We can get some insight into the question of how frequently we can expect

the method to work by considering the following analogous problem (it is, in fact, a special

case of our general problem but we will not bother to make the exact connection).  Suppose

that we have a number of points in the complex plane, $z_n$, and that we wish to find a point $z$

such that $\underset{n}{\text{Max}} \, |z - z_n|$ is made as small as possible.  A method of attacking this problem

which is exactly analogous to the method described above is the following.  Find the pair

or points, $z_n$ and $z_m$, from the given set which maximize $|z_m - z_n|$ (this is analogous

to maximizing $\frac{1}{\sum |G_j|}$ ).  Then let $z = (z_m + z_n)/2$ .  This value of $z$ will sometimes

solve the problem, and sometimes not.  It depends on whether the rest of the points in the

set lie inside the circle having $z$ as a center and $|z_m - z_n|/2$ as a radius.  In the figure

below (Figure 3-2) we show some sets of points for which the method would work, and

some for which it would not work.

Among the cases where this method does work is the design of a broadside linear array where the results of this method coincide with those of the Dolph-Chebychev method. We can certainly expect the method to work also in cases which do not differ too radically from this one, as well as in some of the cases which do differ radically. It is expected that future study will yield methods which work in all cases.



The method works for the following four sets of points:

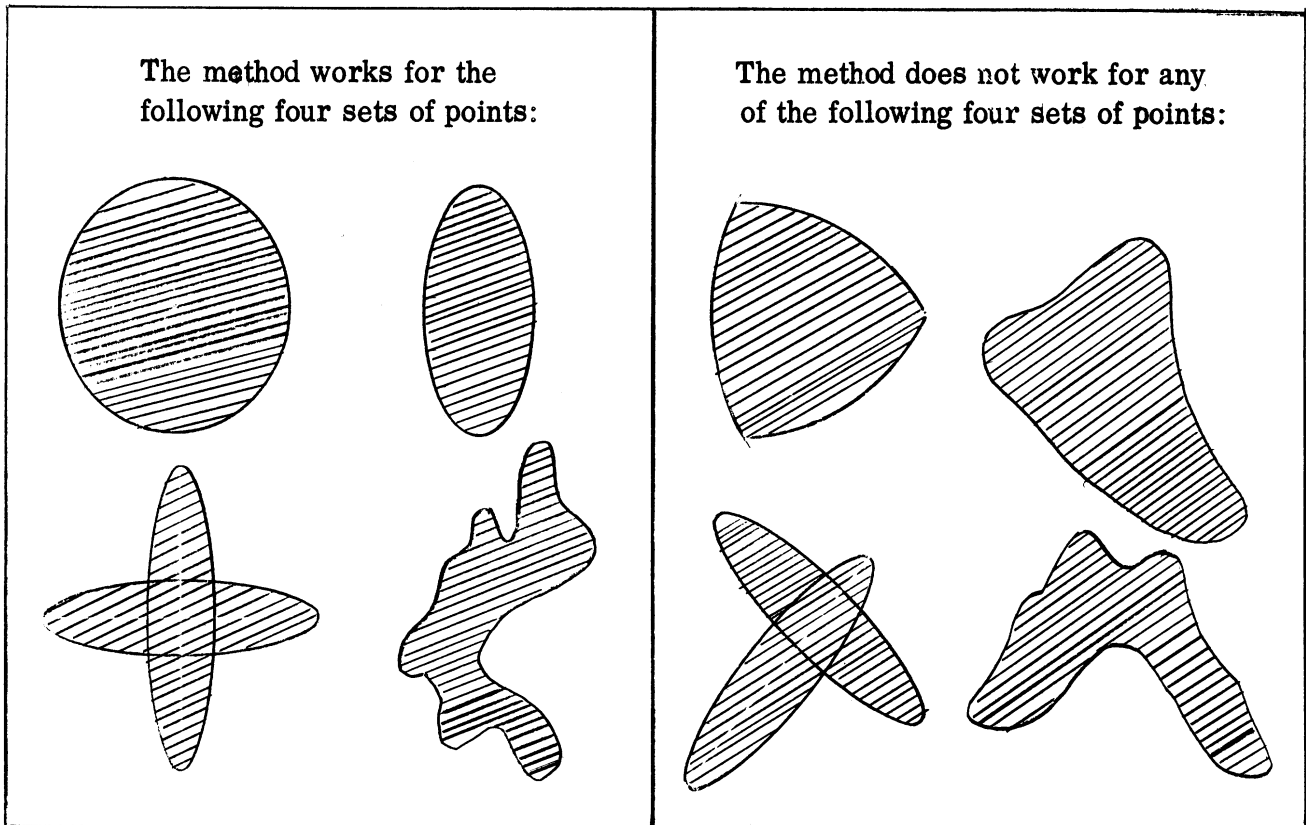The method does not work for any of the following four sets of points:

FIG. 3-2: THE PROBLEM OF MINIMIZING $\max_n \left| z - z_n \right|$ - EXAMPLES OF SETS OF POINTS FOR WHICH METHOD WORKS AND SETS OF POINTS FOR WHICH METHOD DOES NOT WORK

In order to give an idea of how this method goes we will now consider a very simple numerical example. We will take the case of a linear broadside array of four isotropic elements where the ratios of the currents in the elements is to be chosen so as to produce a low side-lobe level. This problem can also be treated by standard methods so that we have a standard of comparison.

Let the inter-element spacing be $\lambda/2$. We will consider the case where there are only four elements which we take to be located at

$$x = y = 0 \; ; \; z = \pm \lambda/4, \; \pm 3\lambda/4 \; . \tag{3.12}$$

The radiated field in the direction $(\theta, \phi)$ is given by

$$E = \frac{e^{ikr}}{r} \quad F = A_{-2} \; \frac{\exp\left[ik(r + \frac{3\lambda}{4}\cos\theta)\right]}{r} \; + A_{-1} \; \frac{\exp\left[ik(r + \frac{\lambda}{4}\cos\theta)\right]}{r} \tag{3.13}$$

$$+ A_1 \; \frac{\exp\left[ik(r - \frac{\lambda}{4}\cos\theta)\right]}{r} \; + A_2 \; \frac{\exp\left[ik(r - \frac{3\lambda}{4}\cos\theta)\right]}{r} \; .$$

Let us first of all consider a standard design of such an array. In the Dolph-Chebychev design we would have $A_1 = A_{-1}$, $A_2 = A_{-2}$, $A_1$ and $A_2$ real. In this case we get

$$F = 2A_1 \; \cos\left(\frac{\pi}{2}\cos\theta\right) + 2A_2 \; \cos\left(\frac{3\pi}{2}\cos\theta\right) \; . \tag{3.14}$$

Now the field broadside $(\theta = \pi/2)$ is $F_0 = 2(A_1 + A_2)$. There will be sidelobes symmetrically situated relative to $\theta = \pi/2$ which are located by the condition $\frac{\partial F}{\partial \cos\theta} = 0$ or

$$-\pi A_1 \; \sin\left(\frac{\pi}{2}\cos\theta\right) - 3\pi A_2 \; \sin\left(\frac{3\pi}{2}\cos\theta\right) = 0 \; . \tag{3.15}$$

Making use of the relation $\sin 3x = \sin x (3 - 4 \sin^2 x)$ we put (3.15) in the form

$$A_1 + 9A_2 = 12A_2 \sin^2 ( \frac{\pi}{2} \cos \theta)$$

(3.16)

$$\sin( \frac{\pi}{2} \cos \theta) = \sqrt{\frac{A_1 + 9A_2}{12A_2}}.$$

Using this value of $(\theta)$ in (3.14) we get

$$F = 2A_1 \sqrt{\frac{3A_2 - A_1}{12A_2}} + 2A_2 \sqrt{\frac{3A_2 - A_1}{12A_2}} \left\{ 1 - \frac{A_1 + 9A_2}{3A_2} \right\} = -\frac{2}{3} \frac{(3A_2 - A_1)^{3/2}}{\sqrt{3A_2}}$$

(3.17)

The value of $\theta$ for which the main beam has decreased to the value given by (3.17) is

also of interest. It is given by

$$2A_1 \cos( \frac{\pi}{2} \cos \theta) + 2A_2 \cos( \frac{3\pi}{2} \cos \theta) = \frac{2(3A_2 - A_1)^{3/2}}{3\sqrt{3A_2}}$$

or

(3.18)

$$\cos( \frac{\pi}{2} \cos \theta) = \sqrt{\frac{3A_2 - A_1}{3A_2}}.$$

Figure 3-3 gives $\theta$ as given by Equations (3.18) and (3.16) as a function of $A_1/A_2$ while

Figure 3-4 gives the side-lobe level in db down from the main dobe as a function of

$A_1/A_2$.

The results given above from Equation (3.14) on are essentially taken from

Dolph's "A Current Distribution for Broadside Arrays which Optimizes the Relationship

Between Beam Width and Side-Lobe Level". With these results available for comparison

we are prepared to treat the same problem with the method discussed previously.
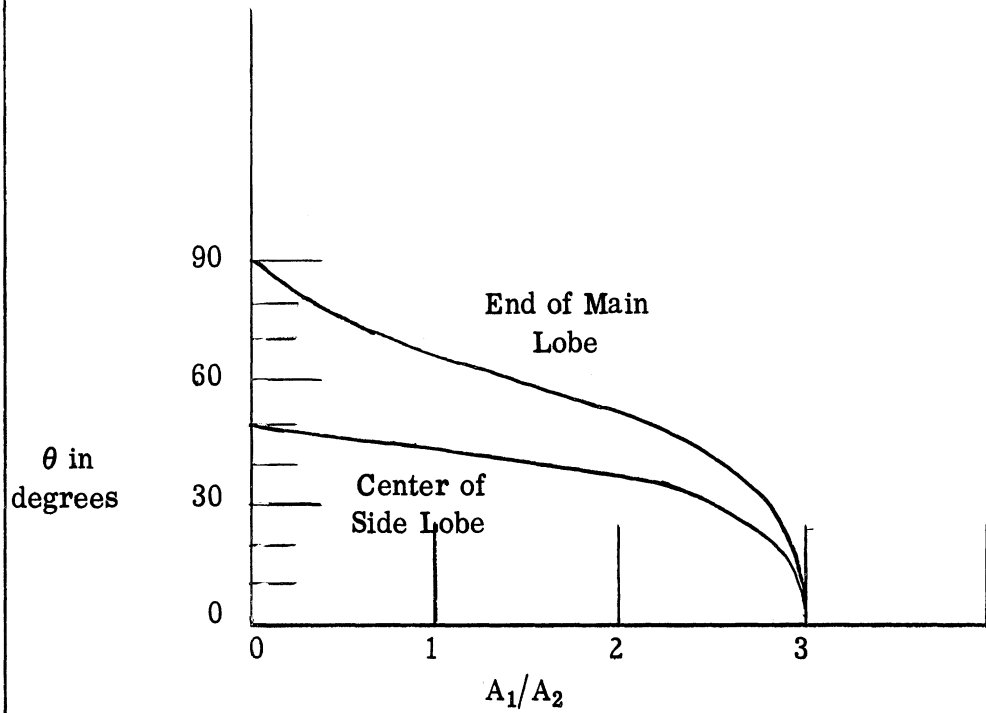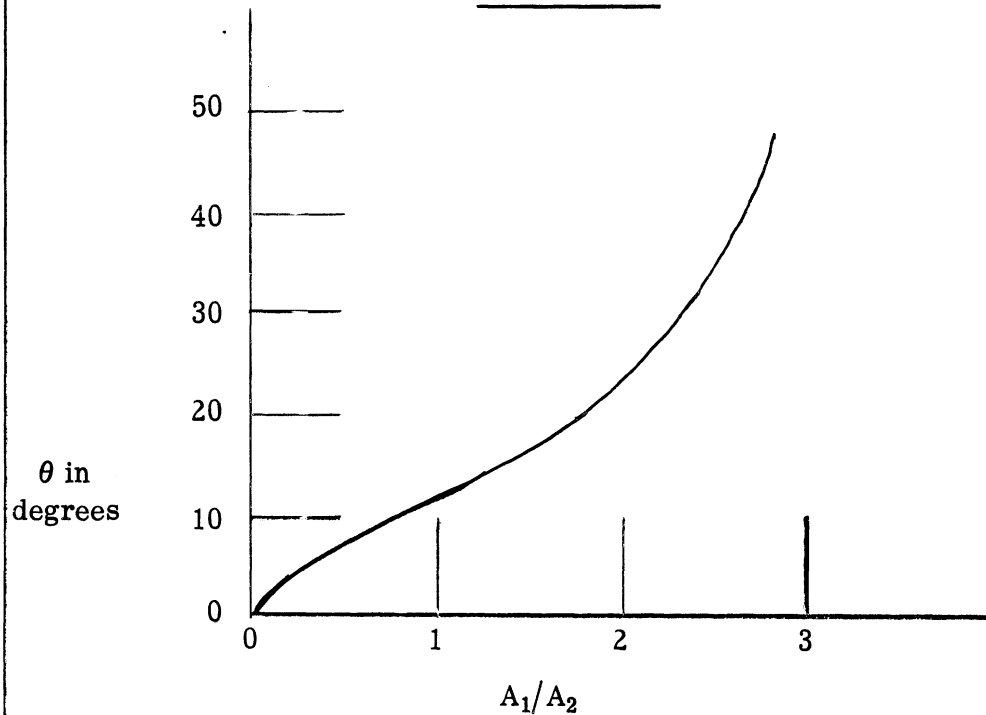
FIG: 3-3



End of Main Lobe

Center of Side Lobe

$\theta$ in degrees

$A_1/A_2$

FIG. 3-4



$\theta$ in degrees

$A_1/A_2$

If we take the main lobe to be constrained to $60^o \le \theta \le 120^o$, then (3.18) and

(3.17) show that the side lobes will be about 17 DB down from the main lobe. The

relationship between the currents is $A_1 = \frac{3}{2} A_2$.

In our method if we were to take the $\theta_i$ to be symmetrically placed about $\theta = 90^o$,

we would obtain symmetric current distributions automatically. We will avoid this by

taking the initial values of $\theta_i$ to be

$$\theta_1 = 0^o$$

$$\theta_2 = 60^o$$

$$\theta_3 = 120^o \tag{3.19}$$

$$\theta_4 = 120^o + \epsilon ,$$

where by $120^o + \epsilon$ we mean to take the limit as $\epsilon \to 0$. Using (3.13) and (3.19) we

find

$$\sum G_n B_n = \sum A_n F_{on} = A_{-2} + A_{-1} + A_1 + A_2 \tag{3.20}$$

$$B_1 = \sum A_n F_{1n} = -i A_{-2} + i A_{-1} - i A_1 + i A_2$$

$$B_2 = \sum A_n F_{2n} = \frac{-1+i}{\sqrt{2}} A_{-2} + \frac{1-i}{\sqrt{2}} A_{-1} + \frac{1-i}{\sqrt{2}} A_1 + \frac{-1-i}{\sqrt{2}} A_2$$

$$B_3 = \sum A_n F_{3n} = \frac{-1-i}{\sqrt{2}} A_{-2} + \frac{1-i}{\sqrt{2}} A_{-1} + \frac{1+i}{\sqrt{2}} A_1 + \frac{-1+i}{\sqrt{2}} A_2$$

$$B_4 = \sum A_n F_{4n} \approx \frac{-1-i}{\sqrt{2}} A_{-2} + \frac{1-i}{\sqrt{2}} A_{-1} + \frac{1+i}{\sqrt{2}} A_1 + \frac{-1+i}{\sqrt{2}} A_2$$

$$+ \epsilon \left[ \frac{3\pi\sqrt{3}}{4\sqrt{2}} (-1+i)A_{-2} + \frac{\pi\sqrt{3}}{4\sqrt{2}} (-1-i)A_{-1} + \frac{\pi\sqrt{3}}{4\sqrt{2}} (-1+i)A_1 + \frac{3\pi\sqrt{3}}{4\sqrt{2}} (-1-i) \right.$$

Rather than solve for the A's in terms of the B's for the special values given by

(3.19) we will find it more profitable to carry through the work for general $\theta_i$.

In the general case

$$\exp\left[\frac{3\pi i}{2}x_1\right]A_{-2} + \exp\left[\frac{\pi i}{2}x_1\right]A_{-1} + \exp\left[-\frac{\pi i}{2}x_1\right]A_1 + \exp\left[-\frac{3\pi i}{2}x_1\right]A_2 = B_1$$

$$\exp\left[\frac{3\pi i}{2}x_2\right]A_{-2} + \exp\left[\frac{\pi i}{2}x_2\right]A_{-1} + \exp\left[-\frac{\pi i}{2}x_2\right]A_1 + \exp\left[-\frac{3\pi i}{2}x_2\right]A_2 = B_2$$

$$\exp\left[\frac{3\pi i}{2}x_3\right]A_{-2} + \exp\left[\frac{\pi i}{2}x_3\right]A_{-1} + \exp\left[-\frac{\pi i}{2}x_3\right]A_1 + \exp\left[-\frac{3\pi i}{2}x_3\right]A_2 = B_3$$

$$\exp\left[\frac{3\pi i}{2}x_4\right]A_{-2} + \exp\left[\frac{\pi i}{2}x_4\right]A_{-1} + \exp\left[-\frac{\pi i}{2}x_4\right]A_1 + \exp\left[-\frac{3\pi i}{2}x_4\right]A_2 = B_4$$

(3.21)

where $x_i = \cos\theta_i$ .

The solution to the set of Equations (3.21) is

$$A_{-2} = \frac{\exp\left[\frac{3\pi i}{2}x_1\right]B_1}{(e^{\pi i x_1}-e^{\pi i x_2})(e^{\pi i x_1}-e^{\pi i x_3})(e^{\pi i x_1}-e^{\pi i x_4})} + \cdots$$

$$A_{-1} = \frac{\exp\left[\frac{3\pi i}{2}x_1\right](e^{\pi i x_2}+e^{\pi i x_3}+e^{\pi i x_4})B_1}{(e^{\pi i x_1}-e^{\pi i x_2})(e^{\pi i x_1}-e^{\pi i x_3})(e^{\pi i x_1}-e^{\pi i x_4})} + \cdots$$

$$A_1 = \frac{\exp\left[\frac{3\pi i}{2}x_1\right](e^{\pi i(x_2+x_3)}+e^{\pi i(x_2+x_4)}+e^{\pi i(x_3+x_4)})B_1}{(e^{\pi i x_1}-e^{\pi i x_2})(e^{\pi i x_1}-e^{\pi i x_3})(e^{\pi i x_1}-e^{\pi i x_4})} + \cdots$$

(3.22)

$$A_2 = \frac{-\exp\left[\frac{3\pi i}{2}x_1\right]e^{\pi i x(x_2+x_3+x_4)}B_1}{(e^{\pi i x_1}-e^{\pi i x_2})(e^{\pi i x_1}-e^{\pi i x_3})(e^{\pi i x_1}-e^{\pi i x_4})} + \cdots$$

where the dots indicate similar terms involving $B_1$, $B_2$, $B_3$, $B_4$ .

From (3.20) and (3.22) we find

$$G_1 = \frac{(1 - e^{\pi i x_2})(1 - e^{\pi i x_3})(1 - e^{\pi i x_4}) \exp\left[\frac{3\pi i}{2} x_1\right]}{(e^{\pi i x_1} - e^{\pi i x_2})(e^{\pi i x_1} - e^{\pi i x_3})(e^{\pi i x_1} - e^{\pi i x_4})} \qquad (3.23)$$

with similar expressions for $G_2, G_3, G_4$. Since we take $B_i = \dfrac{|G_i|}{G_i}$ we have

$$\sum_n G_n B_n = \sum_n |G_n|$$

$$= \left| \frac{\sin\frac{\pi x_2}{2} \sin\frac{\pi x_3}{2} \sin\frac{\pi x_4}{2}}{\sin\frac{\pi(x_1-x_2)}{2} \sin\frac{\pi(x_3-x_1)}{2} \sin\frac{\pi(x_4-x_1)}{2}} \right|$$

$$+ \left| \frac{\sin\frac{\pi x_1}{2} \sin\frac{\pi x_3}{2} \sin\frac{\pi x_4}{2}}{\sin\frac{\pi(x_1-x_2)}{2} \sin\frac{\pi(x_3-x_2)}{2} \sin\frac{\pi(x_4-x_2)}{2}} \right| \qquad (3.24)$$

$$+ \left| \frac{\sin\frac{\pi x_1}{2} \sin\frac{\pi x_2}{2} \sin\frac{\pi x_4}{2}}{\sin\frac{\pi(x_1-x_3)}{2} \sin\frac{\pi(x_2-x_3)}{2} \sin\frac{\pi(x_4-x_3)}{2}} \right|$$

$$+ \left| \frac{\sin\frac{\pi x_1}{2} \sin\frac{\pi x_2}{2} \sin\frac{\pi x_3}{2}}{\sin\frac{\pi(x_1-x_4)}{2} \sin\frac{\pi(x_2-x_4)}{2} \sin\frac{\pi(x_3-x_4)}{2}} \right|$$

In order to restrict the beam in the desired way, we must keep $x_2 = 1/2$, $x_3 = -1/2$.

Thus (3.24) becomes

38

$$\sum |G_n| = \left| \frac{\sin \frac{\pi x_4}{2}}{\cos \pi x_1 \sin \frac{\pi(x_4 - x_1)}{2}} \right| + \left| \frac{\sin \frac{\pi x_1}{2} \sin \frac{\pi x_4}{2}}{\sqrt{2} \sin \left( \frac{\pi x_1}{2} - \frac{\pi}{4} \right) \sin \left( \frac{\pi x_4}{2} - \frac{\pi}{4} \right)} \right|$$

$$+ \left| \frac{\sin \frac{\pi x_1}{2} \sin \frac{\pi x_4}{2}}{\sqrt{2} \sin \left( \frac{\pi x_1}{2} + \frac{\pi}{4} \right) \sin \left( \frac{\pi x_4}{2} + \frac{\pi}{4} \right)} \right| + \left| \frac{\sin \frac{\pi x_1}{2}}{\cos \pi x_4 \sin \frac{\pi(x_1 - x_4)}{2}} \right| . \qquad (3.25)$$

What we now seek is a minimum of (3.25) with respect to $x_1$ and $x_4$ ($|x_1|, |x_4| > 1/2$).

It is clear that it will be simpler to vary $x_4$, then $x_1$, then $x_4$ again, etc. rather than

computing the gradient of (3.25) and varying $x_1$ and $x_4$ along the gradient. Thus,

instead of (3.19) we have initially

$$x_1 = 1$$

$$x_2 = 1/2 \qquad\qquad (3.26)$$

$$x_3 = -1/2$$

where $x_4$ is to be chosen to minimize (3.25), which becomes due to (3.26)

$$\sum |G_n| = \left| \tan \frac{\pi x_4}{2} \right| + \frac{\sqrt{2}}{\left| 1 - \cot \frac{\pi x_4}{2} \right|} + \frac{\sqrt{2}}{\left| 1 + \cot \frac{\pi x_4}{2} \right|} + \frac{1}{\left| \cos \frac{\pi x_4}{2} \cos \pi x_4 \right|} . \qquad (3.27)$$

It is clear that (3.27) is unchanged if we replace $x_4$ by $-x_4$. Thus we will take

$-1 \leq x_4 \leq -1/2$. With this restriction we are able to remove the absolute value

signs in (3.27) obtaining

$$\sum |G_n| = -\tan \frac{\pi x_4}{2} + \frac{\sqrt{2}}{1 - \cot \frac{\pi x_4}{2}} + \frac{\sqrt{2}}{1 + \cot \frac{\pi x_4}{2}} - \frac{1}{\cos \frac{\pi x_4}{2} \cos \pi x_4} \qquad (3.28)$$

$$= \sqrt{\frac{1 - \cos \pi x_4}{1 + \cos \pi x_4}} + \sqrt{2} \frac{\cos \pi x_4 - 1}{\cos \pi x_4} - \frac{\sqrt{2}}{\cos \pi x_4 \sqrt{1 + \cos \pi x_4}} .$$

Figure 3-5 shows the variation of $\sum |G_n|$ with $x_4$ for $x_1 = 1$. The minimum occurs approximately at $x_4 = -0.73$. The value of $\sum |G_n|$ at the minimum is approximately 9.43 (19.5 DB). Since the predicted side lobe level is appreciably below that actually obtainable, the true side lobe level is probably a few DB higher than the ultimate limit. Thus we



FIG. 3-5
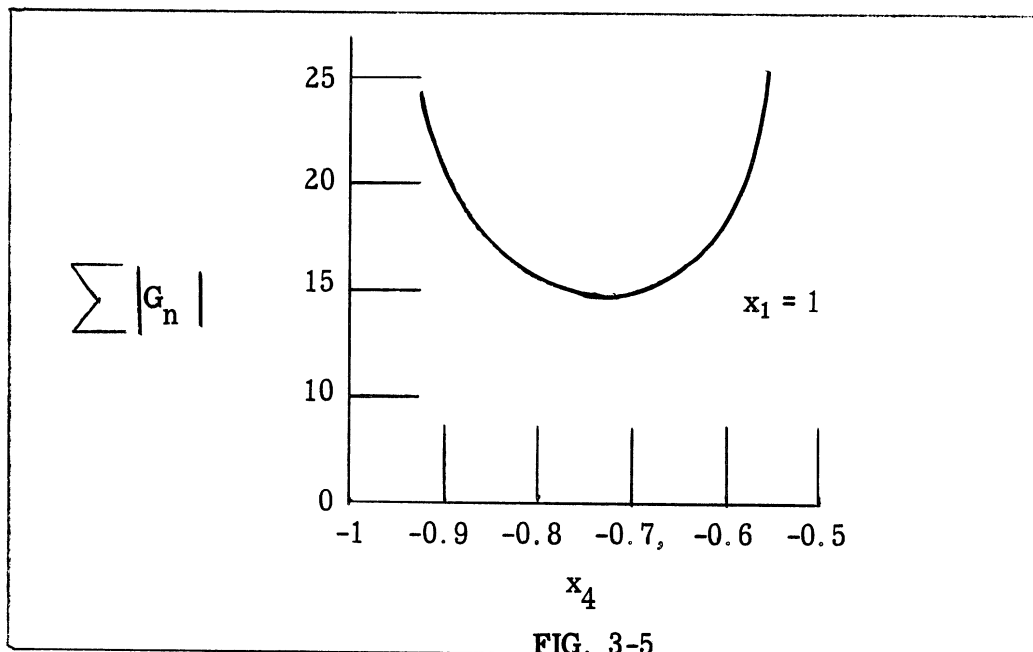
will postpone the calculation of the corresponding current distribution until we have gone through at least one more step. For this step we take
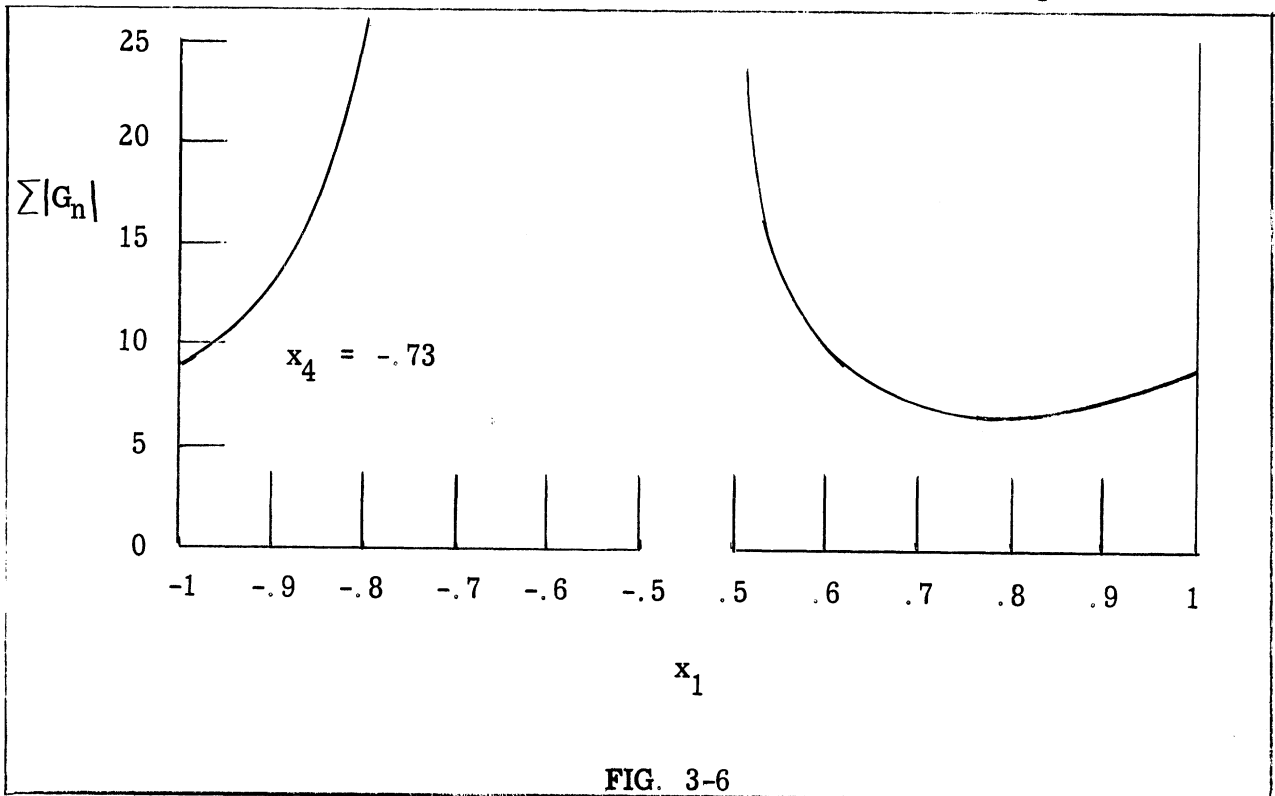
$$x_2 = 1/2$$

$$x_3 = -1/2 \tag{3.29}$$

$$x_4 = -0.73 \ ,$$

and choose $x_1$, so as to minimize (3.25).

Using (3.25) in (3.29) we obtain

$$\sum_{} |G_n| = \left| \frac{\sin 65.7^\circ}{\cos \pi x_1 \sin (65.7^\circ + \frac{\pi x_1}{2})} \right| + \left| \frac{\sin \frac{\pi x_1}{2} \sin 65.7^\circ}{\sqrt{2} \sin (\frac{\pi x_1}{2} - 45^\circ) \sin 69.3^\circ} \right|$$

$$+ \left| \frac{\sin \frac{\pi x_1}{2} \sin 65.7^\circ}{\sqrt{2} \sin (\frac{\pi x_1}{2} + 45^\circ) \sin 20.7^\circ} \right| + \left| \frac{\sin \frac{\pi x_1}{2}}{\cos 48.6^\circ \sin (\frac{\pi x_1}{2} + 65.7^\circ)} \right|$$

<div align="right">(3.30)</div>

$$\sim \frac{.9114}{\left| \cos \pi x_1 \sin (\frac{\pi x_1}{2} + 65.7^\circ) \right|} + .689 \left| \frac{\sin \frac{\pi x_1}{2}}{\sin (\frac{\pi x_1}{2} - 45^\circ)} \right|$$

$$+ 1.824 \left| \frac{\sin \frac{\pi x_1}{2}}{\sin (\frac{\pi x_1}{2} + 45^\circ)} \right| + 1.512 \left| \frac{\sin \frac{\pi x_1}{2}}{\sin (\frac{\pi x_1}{2} + 65.7^\circ)} \right| .$$

Figure 3-6 shows the variation of $\sum |G_n|$ with $x_1$ in the allowable region

$|x_1| > 1/2$ for $x_4 = -0.73$. The minimum occurs approximately at $x_1 = .775$. The



FIG. 3-6

value of $\sum |G_n|$ at the minimum is approximately 7.17 (17.1 DB). Since the predicted

side lobe level is now only slightly below that actually obtainable, we can expect the true

side lobe level to be only slightly above that actually obtainable. Thus we will compute

the actual pattern with

$$x_1 = .775$$

$$x_2 = .5$$

$$x_3 = -.5 \hspace{4cm} (3.31)$$

$$x_4 = -.73$$

We have

$$G_1 = -1.707$$

$$G_2 = 1.553$$

$$G_3 = 1.896 \hspace{4cm} (3.32)$$

$$G_4 = -2.037$$

Since $B_i = \dfrac{|G_i|}{G_i}$ we have $B_1 = B_4 = -1$, $B_2 = B_3 = 1$. For simplicity in

computing the A's it is convenient to rewrite (3.22) in the form

$$A_{-2} = \frac{\exp\left[\frac{\pi i}{2}(1-x_2-x_3-x_4)\right] B_1}{8 \sin \frac{\pi(x_1-x_2)}{2} \sin \frac{\pi(x_1-x_3)}{2} \sin \frac{\pi(x_1-x_4)}{2}} + \ldots = A_2^*$$

$$A_{-1} = \frac{\exp\left[\frac{\pi i}{2}(-1+x_2-x_3-x_4)\right] + \exp\left[\frac{\pi i}{2}(-1-x_2+x_3-x_4)\right] + \exp\left[\frac{\pi i}{2}(-1-x_2-x_3+x_4)\right]}{8 \sin \frac{\pi(x_1-x_2)}{2} \sin \frac{\pi(x_1-x_3)}{2} \sin \frac{\pi(x_1-x_4)}{2}} B_1 + \ldots = A_1^*$$

$$A_1 = \frac{\exp\left[\frac{\pi i}{2}(1-x_2+x_3+x_4)\right] + \exp\left[\frac{\pi i}{2}(1+x_2-x_3+x_4)\right] + \exp\left[\frac{\pi i}{2}(1+x_2+x_3-x_4)\right]}{8 \sin \frac{\pi(x_1-x_2)}{2} \sin \frac{\pi(x_1-x_3)}{2} \sin \frac{\pi(x_1-x_4)}{2}} B_1 + \ldots$$

$$A_2 = \frac{\exp\left[\frac{\pi i}{2}(-1+x_2+x_3+x_4)\right] B_1}{8 \sin \frac{\pi(x_1-x_2)}{2} \sin \frac{\pi(x_1-x_3)}{2} \sin \frac{\pi(x_1-x_4)}{2}} + \ldots , \qquad (3.33)$$

where the fact that $A_{-j} = A_j^*$ follows from the fact that the B's are all real.

The general expression for F is

$$F = A_{-2} \exp\left[\frac{3\pi i}{2} x\right] + A_{-1} \exp\left[\frac{\pi i}{2} x\right] + A_1 \exp\left[-\frac{\pi i}{2} x\right] + A_2 \exp\left[-\frac{3\pi i}{2} x\right]. \quad (3.34)$$

Using the values of the A's given by (3.33) we obtain

$$F = \frac{\sin \frac{\pi(x-x_2)}{2} \sin \frac{\pi(x-x_3)}{2} \sin \frac{\pi(x-x_4)}{2}}{\sin \frac{\pi(x_1-x_2)}{2} \sin \frac{\pi(x_1-x_3)}{2} \sin \frac{\pi(x_1-x_4)}{2}} B_1 + \ldots \qquad (3.35)$$

Figure 3-7 shows the pattern finally obtained after two steps. Figure 3-8 shows the optimum (Dolph-Chebychev) pattern. Figure 3-9 shows the pattern obtained by the above method after only the first step. Upon comparing the patterns of Figures 3-7 and 3-8 we see that the pattern obtained after two steps cannot be differentiated, graphically, from the optimum pattern.

43

In closing, a word is in order about the use of the above method when the fields due to the individual elements are only approximately known. In this case we go ahead with the design procedure as outlined above using the approximate patterns of the elements. We test the result experimentally. In general the side-lobes will not actually be as small as indicated by the design theory. We then use the array and its experimentally determined pattern as one element in an array, with the other elements corresponding to elements in the original array. We then apply the design procedure to these elements. Since we are now only making a small correction to the first design we can expect to get an array whose theoretically predicted pattern agrees well with the experimentally determined one. If necessary, the procedure may be repeated.
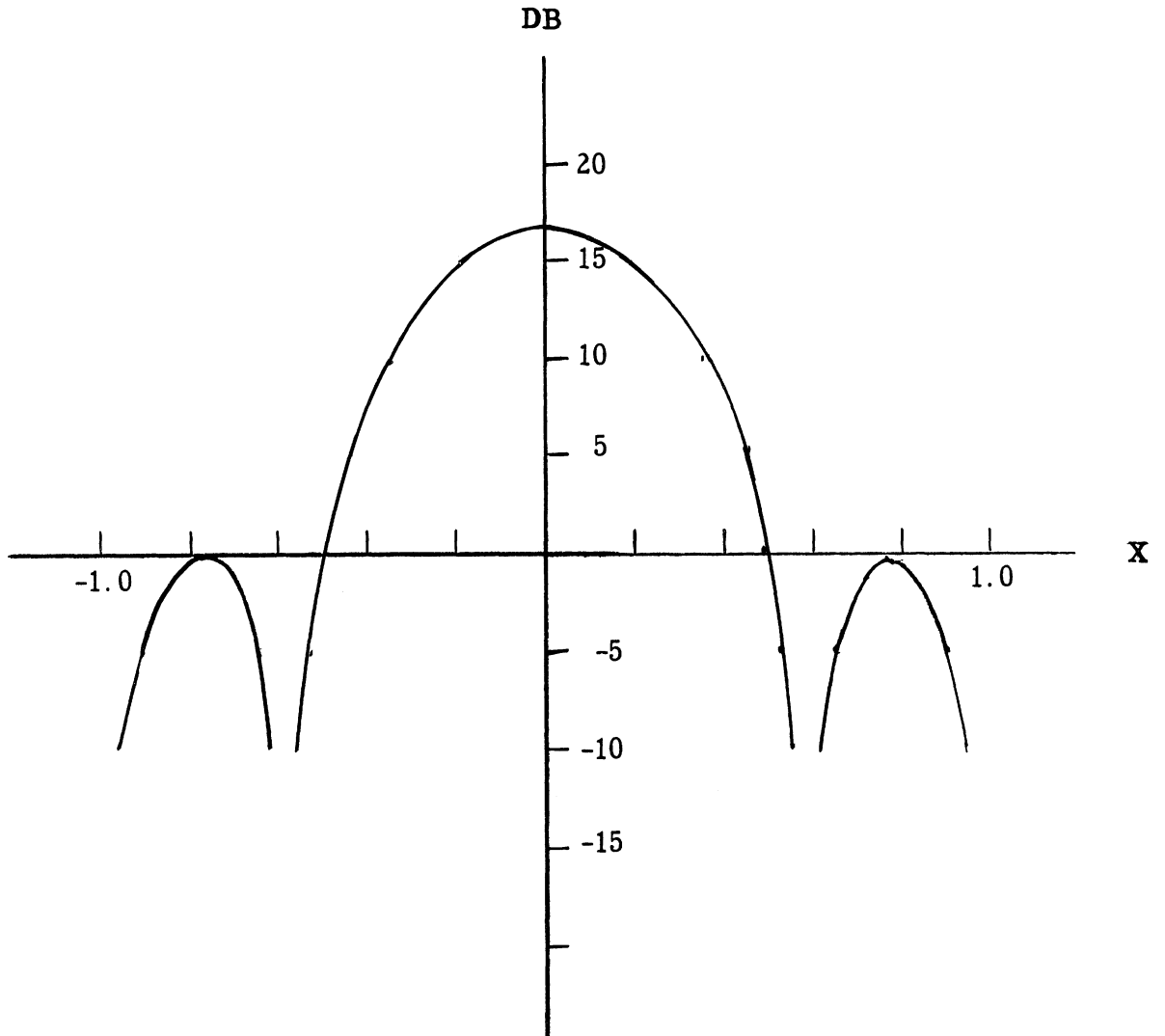
FIG. 3-7: ILLUSTRATIVE EXAMPLE - PATTERN

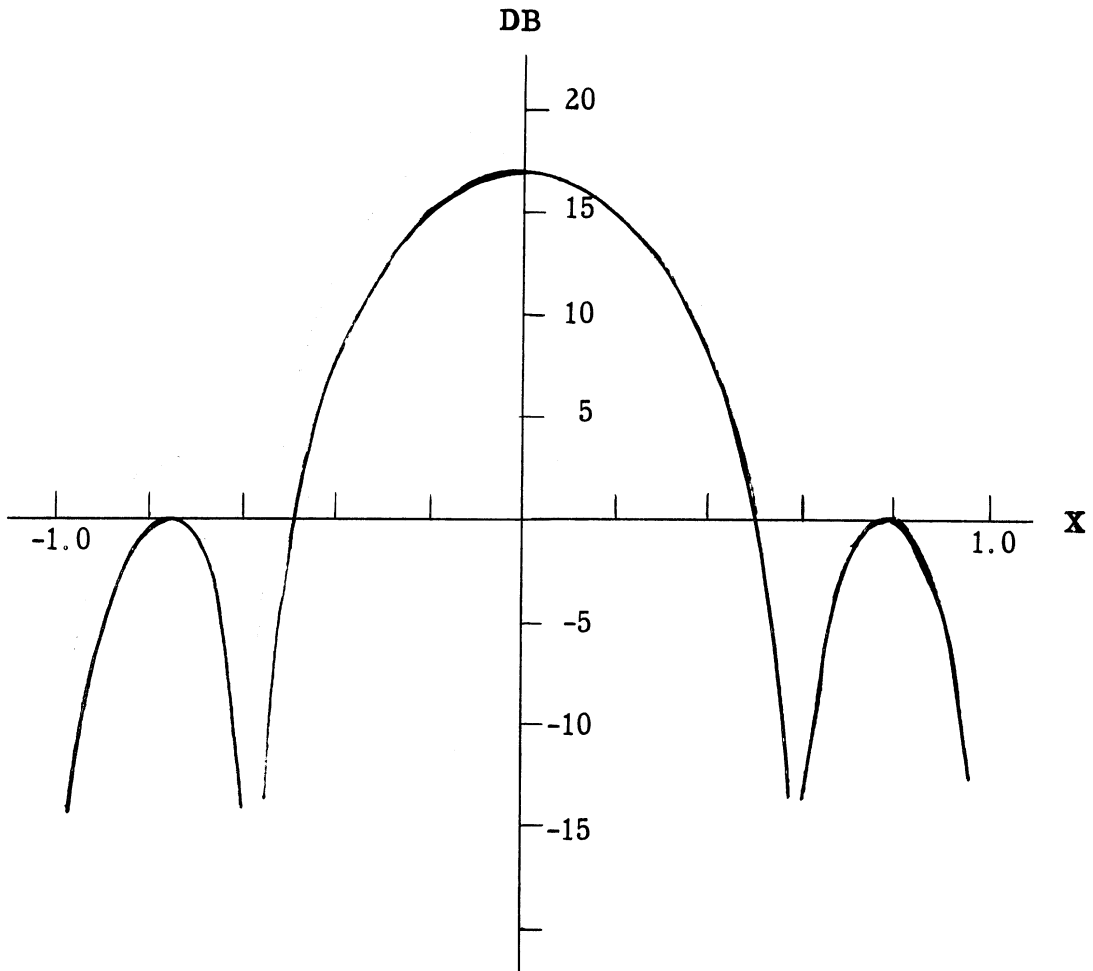OBTAINED UPON THE COMPLETION OF TWO STEPS

FIG. 3-8: ILLUSTRATIVE EXAMPLE -
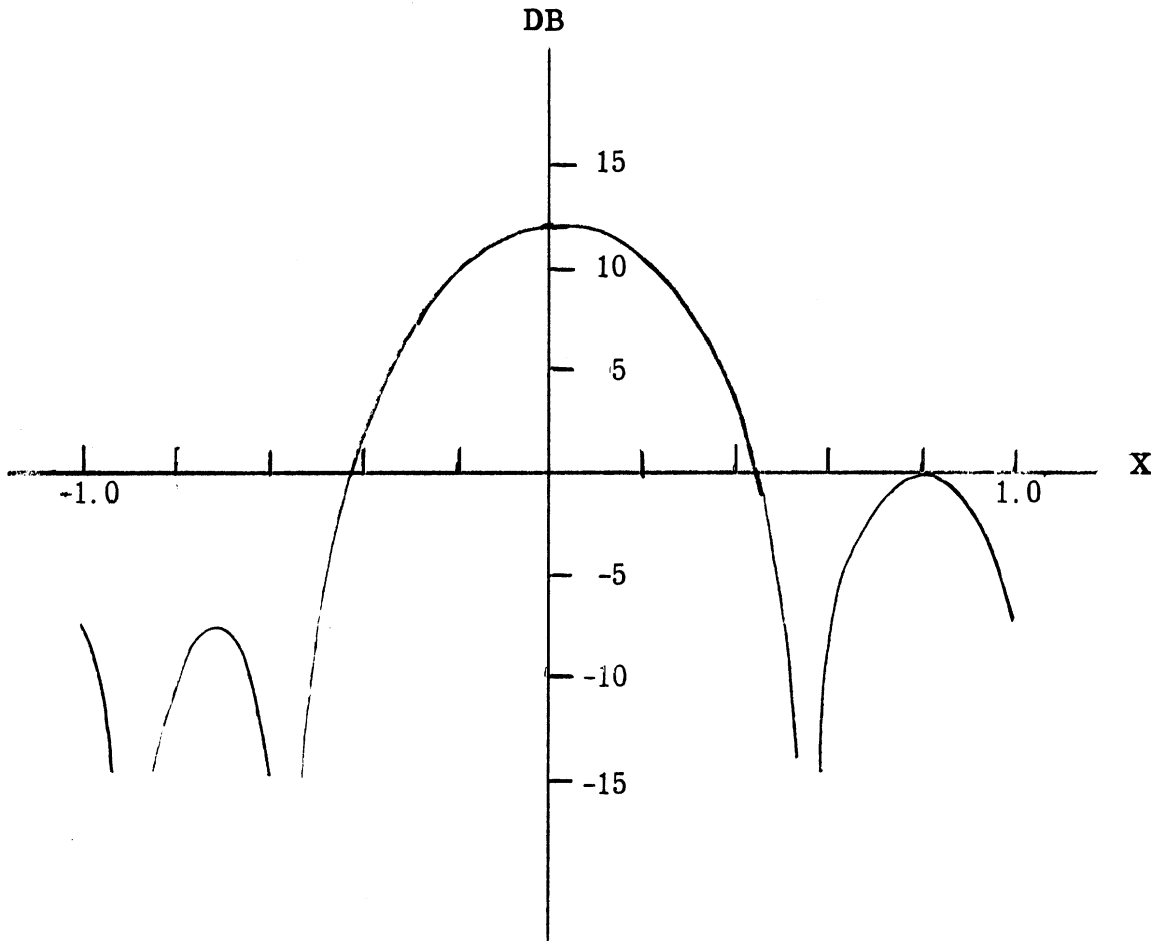
OPTIMUM (DOLPH-CHEBYCHEV) PATTERN

FIG. 3-9: ILLUSTRATIVE EXAMPLE - PATTERN OBTAINED

UPON THE COMPLETION OF THE FIRST STEP

IV

## A THEORY OF MAXIMUM GAIN ANTENNA ARRAYS

To give a broad base to the method of design of surface antennas we now shall

consider a general approach.

We let $\vec{m}(s)$ be a magnetic dipole distribution on a perfectly conducting surface

S. The radiation pattern arising from such a configuration is given by

$$R(\hat{k}) = \int_S \vec{H}(\hat{k}, s) \cdot \vec{m}(s) \, dS, \qquad (4.1)$$

where $\vec{H}$ can be taken as the field induced on S at s by an incident plane wave of

direction $\hat{k}$ and unit amplitude. In briefer notation we put

$$R = H \circ m. \qquad (4.2)$$

The properties of this transformation will be our present concern.

The antenna synthesis problem is that of determining the inverse, i.e. given

a radiation pattern R we need to find

$$m = H^{-1} \circ R. \qquad (4.3)$$

This is very difficult for most surfaces S so we seek to characterize some general

properties of the transformation. What we have accomplished is no more than some

conjectures based on analogy with the better understood case of a line source.

The principle properties we need to know are (1) how to maximize the gain and

(2) how to control the side-lobe levels. We consider these for a line source. In this

relatively simple example the radiation pattern is given by

$$R = \int_{-a}^{a} e^{i\xi z} f(\xi) \, d\xi \qquad (4.4)$$

48

where the length of the source is $2a$, $f$ is the excitation and $z = \frac{2\pi}{\lambda} \cos \theta$. If we

take $a \gg \lambda$ we see that (4.4) approximates a Fourier transform. Hence the gain is

maximized for $f$ = constant and the side lobes are reduced for $f$ approximating a

Gaussian.

By use of our knowledge of Fourier transforms we can characterize the

transformation from the excitation $f$ to the radiation pattern $R$ in such a way as to

enable us to modify the pattern without any detailed treatment of the inverse trans-

formation. Ultimately we wish to find such a technique for our general surface $S$.

Up to now we have considered only the first problem; that of obtaining the

maximum gain configuration. Our progress is yet only a conjecture. By analogy

with the long line source we presume that for large surfaces, i.e. the characteristic

dimensions much larger than a wave length, the maximum gain configuration results

from an excitation which is just the complex conjugate of the field induced on the sur-

face by a plane wave incident from the main beam direction. As an illustration we

give the case of a circumferential slot on a large circular cylinder confining our at-

tention to the principal plane. By reciprocity the radiation pattern at an angle $\phi$ due

to a source at $\phi'$ on the surface is given by the field induced at $\phi'$ by a plane wave

incident in the direction $\phi$. Let this be denoted by $k(\phi, \phi')$; then, for an excitation

$f(\phi)$ we have the radiation pattern

$$R(\phi) = \int k(\phi, \phi') f(\phi') \, d\phi'$$

or

$$R(\phi) = K \circ f(\phi)$$

(4.5)
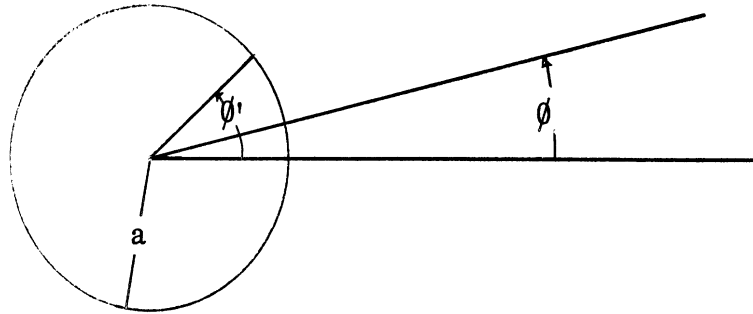
The problem is to determine the excitation f such that the side-lobe levels meet the requirements of a particular application, i. e. if the main beam is in the direction $\phi = 0$ and the side lobes are required to be down A db, we have for the set $\left\{ \phi_n \right\}$, which are solutions of

$$\frac{\partial R(\phi)}{\partial \phi} = 0, \quad \phi_n \neq 0,$$

that

$$\min_{n} 10 \log \left[ \frac{R(0)}{R(\phi_n)} \right]^2 \geqslant A .$$

(4.6)

In our example we can express (4.6) in terms of the Fourier coefficients of the functions $R$, $k$, $f$,

$$R_n = k_n f_n$$

(4.7)

where we use the fact that

$$k(\phi, \phi') = \sum e^{in(\phi - \phi')} k_n .$$

So the inversion of the operator K results in

$$f(\phi) = \sum e^{in\phi} \frac{R_n}{k_n} ,$$

(4.8)

a relatively simple result.

We are interested primarily in the more difficult cases in which S is not such a simple shape. We wish, however, to approach the more difficult problem in terms of the simpler one; so instead of solving (4.8) we will look for a method of choosing f which can be used in the more general cases.

In our example, if we choose the main beam to be in the direction $\phi = 0$ we know that we control the side-lobe levels by tapering the excitation, i.e. $f(\phi)$ should decrease as $|\phi|$ increases in order to decrease the side lobes as compared, say, with those resulting from a uniform excitation, $f = const.$ A readily available tapered excitation is just the complex conjugate of the field induced by a plane wave

$$f(\phi) = \overline{k(\phi, 0)} \tag{4.9}$$

where we take the complex conjugate in order that the phase be such that the radiation pattern be maximized for this case. This gives

$$R(\phi) = K \circ K' \circ \delta(\phi) , \tag{4.10}$$

where $\delta(\phi)$ is the Dirac delta.

This has been computed (Fig. 4-1) in the case $ka = 10$ where $a$ is the radius of the cylinder and $k = 2\pi/\lambda$, $\lambda$ is the wavelength. This gives a side-lobe level of approximately 18 db.

If such an excitation were to be used the origin of it suggests a novel means of producing this excitation. Since the excitation is, in fact, the complex conjugate of the field induced on the surface by a plane wave, we can then devise an analog device in which we model the antenna surface, illuminate it by a plane wave, and use the measured surface

FIG. 4-1 RADIATION PATTERN FOR A CIRCULAR CYLINDER
WITH A CIRCUMFERENTIAL SLOT EXCITATION
(ka = 10)

∅ in degrees
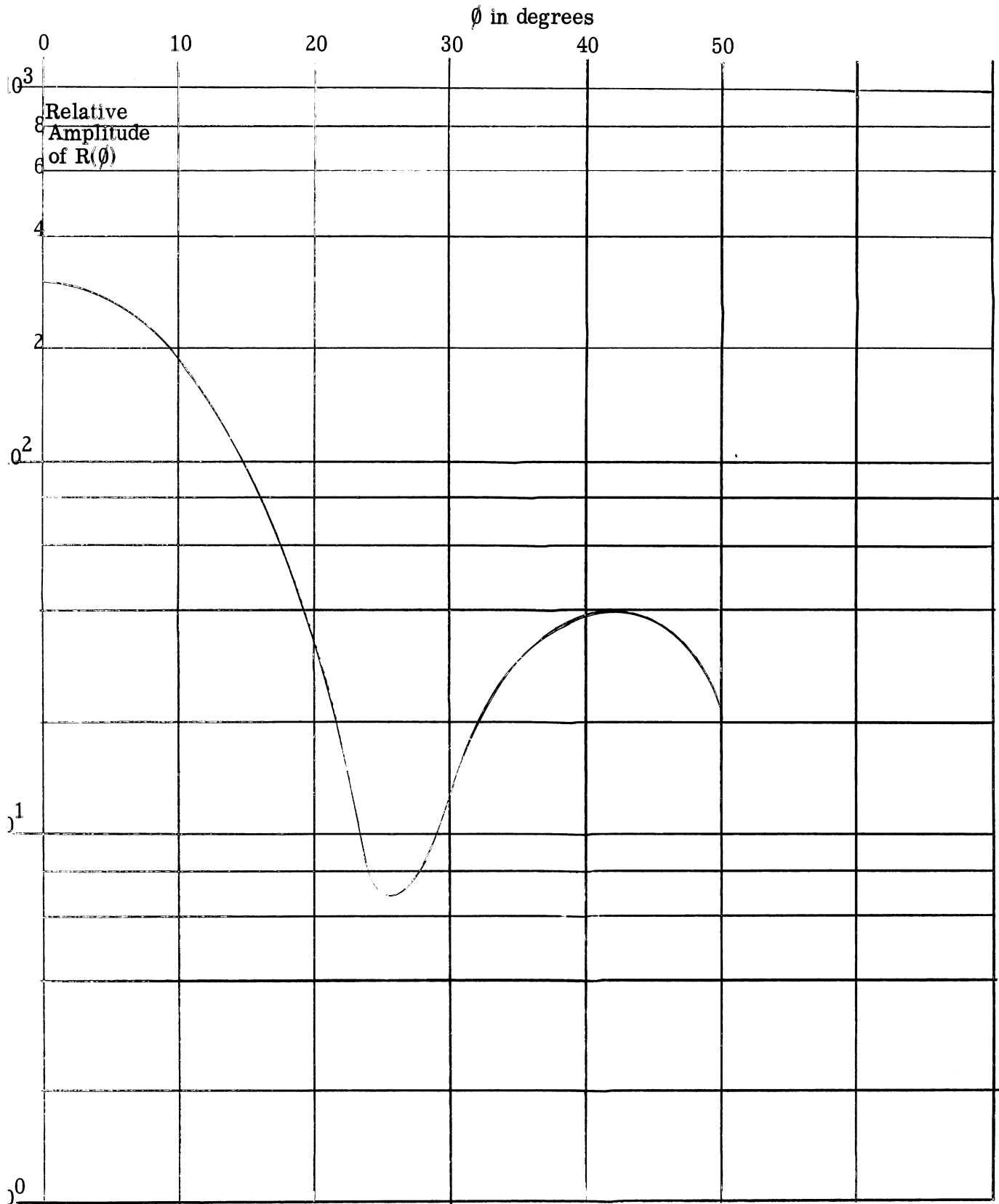
field after an appropriate phase change of $180^{\circ}$ as the input of the excitation on the actual antenna surface. Alternatively, the measurements could be made in the laboratory and recorded on tape to be used in some sort of digital computer to control the excitation.

Since the above scheme uses an approximation to a continuous distribution, we must solve two additional problems. The first is to discover the density of slot radiators necessary for a sufficiently close approximation; the second is the method of exciting these elementary radiators. It may be that the second problem is too difficult; i.e. if we need control over each of the elements the scheme may not be useful for the type of antenna we finally wish to construct. To this point little effort has been spent on this problem.

APPENDIX A

## THE 65-SLOT PROBLEM - THE METHOD OF COMPUTATION

## AND THE RESULTS OBTAINED

### A.1   The Method of Computation

In this Appendix we present the formulas employed in the 65-slot problem together with a discussion of the method of computation and the results obtained.   The single slot expressions needed for such calculations have been discussed in Section II (these single slot expressions also appear as Equations (4.2.4), (4.2.5), and (4.2.11) for Geometric Optics, Fock Theory, and Physical Optics respectively in Reference 16.

In the expressions for the 65-slot calculations given in this Appendix the polarization, $\hat{p}$, will denote directions of the magnetic field with $\hat{p}_1 = \theta$ and $\hat{p}_2 = \phi$.

The following parameter values are fixed throughout:

$\theta_B$   = (main beam direction) = $70^o$, $50^o$, $30^o$, $10^o$ .

$\theta_0$   = $165^o$, denotes cone surface

$d_0$   = (distance from tip of cone to first slot = $16\lambda$.

$d_j$   = (distance from tip of cone to $j\underline{\text{th}}$ slot), $j = 0, 1, 2, \ldots, 64$.

$d$   = $d_{j+1} - d_j$ = (distance between slots) = $0.4\lambda$.

In performing the calculations for the 65-slot problem, each of the 65 values of $\vec{H}$ determined according to the methods of Geometric Optics, Physical Optics, or Fock Theory (corresponding to $j = 0, 1, 2, \ldots, 64$) are multiplied by the corresponding phase factor, $\exp(ikd_j(\theta_B - \theta_0))$, and the resulting 65 expressions summed.

We now turn our attention to the formulas employed in the 65-slot computations;

the derivations of these expressions have been discussed in Section II.

A.1.1.  The Geometric Optics Formulas

In determining the magnitudes of the Geometric Optics contributions in the 65-slot

problem we employed the following formulas.

For a single slot

$$\frac{\vec{H}_{GO}}{C \frac{e^{ikr}}{r}} = 2\, e^{-ikd_0 D} (\cos \theta \sin \phi \; \hat{p}_1 + \cos \phi \; \hat{p}_2),$$

where $d_0$ = distance from tip to slot,

$$D = \cos \theta \cos \theta_0 + \sin \theta \sin \theta_0 \cos \phi, \text{ and}$$

$$2C = ikV_0 L/2\pi ,$$

with $V_0$ = the voltage across the slot and  L = the length of the slot.

In the general case of  N  slots with  $d_j$ = distance from tip to the $j^{\underline{th}}$ slot

$$\frac{\vec{H}_{GO}}{C \frac{e^{ikr}}{r}} = 2 (\cos \theta \sin \phi \; \hat{p}_1 + \cos \phi \; \hat{p}_2) \sum_{j=1}^{N} \exp\left[ ikd_j (-D + \cos(\theta_B - \theta_0)) \right] .$$

This becomes, for 65 slots,

$$\frac{\vec{H}_{GO}}{C \frac{e^{ikr}}{r}} = 2 (\cos \theta \sin \phi \; \hat{p}_1 + \cos \phi \; \hat{p}_2) \frac{\sin (65(0.4\pi x) )}{\sin (0.4\pi x)} e^{-57.6\pi ix} ,$$

where  $x = D - \cos (\theta_B - \theta_0)$.

## A.1.2. The Physical Optics Formulas

In determining the magnitudes of the Physical Optics contributions in the 65-slot

problem we employed for the entire set of 65 slots

$$\frac{\vec{H}}{C \frac{e^{ikr}}{r}} = \frac{iT}{4\pi^2} \left\{ \left[ -f_x \sin\theta \cos\theta_0 \sin\phi + f_y(-\cos\theta \sin\theta_0 + \sin\theta \cos\theta_0 \cos\phi) \right. \right.$$

$$\left. \left. -f_z \cos\theta \cos\theta_0 \sin\phi \right] \hat{p}_1 - \left[ f_x \sin\theta_0 + f_z \cos\theta_0 \cos\phi \right] \hat{p}_2 \right\}^*$$

where $T = \lambda \sum\limits_{j=0}^{64} (1/d_j) \exp\left[ ikd_j + ikd_j \cos(\theta_B - \theta_0) \right]$,

$$d_j = d_0 + jd,$$

$$f_x = \sin\theta_0 \cos\theta_0 \left[ \frac{2c^2 \sin x - 2q \sin x (q + b \cos x)}{(\,(q + b \cos x)^2 - c^2 \sin^2 x\,)\,Q} + 2bA \right],$$

$$f_y = \sin\theta_0 \cos\theta_0 \left[ \frac{-2bc \sin x - 2qc \sin x \cos x}{(\,(q + b \cos x)^2 - c^2 \sin^2 x\,)\,Q} + 2cA \right],$$

$$f_z = \sin^2\theta_0 \left[ \frac{-2c^2 \sin x \cos x - 2b \sin x (q + b \cos x)}{(\,(q + b \cos x)^2 - c^2 \sin^2 x\,)\,Q} + 2qA \right],$$

and

$$A = Q^{-3/2} \arctan\left[ Q^{1/2} \sin x / (q \cos x + b) \right],$$

$$Q = q^2 - b^2 - c^2,$$

$$q = \cos\theta_0 (\cos\theta_0 + \cos\theta),$$

---

* In the one slot case the expression is the same except that the factor $iT/4\pi^2$ is replaced by the factor $\dfrac{i\lambda e^{ikd_0}}{4\pi^2 d_0}$ with $d_0$ being the distance from the tip to the slot.

$$b = \sin \theta_0 \, (\cos \phi \, \sin \theta_0 + \sin \theta) \; ,$$

$$c = \sin \phi \, \sin^2 \theta_0 \; , \text{ and}$$

$$x = \arccos \left( \frac{\tan \theta_0}{\tan \theta} \right) \; .$$

The values of $T$ corresponding to the four values of $\theta_B$ studied are

$$T = 0.11193 + 0.34491 \; i \quad \text{for} \; \theta_B = 10^\circ,$$

$$= 0.0273 \; + 0.112 \quad i \quad \text{for} \; \theta_B = 30^\circ,$$

$$= 0.0211 \; + 0.0209 \; i \quad \text{for} \; \theta_B = 50^\circ, \text{ and}$$

$$= 0.0276 \; + 0.0265 \; i \quad \text{for} \; \theta_B = 70^\circ \; .$$

The $C$ appearing in the above expression is defined in the same manner as in the Geometric Optics expressions.

## A.1.3 Fock Theory Expressions

To determine the contribution for each of the 65 slots as determined by Fock Theory we use the following expressions:

$$\frac{\vec{H} \cdot \hat{p}}{C \dfrac{e^{ikr}}{r}} =$$

$$\left[ \sum_{n=0}^{*} e^{iA_n} \left\{ c_1 \, g(\xi_n) \sin \left[ (2n\pi + \phi - \phi_s) \sin \theta_0 + \pi/2 - \psi \right] \right. \right.$$

$$+ (ic_2/m_n) \, f(\xi_n) \cos \left[ (2n\pi + \phi - \phi_s) \sin \theta_0 + \pi/2 - \psi \right]$$

$$+ \sum_{n=1}^{*} e^{iA_n'} \left\{ c_1 \, g(\xi_n') \sin \left[ (2n\pi - \phi - \phi_s) \sin \theta_0 + \pi/2 - \psi \right] \right.$$

$$\left. + (ic_2/m_n') \, f(\xi_n') \cos \left[ (2n\pi - \phi - \phi_s) \sin \theta_0 + \pi/2 - \psi \right] \right]$$

where $\cos \phi_s = (\tan \theta_0)/(\tan \theta)$ ; $\cos \psi = - \cos \theta / \cos \theta_0$ ; $\phi > \phi_s$ ; $k = 2\pi/\lambda$,

$$A_n(a_n, \phi) = - ka_n \left( \sin \theta_0 \sin \theta \cos \phi_s + \cos \theta_0 \cos \theta \right) + \frac{kd_j \sin \left[ (2n\pi + \phi - \phi_s) \sin \theta_0 \right]}{\sin \psi},$$

$$A_n' = A_n \left( a_n', - \phi \right),$$

$$a_n (\phi) = \frac{d_j \cos \left[ (2n\pi + \phi - \phi_s) \sin \theta_0 + \pi/2 - \psi \right]}{\sin \psi}$$

$$a_n' = a_n (-\phi),$$

$d_j$ = distance from tip to $j\underline{\text{th}}$ slot,

$*$ = sums cut off when argument of the cosine reaches $\pi/2$ ,

$$m_n (a_n) = \left\{ \frac{kd_j^{\,3}}{2a_n^{\,2}} \frac{|\tan \theta_0|}{\sin^2 \psi} \right\}^{1/3},$$

$$m_n' = m_n (a_n'),$$

$$\xi_n (a_n, \phi) = \left\{ \frac{ka_n \sin \psi}{2 \tan^2 \theta_0} \right\}^{1/3} (2n\pi + \phi - \phi_s) \sin \theta_0 ,$$

$$\xi_n' = \xi_n (a_n', -\phi) , \text{ and}$$

$2 C = ikV_0 L/2\pi$ where $V_0 =$ the voltage across the slot and $L$ is the length of the slot.

For $\hat{p} = \hat{p}_2$ ,       $c_1 = - \sin \theta_0 / \sin \theta$ ,

$c_2 = \cos \theta_0 \sin \phi_s$ , and

for $\hat{p} = \hat{p}_1$ ,       $c_1 = - \cos \theta_0 \sin \phi_s$ ,

$c_2 = - \sin \theta_0 / \sin \theta$ .

The expressions f( ) and g( ) are the Fock functions which are tabulated (Ref. 17).

In the conical cut computations, described more fully in A.3, $\hat{p}$ was taken

in $5^o$ intervals from $\phi = \phi_s$ to $\phi = 175^o$ and the corresponding $\theta$ value was

determined from the following

$$\cos \theta = \frac{\cos(\theta_0 - \theta_B) \cdot \cos \theta_0 + \sin \theta_0 \cos \phi \sqrt{\cos^2 \theta_0 + \sin^2 \theta_0 \cos^2 \phi - \cos^2(\theta_0 - \theta_B)}}{\cos^2 \theta_0 + \sin^2 \theta_0 \cos^2 \phi}$$

In the limiting case of $\phi = \phi_S$ we have (on the conical cut)

$$\cos \phi_S = \frac{\sin \theta_0 \cos(\theta_0 - \theta_B)}{\sqrt{1 - \cos^2 \theta_0 \cos^2(\theta_0 - \theta_B)}} \quad .$$

Upon multiplying each of the single slot expressions by the corresponding phase

factor $\exp(ikdj(\theta_B - \theta_0))$ and summing, we obtain an expression of the form

$$\sum_{j=0}^{N} F(j) e^{i\alpha j} \quad .$$

Approximating the function $F(j)$ by $F(0) \left(\frac{F(N)}{F(0)}\right)^{j/N}$ we obtain

$$\sum_{j=0}^{N} F(j) e^{i\alpha j} \approx F(0) \left\{ \frac{1 - e^{i\alpha(N+1)} \left[F(N)/F(0)\right]^{\frac{N+1}{N}}}{1 - e^{i\alpha} \left[F(N)/F(0)\right]^{\frac{1}{N}}} \right\} \quad .$$

This approximate summation method was employed for all four cases (i.e. for

$\theta_B = 10^o, 30^o, 50^o$, and $70^o$); the actual sum was obtained only for the $\theta_B = 70^o$ case.

A comparison of the sums obtained in the $\theta_B = 70^o$ case indicated a maximum difference

of about 20 per cent between the actual sum and the result obtained using the approximate

summation method described above. The nature of this approximate summation process

is such as to lead one to expect the greatest accuracy in the middle of the interval

between the shadow boundary and $\phi = 180^o$.

## A.2  Beam Direction

The relative maximum in $\theta$ for a given $\phi$ and main beam direction $\theta_B$ is given, in the illuminated region, by the cone

$$\sin \theta_B \sin \theta \cos \phi + \cos \theta_B \cos \theta = \cos (\theta_0 - \theta_B)$$

about the slot array as axis, while in the shadow region, the locus of the relative maximum departs from the conical surface and is given parametrically by

$$\theta_B + \alpha = \psi - (\phi - \phi_S) \sin \alpha \quad,$$

$$\cos \psi = \frac{\cos \theta}{\cos \alpha} \quad,$$

$$\cos \phi_S = -\frac{\tan \alpha}{\tan \theta} \quad, \text{ and}$$

$$\alpha = \pi - \theta_0 \quad.$$

Plots of the beam direction for $\theta_B = 10^\circ, 30^\circ, 50^\circ, 70^\circ$ are included here in Figure A.2-1, showing $\theta$ as a function of $|\phi|$ . Although the locus of the relative maximum in $\theta$ is continued until it reaches the cone surface, $\theta = 165^\circ$, the field is dominated by that arising at the other shadow boundary when $\phi > 180^\circ$. The relative maximum in $\theta$ coincides with the conical cut out to about $\phi \approx 135^\circ$; this is also shown in Figure A.2-1.

FIG. A. 2-1   THE RELATIVE MAXIMUM IN $\theta$ FOR A GIVEN
$\phi$ AND MAIN BEAM DIRECTION $\theta_B$
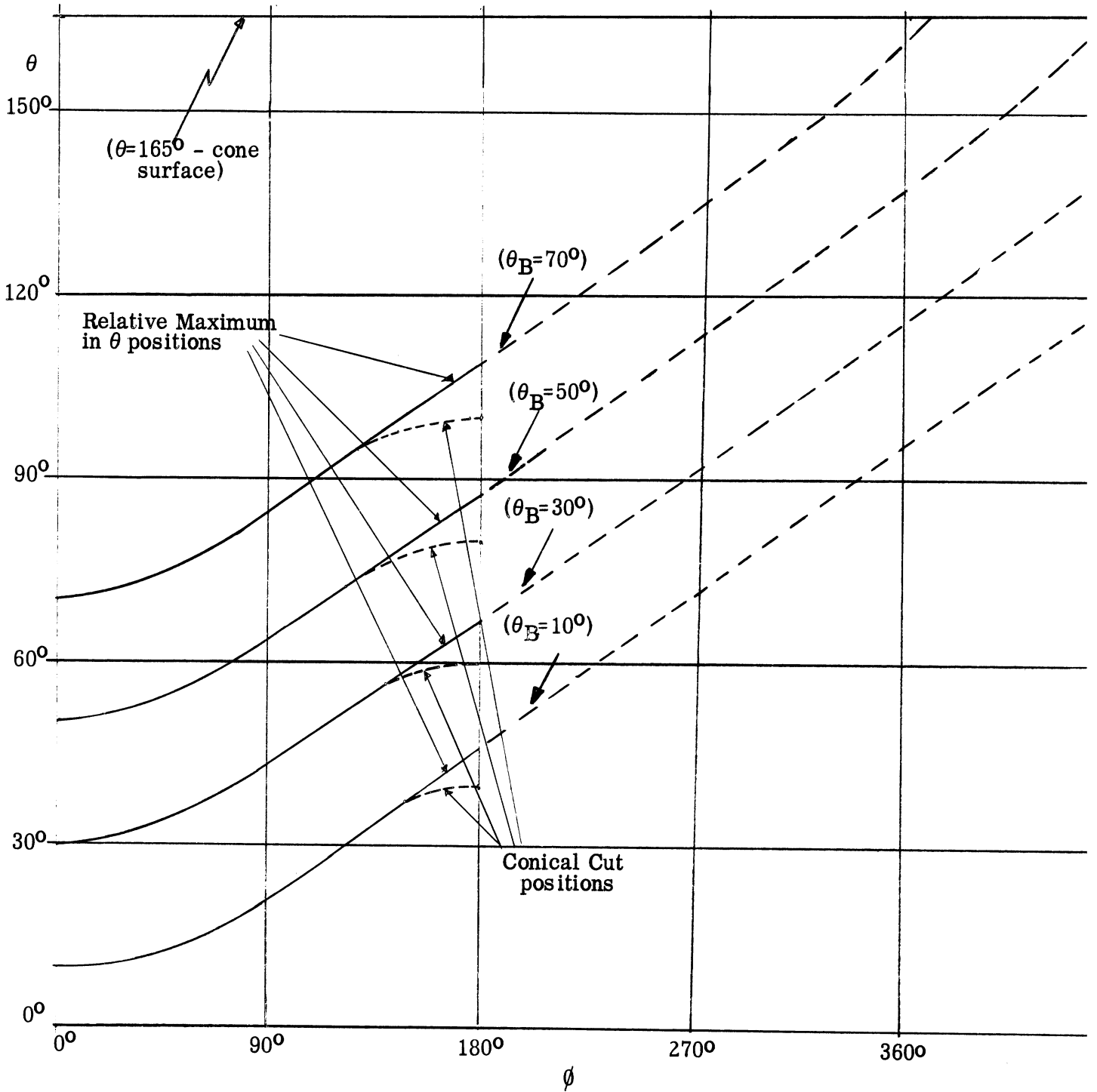
## A.3 Results of the 65-Slot Computations

As pointed out at the beginning of this Appendix and in Section I computations

were performed for four different beam directions,

$$\theta_B = 10^\circ, 30^\circ, 50^\circ, \text{ and } 70^\circ,$$

for the 65 slots located on a generator of a cone of half-angle $15^\circ$. For each beam angle

computations were performed on two "cuts":

(1) a conical cut for which the receiver is restricted to lie on a conical surface

whose axis is the extension of the generator containing the slots and which has

a half-angle equal to $15^\circ + \theta_B$, and

(2) a plane cut for which the receiver is restricted to lie in the plane of the

generator containing the slots and the axis of the $15^\circ$ cone.

These two geometries are displayed in Figure 1-1 of Section I.

Values of $|H_\theta|^2$ and $|H_\phi|^2$ were computed at appropriate intervals in $\phi$ (or $\theta$)

using Geometric Optics, Physical Optics, and Fock Theory in their regions of applica-

bility. The space regions of the applicability of these three methods is shown graphically

in Figure 1-6 in Section I.

The results were obtained in <u>db below the Geometric Optics maximum</u> and are

tabulated in Tables A.3.1 through A.3.4. Only the Geometric Optics and Fock Theory

results are given in these tables; it was found that the Physical Optics results were

negligible.* Graphical presentations of these Physical Optics results are given in

---

\* As will be noted by an examination of Tables A.3.1 through A.3.4, only values less
than 60 were recorded; that is, a value which was more than 60 db down from the
Geometric Optics maximum was not included in the final summary.

Figure A. 3-1 for the conical cut cases and a brief examination of the data contained in

Figure A. 3-1 indicates that the Physical Optics contribution is negligible in comparison

with the "Fock Theory" contributions in the shadow region.

In the lit region where the Geometric Optics results were used, only the relative

maxima were computed except in the vicinity of the main beam.

At the time of the writing of this report experimental results were available for

the two beam directions $\theta_B = 10^0$ and $\theta_B = 30^0$. The theoretical results of Tables A. 3. 1

and A. 3. 2 are compared with the experimental data in Figures 1-2 through 1-5 in Section I.

The theoretical data is superimposed upon copies of the actual patterns obtained from the

Hughes Aircraft Company. For the plane cuts the experimental data was not normalized

and thus the peak value (which would be 0 db) appears on the experimental curves as

approximately -4. 5 db. Thus, in making the comparisons between theory and experiment,

the theoretical data has been normalized to the experimental peak value; i. e. each theo-

retical value, x, is plotted in Figures 1-2 and 1-3 as the quantity, -(x + 4. 5). The

slight angular variation between the theoretical and experimental patterns which can be

observed in Figures 1-2 and 1-3 is due to a slight missalignment in the experimental

tests (in fact, the main beam direction in the $30^0$-experimental-test was actually $29^0$);

no attempt has been made to normalize angularly the results in the plane cut.

On the "conical cut", this normalization is partially accomplished since the

comparison between theory and experiment shown in Figures 1-4 and 1-5 is actually a

comparison between theoretical values for receiver positions on the conical cut while the

experimental values are for "relative maxima in $\theta$" positions. Examination of Figure A. 2-1

indicates that such a comparison loses validity only near $\emptyset = 180^{\circ}$. Also, since the

summation technique employed to obtain the Fock results was expected to be least

accurate near $\emptyset = 180^{\circ}$, we expect the greatest deviation between theory and

experiment in Figures 1-4 and 1-5 to occur near $\emptyset = 180^{\circ}$. *

This program of experimentation and theoretical calculation was set up

primarily as a feasibility study and thus one would not expect "extreme" precision

in the results. We feel that the excellent agreement between theory and experiment

displayed in the comparisons of Section I definitely establishes that radiation patterns

for slot arrays on conical surfaces can be theoretically determined.

---

* During the final editing stage, the experimental data for $\theta_B = 50^{\circ}$ became available. These results are compared with the theoretical estimates in Figures A.3-2 and A.3-3. For this case in addition to the slight angular misalignment, it was found necessary to locate the slots in a manner slightly different from that used in the $\theta_B = 60^{\circ}$ and $\theta_B = 30^{\circ}$ cases; that is, the slots were tilted a few degrees from the transverse position. This slight tilt in the positioning of the slots could be expected to lead to larger differences between theory and experiment due to the polarization effects and thus the relatively poor agreement between theory and experiment for the $H_{\emptyset}$ case shown in Figure A.3-3 is not unexpected.

## TABLE A.3.1
### Results Obtained for $\theta_B = 10°$

| Conical Cut | | | | Plane Cut | | | |
|---|---|---|---|---|---|---|---|
| $\phi°$ | $\theta°$ | $|H_\theta|^2$ * | $|H_\phi|^2$ * | $\phi°$ | $\theta°$ | $|H_\theta|^2$ * | $|H_\phi|^2$ * |
| 0 | 10. | >60 | 0 | 0 | 150 | >60 ** | 33.3 |
| 30 | 10.5 | 6.2 | 1.2 | 0 | 135 | >60 | 34.3 |
| 60 | 14 | 1.5 | 6.0 | 0 | 120 | >60 | 35.4 |
| 90 | 20.3 | .6 | >60 | 0 | 105 | >60 | 36.1 |
| 100 | 23.1 | .9 | 15.2 | 0 | 90 | >60 | 36.2 |
| 105 | 24.6 | 1.1 | 11.7 | 0 | 75 | >60 | 35.4 |
| 110 | 26.1 | 1.5 | 9.3 | 0 | 60 | >60 | 33.5 |
| 15 | 27.7 | 1.9 | 7.6 | 0 | 45 | >60 | 30.0 |
| 20 | 29.2 | 5.8 | 9.6 | 0 | 28 | >60 | 22.5 |
| 125 | 30.7 | 6.6 | 11.1 | 0 | 24 | >60 | 20.8 |
| 130 | 32.2 | 7.8 | 12.6 | 0 | 22.5 | >60 | >60 |
| 135 | 33.5 | 9.1 | 14.3 | 0 | 21 | >60 | 17.9 |
| 140 | 34.8 | 10.7 | 16.2 | 0 | 19 | >60 | >60 |
| 145 | 36 | 12.5 | 18.3 | 0 | 17 | >60 | 13.5 |
| 150 | 37 | 13.9 | 20.2 | 0 | 15 | >60 | >60 |
| 155 | 37.9 | 15.6 | 22.0 | 0 | 12.5 | >60 | 4.0 |
| 160 | 38.6 | 17.8 | 24.4 | 0 | 10 | >60 | 0 |
| 165 | 39.2 | 21.4 | 28.2 | 0 | 7 | >60 | 4.0 |
| 170 | 39.7 | 30.3 | 37.1 | 0 | 4 | >60 | >60 |
| 175 | 39.9 | 28.7 | 35.8 | 0 | 0 | >60 | 13.5 |
| 180 | 40 | 32.3 | 39.1 | 180 | 8 | >60 | >60 |
| | | | | 180 | 16 | >60 | 17.9 |
| | | | | 180 | 20 | 22.2 | 20.9 |
| | | | | 180 | 30 | 34.9 | 39.0 |
| | | | | 180 | 40 | 32.3 | 39.1 |
| | | | | 180 | 50 | 23.9 | 32.6 |
| | | | | 180 | 60 | 47.5 | 57.1 |
| | | | | 180 | 70 | 55.1 | >60 |
| | | | | 180 | 80 | 59.2 | >60 |

\* Measured in db down from the Geometrics Optics Maximum
\*\* Geometric Optics result only

## TABLE A.3.2
### Results Obtained for $\theta_B = 30^\circ$

| | Conical Cut | | | | Plane Cut | | |
|---|---|---|---|---|---|---|---|
| $\phi^\circ$ | $\theta^\circ$ | $\|H_\theta\|^2$ * | $\|H_\phi\|^2$ * | $\phi^\circ$ | $\theta^\circ$ | $\|H_\theta\|^2$ * | $\|H_\phi\|^2$ * |
| 0 | 30 | >60 | 0 | 0 | 150 | >60 ** | 35 |
| 30 | 31.4 | 7.4 | 1.2 | 0 | 135 | >60 | 35.6 |
| 60 | 35.8 | 3.1 | 6.0 | 0 | 120 | >60 | 36.1 |
| 90 | 42.9 | 2.7 | >60 | 0 | 105 | >60 | 36.3 |
| 100 | 45.7 | 3.2 | 15.2 | 0 | 90 | >60 | 35.6 |
| 105 | 47 | 6.2 | 14.4 | 0 | 75 | >60 | 34.1 |
| 110 | 48.4 | 7.9 | 15.6 | 0 | 60 | >60 | 30.7 |
| 115 | 49.8 | 9.2 | 17 | 0 | 43 | >60 | 22.5 |
| 120 | 51.1 | 10.6 | 18.6 | 0 | 40 | >60 | 20.8 |
| 125 | 52.4 | 12.2 | 20.4 | 0 | 38.5 | >60 | >60 |
| 130 | 53.6 | 13.9 | 22 | 0 | 37 | >60 | 17.9 |
| 135 | 54.7 | 15.9 | 24.5 | 0 | 36 | >60 | >60 |
| 140 | 55.8 | 18.3 | 27.6 | 0 | 35 | >60 | 13.5 |
| 145 | 56.7 | 21.4 | 30.4 | 0 | 33 | >60 | >60 |
| 150 | 57.6 | 25.8 | 35.1 | 0 | 31.5 | >60 | 4 |
| 155 | 58.3 | 32.2 | 41.7 | 0 | 30 | >60 | 0 |
| 160 | 58.9 | 41.1 | 50.1 | 0 | 28.5 | >60 | 4 |
| 165 | 59.4 | 37.4 | 46.9 | 0 | 27 | >60 | >60 |
| 170 | 59.7 | 38.1 | 47.8 | 0 | 25 | >60 | 13.5 |
| 175 | 59.9 | >60 | >60 | 0 | 23 | >60 | >60 |
| 180 | 60 | 40.9 | 50.7 | 0 | 21 | >60 | 17.9 |
| | | | | 0 | 19.5 | >60 | >60 |
| | | | | 0 | 18 | >60 | 20.9 |
| | | | | 0 | 0 | >60 | 26 |
| | | | | 180 | 15 | >60 | 27.3 |
| | | | | 180 | 20 | 32.3 | 31.0 |
| | | | | 180 | 30 | 38.4 | 42.7 |
| | | | | 180 | 40 | 41.8 | 48.6 |
| | | | | 180 | 50 | 40.9 | 49.6 |
| | | | | 180 | 60 | 40.9 | 50.7 |
| | | | | 180 | 70 | 33.5 | 44.2 |
| | | | | 180 | 80 | 55.4 | >60 |

* Measured in db down from the Geometric Optics Maximum
** Geometric Optics result only

66

TABLE A.3.3
Results Obtained for $\theta_B = 50°$

| Conical Cut | | | | Plane Cut | | | |
|---|---|---|---|---|---|---|---|
| $\phi°$ | $\theta°$ | $|H_\theta|^2$ * | $|H_\phi|^2$ * | $\phi°$ | $\theta°$ | $|H_\theta|^2$ * | $|H_\phi|^2$ * |
| 0 | 50 | >60 | 0 | 0 | 150 | >60 ** | 36.1 |
| 30 | 51.6 | 11.4 | 1.2 | 0 | 135 | >60 | 36.3 |
| 60 | 56.6 | 6.4 | 6 | 0 | 120 | >60 | 36.1 |
| 90 | 64 | 7.2 | >60 | 0 | 105 | >60 | 35.5 |
| 100 | 66.7 | 12.2 | 18.7 | 0 | 90 | >60 | 33.9 |
| 105 | 68.1 | 13 | 19.8 | 0 | 75 | >60 | 30.3 |
| 110 | 69.4 | 14.4 | 21.6 | 0 | 61 | >60 | 22.5 |
| 115 | 70.7 | 16.1 | 23.6 | 0 | 58 | >60 | 20.8 |
| 120 | 71.9 | 17.8 | 25.7 | 0 | 57 | >60 | >60 |
| 125 | 73.1 | 19.9 | 28.1 | 0 | 56 | >60 | 17.9 |
| 130 | 74.2 | 22.1 | 31.6 | 0 | 55 | >60 | >60 |
| 135 | 75.3 | 27.4 | 36.5 | 0 | 54 | >60 | 13.5 |
| 140 | 76.2 | 28.5 | 38.7 | 0 | 53 | >60 | >60 |
| 145 | 77.1 | 35.6 | 39.1 | 0 | 51.5 | >60 | 4 |
| 150 | 77.8 | 46.4 | 55.3 | 0 | 50 | >60 | 0 |
| 155 | 78.5 | >60 | >60 | 0 | 49 | >60 | 4 |
| 160 | 79 | >60 | >60 | 0 | 48 | >60 | >60 |
| 165 | 79.5 | 52.4 | >60 | 0 | 46 | >60 | 13.5 |
| 170 | 79.8 | 52 | >60 | 0 | 45 | >60 | >60 |
| 175 | 79.9 | 58.5 | >60 | 0 | 44 | >60 | 17.9 |
| 180 | 80 | 51.3 | >60 | 0 | 42.5 | >60 | >60 |
| | | | | 0 | 41 | >60 | 20.8 |
| | | | | 0 | 30 | >60 | 26.9 |
| | | | | 0 | 15 | >60 | 30.7 |
| | | | | 0 | 0 | >60 | 32.1 |
| | | | | 180 | 15 | >60 | 32.7 |
| | | | | 180 | 20 | 54.8 | 58.8 |
| | | | | 180 | 30 | 52.3 | 46.5 |
| | | | | 180 | 40 | 46.6 | 53.3 |
| | | | | 180 | 50 | 56.7 | >60 |
| | | | | 180 | 60 | 51.4 | >60 |
| | | | | 180 | 70 | 52.9 | >60 |
| | | | | 180 | 80 | 51.3 | >60 |

* Measured in db down from the Geometric Optics Maximum

** Geometric Optics result only
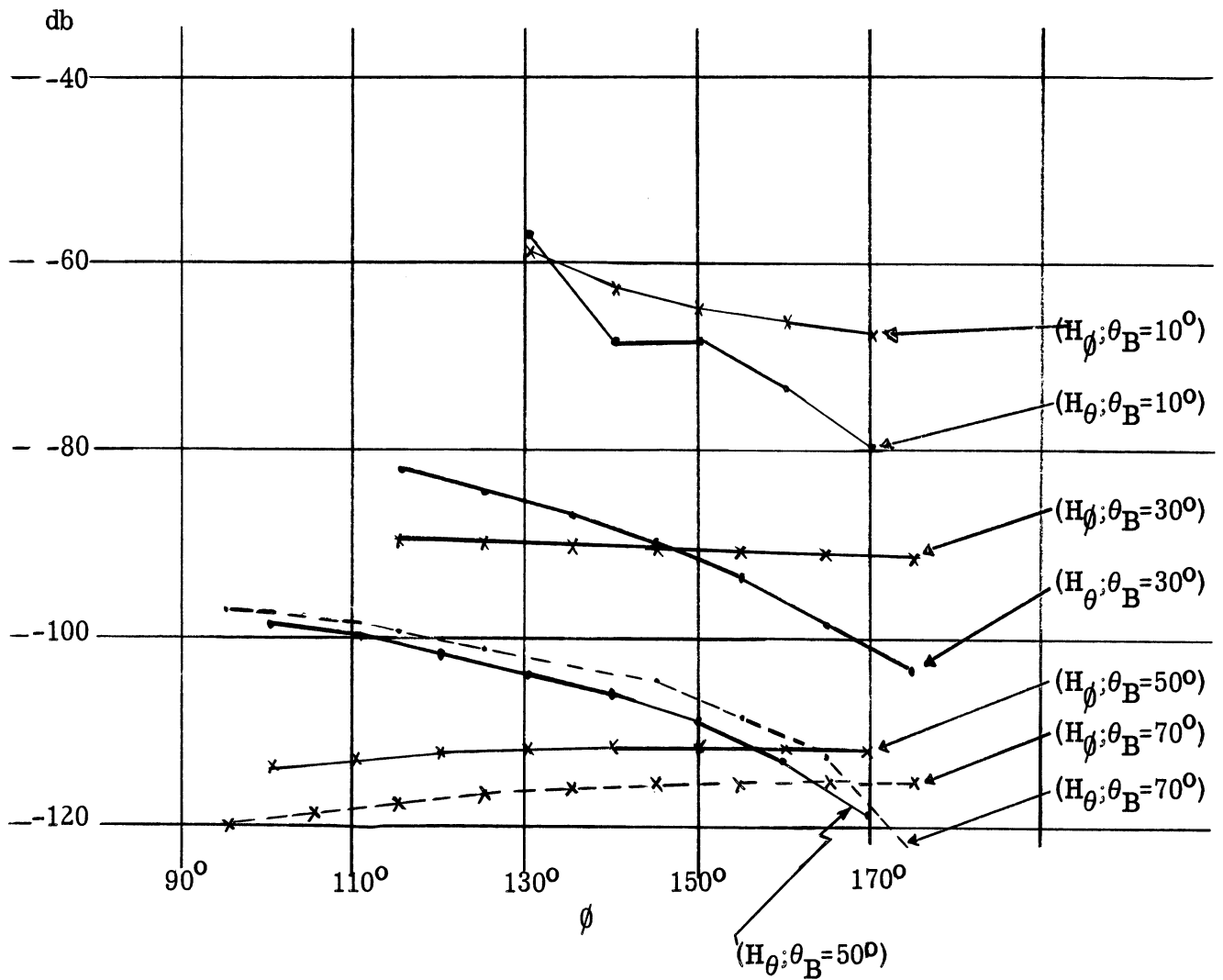
TABLE A. 3. 4

Results Obtained for $\theta_B = 70^\circ$

| Conical Cut | | | | Plane Cut | | | |
|---|---|---|---|---|---|---|---|
| $\phi^\circ$ | $\theta^\circ$ | $\|H_\theta\|^2$ * | $\|H_\phi\|^2$ * | $\phi^\circ$ | $\theta^\circ$ | $\|H_\theta\|^2$ * | $\|H_\phi\|^2$ * |
| 0 | 70 | >60 | 0 | 0 | 150 | >60 ** | 36 |
| 30 | 71.9 | 16.2 | 1.2 | 0 | 135 | >60 | 35.6 |
| 60 | 77.2 | 14.4 | 6 | 0 | 120 | >60 | 34.7 |
| 90 | 84.8 | 20.9 | >60 | 0 | 105 | >60 | 32.8 |
| 95 | 86.2 | 24.7 | 19.7 | 0 | 90 | >60 | 28.6 |
| 100 | 87.5 | 26.8 | 22.6 | 0 | 80.5 | >60 | 22.5 |
| 105 | 88.8 | 28.8 | 25.8 | 0 | 78 | >60 | 20.8 |
| 110 | 90.1 | 30.7 | 29 | 0 | 77 | >60 | >60 |
| 115 | 91.3 | 32.6 | 32.5 | 0 | 76 | >60 | 17.9 |
| 120 | 92.5 | 34.5 | 36.2 | 0 | 74.5 | >60 | >60 |
| 125 | 93.6 | 36.5 | 39.9 | 0 | 73 | >60 | 13.5 |
| 130 | 94.7 | 39.3 | 44.6 | 0 | 72 | >60 | >60 |
| 135 | 95.6 | 43.4 | 50.2 | 0 | 71 | >60 | 4 |
| 140 | 96.5 | 51.3 | 58.4 | 0 | 70 | >60 | 0 |
| 145 | 97.3 | 58.5 | >60 | 0 | 69 | >60 | 4 |
| 150 | 98 | 53.1 | >60 | 0 | 68 | >60 | >60 |
| 155 | 98.6 | 58.9 | >60 | 0 | 67 | >60 | 13.5 |
| 160 | 99.1 | >60 | >60 | 0 | 66 | >60 | >60 |
| 165 | 99.5 | >60 | >60 | 0 | 65 | >60 | 17.9 |
| 170 | 99.8 | >60 | >60 | 0 | 64 | >60 | >60 |
| 175 | 99.9 | >60 | >60 | 0 | 62.5 | >60 | 20.8 |
| | | | | 0 | 45 | >60 | 30.2 |
| | | | | 0 | 30 | >60 | 33.2 |
| | | | | 0 | 15 | >60 | 34.7 |
| | | | | 0 | 0 | >60 | 35.3 |
| | | | | 180 | 15 | >60 | 35.5 |
| | | | | 180 | 20 | 42.3 | 41 |
| | | | | 180 | 30 | 44.8 | 49.1 |
| | | | | 180 | 40 | 49.3 | 56.2 |
| | | | | 180 | 50 | 53.7 | >60 |
| | | | | 180 | 60 | 56.3 | >60 |
| | | | | 180 | 70 | 58.3 | >60 |
| | | | | 180 | 80 | >60 | >60 |

\* Measured in db down from the Geometric Optics Maximum

\*\* Geometric Optics result only

FIG. A. 3-1: PHYSICAL OPTICS RESULTS OBTAINED FOR
THE CONICAL CUTS

$$\left| \frac{|H_{PO}|^2}{|H_{GO(max)}|^2} \quad IN \ DB \right|$$
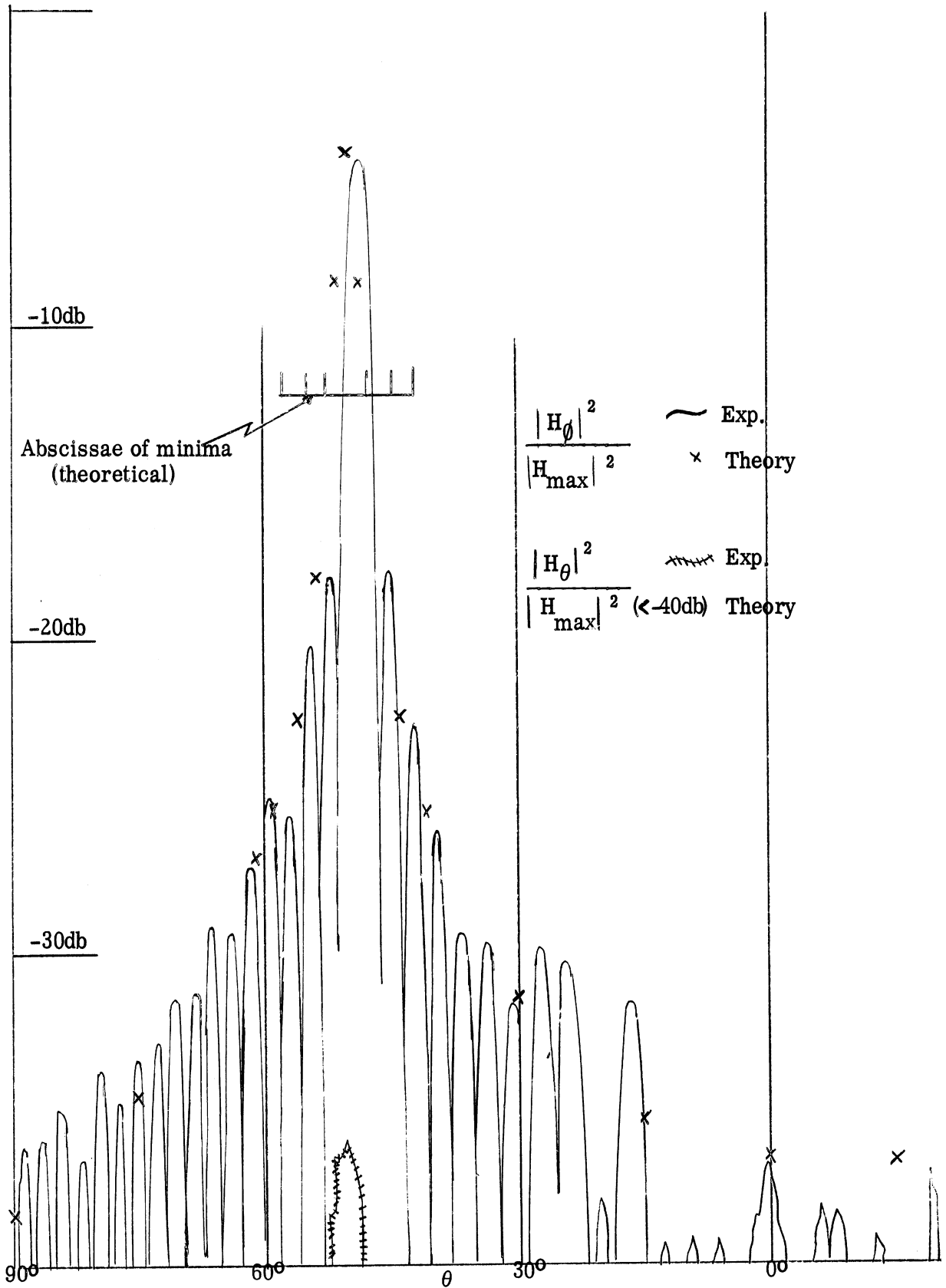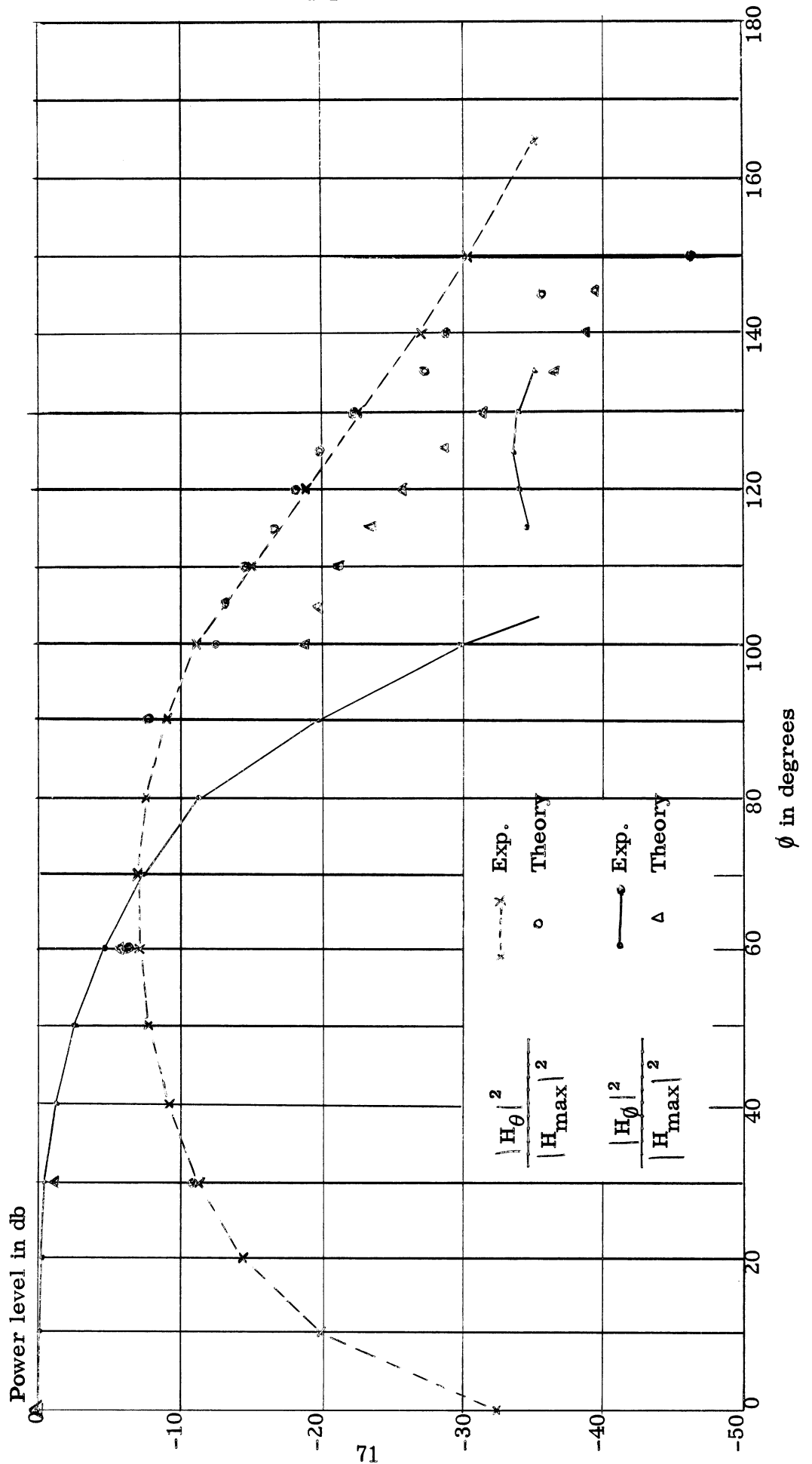
-10db

Abscissae of minima
(theoretical)

-20db

-30db

$$\frac{\left|H_{\phi}\right|^{2}}{\left|H_{max}\right|^{2}} \qquad \begin{array}{l} \sim \quad \text{Exp.} \\ \times \quad \text{Theory} \end{array}$$

$$\frac{\left|H_{\theta}\right|^{2}}{\left|H_{max}\right|^{2}} \ (<-40db) \quad \begin{array}{l} \text{Exp.} \\ \text{Theory} \end{array}$$

$90^{o}$    $60^{o}$    $\theta$    $30^{o}$    $0^{o}$

FIG. A. 3-2:  COMPARISON BETWEEN THEORY AND EXPERIMENT FOR A PLANE
CUT ($\theta_{B}$= 50°, $\phi$ = 0°)

FIG. A. 3-3: COMPARISON BETWEEN THEORY AND EXPERIMENT FOR A CONICAL CUT ($\theta_B = 50^\circ$)
(see footnote on page 64)

## APPENDIX B

## A FURTHER ANALYSIS OF TIP SCATTERING

It will be recalled that in Section 2.4 we obtained an expression for the field scattered by the tip of a cone. It was noted at that time that the approximation which was employed gave rise in some cases to divergent integrals.

In this Appendix we shall examine these cases more closely. We start with the Kirchhoff expression for the scattered magnetic field

$$\vec{H}_s = \frac{1}{4\pi} \int_S (\hat{n} \times \vec{H}) \times \nabla \frac{e^{ikR}}{R} \, dS, \tag{B.1}$$

where

$\hat{n}$ is the unit outward normal,

$R$ is the distance from the integration point $(x'', y'', z'')$ to the field point $(x', y', z')$,

$k = \frac{2\pi}{\lambda}$,

$S$ is the entire surface area, and time dependence $e^{-iwt}$ has been assumed.

Our problem concerns a plane wave incident on a conical surface. The incident field at any point $(x', y', z')$ is given by

$$H_i = \hat{p} H_o e^{-ik\hat{r} \cdot \vec{r}'},$$

where

$\hat{p}$ is the unit vector in the polarization direction,

$\hat{r}$ is a unit vector toward transmitter,

$\vec{r}'$ position vector for field point.

Points on the surface will be denoted by $r''$. ($\wedge$ will denote unit vectors while $\rightarrow$ will denote vectors of arbitrary magnitude).

As before, we employ the Physical Optics approximation, i.e. (1) the magnetic field on the surface is taken to be

$$\vec{H} = 2 H_o e^{-ik\hat{r} \cdot \vec{r}''} \vec{p}_t$$

where $\vec{p}_t$ is the tangential component of $\hat{p}$ and (2) S is the illuminated area.

Thus, we may rewrite B.1, remembering that $\hat{n} \times \hat{p} \equiv \hat{n} \times \vec{p}_t$, as follows

$$\vec{H}_s = \frac{H_o}{2\pi} \int_{\substack{\text{illuminated} \\ \text{area}}} \left[ (\hat{n} \times \hat{p}) \times \nabla \frac{e^{ikR}}{R} \right] e^{-ik\hat{r} \cdot \vec{r}''} \, dS \ . \tag{B.2}$$

However, $\nabla \dfrac{e^{ikR}}{R} = \left[ \dfrac{-e^{ikR}}{R^2} + i k \dfrac{e^{ikR}}{R} \right] \nabla R$

$$= \left[ \frac{-e^{ikR}}{R^2} + i k \frac{e^{ikR}}{R} \right] \hat{R}$$

$$= \left[ \frac{-e^{ikR}}{R^2} + i k \frac{e^{ikR}}{R} \right] \frac{(\vec{r}' - \vec{r}'')}{|\vec{r}' - \vec{r}''|}$$

and

$$(\hat{n} \times \hat{p}) \times (\vec{r}' - \vec{r}'') = \left[ (\vec{r}' - \vec{r}'') \cdot \hat{n} \right] \hat{p} - \left[ (\vec{r}' - \vec{r}'') \cdot \hat{p} \right] \hat{n} \ ,$$

hence, (B.2) becomes

$$\vec{H}_s = \frac{H_o}{2\pi} \int_{\substack{\text{illuminated} \\ \text{area}}} \frac{\left[ (\vec{r}' - \vec{r}'') \cdot \hat{n} \right] \hat{p} - \left[ (\vec{r}' - \vec{r}'') \cdot \hat{p} \right] \hat{n}}{|\vec{r}' - \vec{r}''|} \left( -\frac{e^{ikR}}{R^2} + i k \frac{e^{ikR}}{R} \right) e^{-ik\hat{r} \cdot \vec{r}''} dS.$$

$$\tag{B.3}$$

73

The usual far zone assumptions are:

(1) $\quad \dfrac{\vec{r'} - \vec{r''}}{|\vec{r'} - \vec{r''}|} \sim \hat{r'} ,$

(2) $\quad -\dfrac{1}{R^2} + \dfrac{ik}{R} \sim \dfrac{ik}{R} ,$  (B.4)

(3) $\quad R \approx \begin{cases} r' & \text{when evaluating magnitude} \\ r' - \hat{r'} \cdot \vec{r''} & \text{when evaluating phase} \end{cases}$ .

Utilizing Equations (B.4) in (B.3) we obtain

$$\vec{H}_s = \dfrac{H_0}{2\pi} \int_{\substack{\text{illuminated} \\ \text{area}}} \left[ (\hat{r'} \cdot \hat{n}) \, \hat{p} - (\hat{r'} \cdot \hat{p}) \hat{n} \right] \dfrac{ike}{r'}^{ik(r' - \hat{r'} \cdot \vec{r''})} e^{-ik\hat{r} \cdot \vec{r''}} \, dS .$$  (B.5)

Let us re-examine our far zone assumption B.4 (3), retaining the next higher

order terms. That is,

$$R = \sqrt{r'^2 + r''^2 - 2\vec{r'} \cdot \vec{r''}}$$

$$= r' \sqrt{1 + \dfrac{r''^2}{r'^2} - \dfrac{2\vec{r'} \cdot \vec{r''}}{r'^2}}$$

$$= r' \left[ 1 + \dfrac{1}{2} \left( \dfrac{r''^2}{r'^2} - \dfrac{2\vec{r'} \cdot \vec{r''}}{r'^2} \right) - \dfrac{1}{8} \left( \dfrac{r''^2}{r'^2} - \dfrac{2\vec{r'} \cdot \vec{r''}}{r'^2} \right)^2 + \cdots \right]$$  (B.6)

$$= r' \left[ 1 - \dfrac{\vec{r'} \cdot \vec{r''}}{r'} + \dfrac{r''^2}{2r'^2} - \dfrac{1}{2} \dfrac{(\hat{r'} \cdot \vec{r''})^2}{r'^2} + O\left( \dfrac{1}{r'^3} \right) \right]$$

$$\sim r' - \hat{r'} \cdot \vec{r''} + \dfrac{r''^2 - (\hat{r'} \cdot \vec{r''})^2}{2r'} .$$

Now we rewrite (B.5) using (B.6)

$$\vec{H}_s = \frac{H_0 \; ike^{ikr'}}{2 \pi r'} \int_{\substack{\text{illuminated} \\ \text{area}}} \left[ (\hat{r}' \cdot \hat{n}) \; \hat{p} - (\hat{r}' \cdot \hat{p}) \; \hat{n} \right] \quad \exp \left[ i \; k \; (-\vec{r}'' \cdot (\hat{r}' + \hat{r}) + \frac{r'^2 - (\hat{r}' \cdot \vec{r}'')^2}{2 \; r'}) \right] \; d \; S .$$

$$(B.7)$$

Equation (B.5) gave rise, in Section II, to the integral

$$\vec{f} = \int_{\substack{\text{illuminated} \\ \text{area}}} \hat{n} \; e^{-ik\vec{r}'' \cdot (\hat{r}' + \hat{r})} \quad r'' \sin \alpha \; d \; r'' d \; \phi''$$

which proved troublesome for values of $\phi''$ such that $\vec{r}'' \cdot (\hat{r}' + \hat{r}) = 0$. It is true that,

as written, $\vec{f}$ diverges if there is a $\phi''$ in the range of integration for which $\vec{r}'' \cdot (\hat{r}' + \hat{r}) = 0$.

If at the same point $(x'', y'', z'')$ we also have $\hat{n} \times (\hat{r}' + \hat{r}) = 0$, then of course, we have a

specular reflection situation and we would use Geometric Optics to describe the scattered

field. However, let us assume that there is such a $\phi''$, say $\phi''_0$, where $\vec{r}'' \cdot (\hat{r}' + \hat{r}) = 0$

but $\hat{n} \times (\hat{r}' + \hat{r}) \neq 0$ and examine the following three cases, using (B.7) instead of (B.5)

(1) $\quad \vec{r}'' \cdot \hat{r}' = 0$ ,

(2) $\quad \vec{r}'' \cdot \hat{r}' = r'' \cos \gamma$ where $0 < \cos^2 \gamma < 1$ ,

(3) $\quad \vec{r}'' \cdot \hat{r}' = \pm r''$ .

In the following we will treat (B.7) as consisting of two contributions

$$\vec{H} = \int_{\substack{\text{illuminated} \\ \text{area}}} = \int_{S_1} + \int_{S_2}$$

where $S_2$ contains $\phi''_0$ and $S_1 + S_2 =$ illuminated area. We will concern ourselves only

with $\int_{S_2}$ since $\int_{S_1}$ presents no problem.

75

<u>CASE I</u>

In the neighborhood of $\phi_0''$ we have

$$\vec{r}'' \cdot (\hat{r}' + \hat{r}) = 0 \quad \text{and} \quad \vec{r}'' \cdot \hat{r}' = 0 \quad,$$

hence we may write (B. 7) as

(B. 8)

$$\vec{H}_s = \int_{S_1} + \frac{H_0 \, ike^{ikr'}}{2\pi r'} \int_{\phi_0'' - \epsilon}^{\phi_0'' + \epsilon} \int_0^\infty \left[ (\hat{r}' \cdot \hat{n}) \, \hat{p} - (\hat{r}' \cdot \hat{p}) \, \hat{n} \right] \exp\left( ik \frac{r''^2}{2r'} \right) r'' \sin\alpha \, d\,r'' d\,\phi''$$

The $r''$ integration can be performed by an Abelian limit argument as follows

$$\int_0^\infty \exp\left( ik \frac{r''^2}{2r'} \right) r'' d\,r'' = \lim_{\delta \to 0} \int_0^\infty \exp\left[ \left( \frac{ik}{2r'} - \delta \right) r''^2 \right] r'' \, d\,r''$$

$$= \lim_{\delta \to 0} \left[ \frac{\exp\left[ \left( \frac{ik}{2r'} - \delta \right) r''^2 \right]}{2 \left( \frac{ik}{2r'} - \delta \right)} \Bigg|_0^\infty \right]$$

$$= \frac{r'}{ik} \quad.$$

Thus (B. 8) becomes

$$\vec{H}_s = \int_{S_1} + \frac{H_0 \, e^{ikr'}}{2\pi} \sin\alpha \int_{\phi_0'' - \epsilon}^{\phi_0'' + \epsilon} \left[ (\hat{r}' \cdot \hat{n}) \, \hat{p} - (\hat{r}' \cdot \hat{p}) \, \hat{n} \right] d\,\phi'' \quad.$$

Applying the mean value theorem, we obtain

$$\vec{H}_s = \int_{S_1} + \frac{H_0 \, e^{ikr'}}{\pi} \sin\alpha \left[ (\hat{r}' \cdot \hat{n}) \, \hat{p} - (\hat{r}' \cdot \hat{p}) \, \hat{n} \right] \epsilon$$

$$\text{for } \hat{n} = \hat{n}(\phi_1'') \,, \quad \phi_0'' - \epsilon \leq \phi_1'' \leq \phi_0'' + \epsilon \quad.$$

$$\text{Thus } \vec{H}_s \approx \int_{S_1}$$

where $\int_{S_1}$ can be evaluated by the method of Section II.

## CASE II

In the neighborhood of $\emptyset_0''$ we have $\vec{r}'' \cdot (\hat{r}' + \hat{r}) = 0$ and $\vec{r}'' \cdot \hat{r}' = r'' \cos \gamma$

where $\cos^2 \gamma$ is bounded away from 0 and 1. In this case, we may write (B.7) as

$$\vec{H}_s = \int_{S_1} + \frac{H_0 ike^{ikr'}}{2\pi r'} \sin \alpha \int_{\emptyset_0''-\epsilon}^{\emptyset''+\epsilon} \int_0^\infty \left[ (\hat{r}' \cdot \hat{n})\hat{p} - (\hat{r}' \cdot \hat{p})\hat{n} \right] \exp \left[ \frac{ikr''^2}{2r'} \sin^2 \gamma \right] r'' dr'' d\emptyset''$$

$$(B.9)$$

Since $\sin^2 \gamma$ is bounded away from zero, we proceed exactly as in Case I obtaining

$$\vec{H}_s = \int_{S_1} + \frac{H_0 e^{ikr'}}{\pi \sin^2 \gamma} \sin \alpha \left[ (\hat{r}' \cdot \hat{n})\hat{p} - (\hat{r}' \cdot \hat{p})\hat{n} \right] \epsilon$$

$$\text{for } \hat{n} = \hat{n}(\emptyset_1''), \quad \emptyset_0'' - \epsilon \leq \emptyset_1'' \leq \emptyset_0'' + \epsilon \quad .$$

Thus again we see that the contribution from the neighborhood containing $\emptyset_0''$ vanishes

with $\epsilon$ and

$$\vec{H}_s \approx \int_{S_1} .$$

## CASE III

In the neighborhood of $\emptyset_0''$ we have $\vec{r}'' \cdot (\hat{r}' + \hat{r}) = 0$ and $\vec{r}'' \cdot \hat{r}' = \pm r''$. Thus

either (a), $\vec{r}'' \cdot \hat{r}' = r''$ and $\vec{r}'' \cdot \hat{r} = -r''$ or (b), $\vec{r}'' \cdot \hat{r}' = -r''$ and $\vec{r}'' \cdot \hat{r} = r''$. In (a) we

have the receiver on a cone generator and the transmitter on the extension of that

generator while in (b) the transmitter is on the generator and the receiver is on the

extension. These are the transition cases which we cannot handle by these techniques

and must exclude from our analysis.

# APPENDIX C

## IDEAL CURRENT DISTRIBUTION FOR A CONICAL ANTENNA

It was pointed out in Section I that it was theoretically possible to duplicate a pattern produced by one type of antenna with another antenna of equal or greater aperture. It was pointed out there that the problems involved in attempting to instrument the current distribution required appeared to be of such complexity that a serious attempt at instrumentation would not be warranted since this is not an optimal array. In this Appendix we consider this problem of duplicating a given pattern. Specifically, for illustration, we consider the pattern produced by an ideal parabolic dish and calculate the current distribution which, if activated on a cone surface in any manner whatsoever, would make the cone yield a pattern identical with the dish pattern.

Consider a conical surface behind which a dish antenna is pivoted about the point 0. By application of Huygens Principle the field at a point P outside a surface S can be obtained from knowledge of the tangential field produced by the source at the surface. In this case the source is a dish and the surface a cone. The field of a dish is approximated by a plane wave; the tangential component on the cone surface will be studied.

An $\hat{i}, \hat{j}, \hat{k}$ coordinate system is considered to be affixed to the cone as in Figure C-1. A plane wave is considered to be produced from the dish with polarizations as follows in the two cases to be considered here:
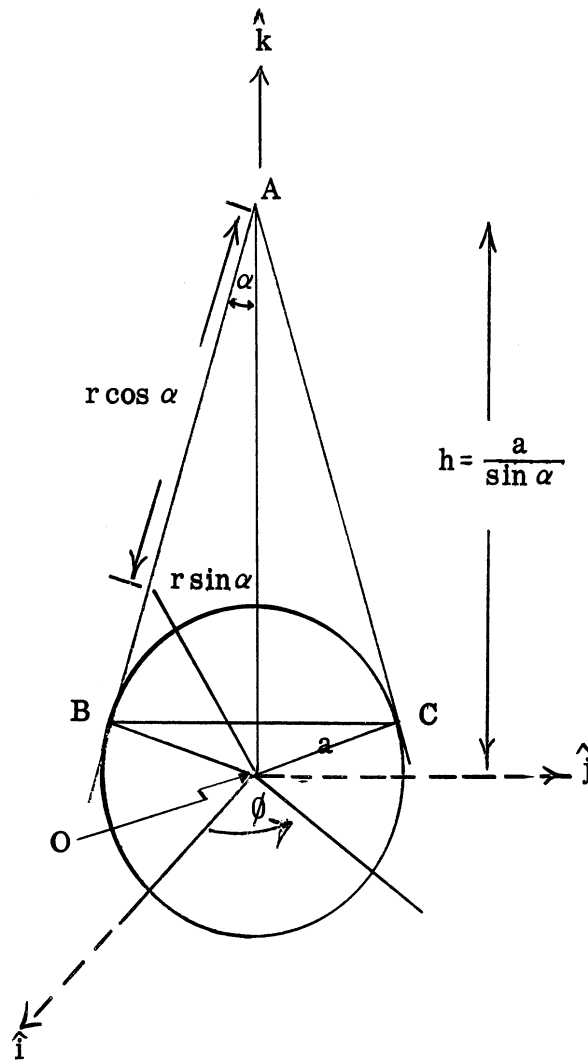
FIG. C-1

$$\vec{E_1} = (\hat{i}\cos\beta - \hat{k}\sin\beta)\, e^{i\vec{k}\cdot\vec{r}} \tag{C.1}$$

$$\vec{E_2} = \hat{j}\, e^{i\vec{k}\cdot\vec{r}} \tag{C.2}$$

in which the $e^{iwt}$ time dependence is assumed. $\vec{E_1}$ lies in the y-plane and $\vec{E_2}$ is $\perp$ to the

y-plane.

In each case the beam is considered to take the orientations

$$\beta = 0^\circ, 20^\circ, 40^\circ, 60^\circ, 80^\circ.$$

In order to graph the amplitude, phase and direction of the field, the cone is

unrolled and forms a two-dimensional cone of apex angle $= 2\pi\sin\alpha$.

The tangential component of the field on the illuminated part of the cone is res-

pectively

$$\hat{n} \times \vec{E_1} = e^{i\vec{k}\cdot\vec{r}}\left[\hat{i}(-\cos\alpha\sin\beta\sin\phi) + \hat{j}(\sin\alpha\cos\beta + \cos\alpha\sin\beta\cos\phi)\right.$$
$$\left. + \hat{k}(-\cos\alpha\cos\beta\sin\phi)\right] \tag{C.3}$$

$$\hat{n} \times \vec{E_2} = e^{i\vec{k}\cdot\vec{r}}\left[\hat{i}(-\sin\alpha) + \hat{k}(\cos\alpha\cos\phi)\right], \tag{C.4}$$

and, in spherical coordinates on the cone surface

$$\hat{n} \times \vec{E_1} = e^{i\vec{k}\cdot\vec{r}}\left[r(\cos\beta\sin\phi) + \phi(\sin\alpha\cos\beta\cos\phi + \sin\beta\cos\alpha)\right] \tag{C.5}$$

$$\hat{n} \times \vec{E_2} = e^{i\vec{k}\cdot\vec{r}}\left[r(-\cos\phi) + \phi(\sin\alpha\sin\phi)\right]. \tag{C.6}$$

The amplitudes and directions of the field on the cone surface are

$$|E_1| = \sqrt{\cos^2\beta\sin^2\phi + (\sin\alpha\cos\beta\cos\phi + \sin\beta\cos\alpha)^2} \tag{C.7}$$

$$|E_2| = \sqrt{\cos^2\phi + \sin^2\alpha\sin^2\phi} \tag{C.8}$$

$$\tan\theta_1 = \frac{\sin\alpha\cos\phi + \tan\beta\cos\alpha}{\sin\phi} \tag{C.9}$$

$$\tan\theta_2 = \frac{\sin\alpha\sin\phi}{-\cos\phi} \tag{C.10}$$
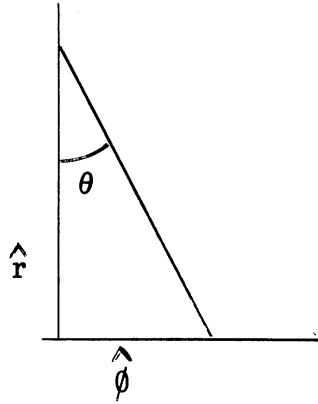
FIG. C-2

Since propagation takes place in $y$ = const. planes, the phase in each case

is given by

$$\vec{k} \cdot \vec{r} = kz \cos \beta + kx \sin \beta \qquad (C.11)$$

We are interested in the phase over the illuminated region of the cone's

surface. From the figure we see that $z = h - r \cos \alpha$ and $x = r \sin \alpha \cos \phi$.

Therefore, the phase angle is given by

$$\frac{2\pi}{3} \left[ \frac{a}{\sin \alpha} - r \cos \alpha \cos \beta + r \sin \alpha \sin \beta \cos \phi \right] \qquad (C.12)$$

To find the minimum distance between two points along a cone generator at

which the radiation is in phase we equate the phase angle above to zero and $2\pi$, we

solve for $r$ (obtaining $r_0$ and $r_{2\pi}$), and then subtract the values of $r$ obtaining

the distance $\ell$

$$\ell = r_0 - r_{2\pi} = \frac{3}{(\cos \alpha \cos \beta - \sin \alpha \sin \beta \cos \phi)} \text{ (cm.)} \qquad (C.13)$$

## Equations for the direction lines

The equations for the direction lines on the cone surface may be obtained in the following manner: Consider a $\xi$, $\eta$ coordinate system on which the unrolled cone is placed as shown in Figure C-3.

Then

$$\frac{dn}{d\xi} = \tan(\theta + \phi^1)$$

$$n = r \sin \phi^1 \frac{dn}{dr} = \sin \phi^1 \frac{dn}{d\phi^1} = r \cos \phi^1$$

$$\xi = r \cos \phi^1 \frac{d\xi}{dr} = \cos \phi^1 \frac{d\xi}{d\phi^1} = r \sin \phi^1$$

then

$$\frac{\sin \phi^1 \, dr + r \cos \phi^1 \, d\phi^1}{\cos \phi^1 \, dr - r \sin \phi^1 d\phi^1} = \tan(\theta + \phi^1) = \frac{\tan \theta + \tan \phi^1}{1 - \tan \theta \tan \phi^1}$$
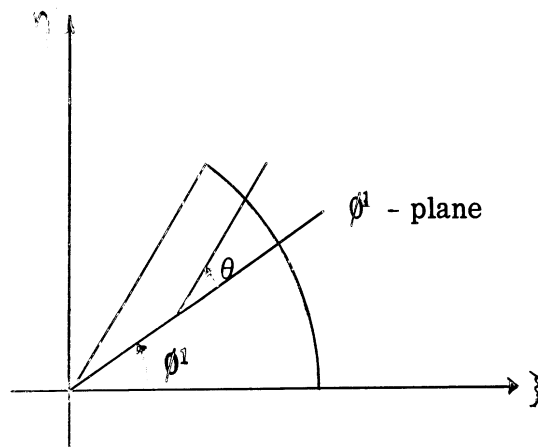


FIG. C-3

$$(\sin \phi^1 \, dr + r \cos \phi^1 \, d\phi^1)(1 - \tan \theta \tan \phi^1) - (\cos \phi^1 \, dr - r \sin \phi^1 \, d\phi^1)(\tan \theta + \tan \phi^1) = 0$$

$$- \tan \theta \, dr + r \, d\phi^1 = 0$$

but

$$d\phi^1 = \sin \alpha \, d\phi$$

$$\frac{dr}{r} = \frac{\sin \alpha \, d\phi}{\tan \theta} \qquad\qquad (C.14)$$

For the two cases considered we have

$$\theta_1 : \qquad r = \frac{r_o}{(\cos \phi \, \frac{\tan \beta}{\tan \alpha})} \qquad\qquad r_o = \text{integration const.} \qquad (C.15)$$

$$\theta_2 : \qquad r = r_o \csc \phi \qquad\qquad r_o = \text{integration const.} \qquad (C.16)$$

The constant $r_o$ is a parameter which takes on all values on a generator of the cone. Due to the discontinuity of the trigonometric functions, the integrations must be performed piecewise resulting in a sign change in the $r_o$ at the points of discontinuity.

## Determination of illuminated region

We will now determine $\phi = \phi(r)$, the envelope of the illuminated region on the cone. We will first find the maximum and minimum intercept points of the beam on the cone. It can be seen from the geometry that the cylinder generators in the $y = 0$ plane intersect the cone at $r_{max}$ and $r_{min}$.

On $\phi = 0$ the range of $r$ is determined by

$$r_{\substack{max \\ min}} = a \left( \frac{\sin \beta \pm \sin \alpha}{\sin \alpha \sin (\alpha + \beta)} \right) \qquad (C.17)$$

$\phi$ is determined as a function of $r$ by solving the equation of the intersection of the cone and cylinder. In a spherical coordinate system passing through the cone apex, the intersection equation is

$$r^2 \sin^2 \alpha \sin^2 \beta (1 - \cos \phi)^2 + 2r \sin \alpha \sin \beta \left[ r \cos (\alpha + \beta) - h \cos \beta \right] (1 - \cos \phi)$$

$$- r^2 \sin^2 (\alpha + \beta) + 2rh \sin \beta \sin (\alpha + \beta) + h^2 (\sin^2 \alpha - \sin^2 \beta) = 0$$

whose solution is

$$(C.18)$$

$$\cos \phi = \frac{(r \cos \alpha - h) \cos \beta + | r - h \cos \alpha |}{r \sin \alpha \sin \beta} \qquad (C.19)$$

the change of sign would occur at

$$r = h \cos \alpha$$

which is the point of maximum possible $\phi$.

In order to obtain the boundary of the illuminated region on the cone we use expression (C.19)

$$\cos \phi = \frac{r \cos \alpha \cos \beta - h \cos \beta + | r - h \cos \alpha |}{r \sin \alpha \sin \beta}$$

having already obtained the range of $r$. For $\phi_{max}$ the phase is zero since the dish touches the cone at that point. Knowing the phase along the boundary of the illuminated region, we can, for given $\phi$, keep laying off the distance $\ell$ along the generators starting at a boundary point until we attain some pre-assigned phase. The phase on the boundary is obtained from (C.12). For laying off successive curves we subtract

FIG. C-4



Phase given
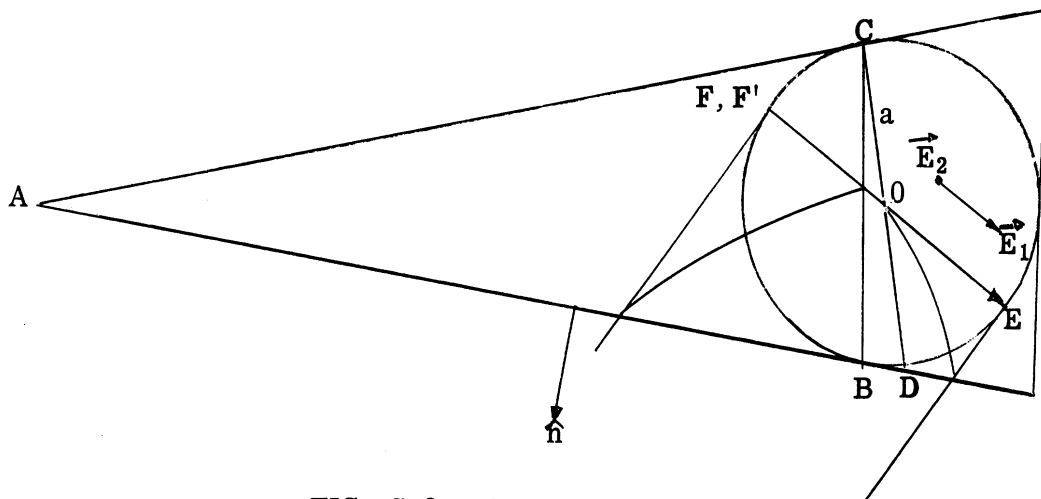in terms of
$2\pi$(e.g. $\nu \cdot 2\pi$)

$\ell$ = period

Line of constant
zero phase
= $\ell_{min} + \nu(\ell)$
as a function of $\phi$
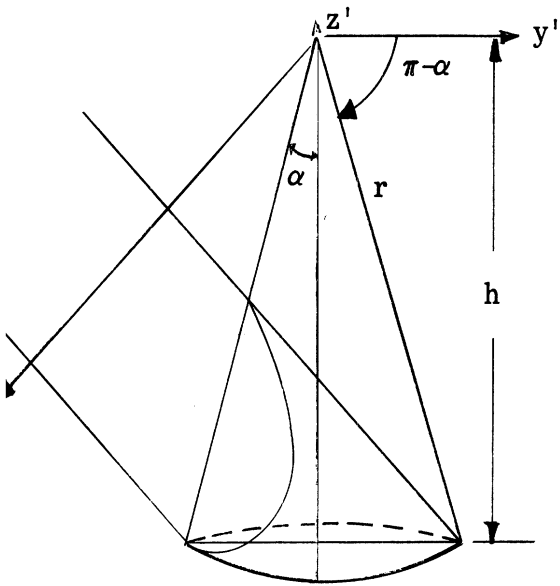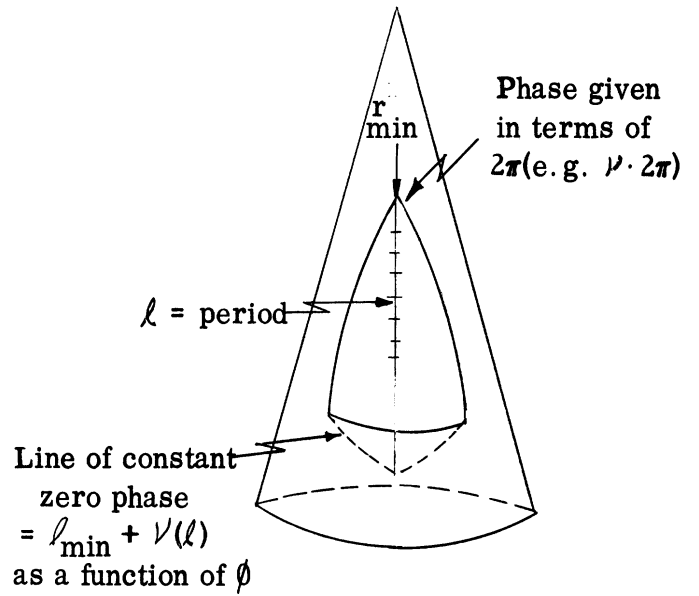
FIG. C-5



FIG. C-6: The cone in the y = 0 plane

some multiple of $2\pi$ from the line of constant zero phase where $\ell = \ell(\phi)$ is used

for the distance equivalent to $2\pi$.

## Discussion of Results:

In order to see, physically, what occurs, we will consider a sphere of radius

"a" equal to the radius of the dish to be inserted into the cone as shown in Figure C-6.

The points of contact will constitute a circle whose two-dimensional projection is BC.

The dish is focused at 0 and has a point of contact C when in the position DC and two

points of contact F, $F^1$ when in the position EF.

The graphs in Figures C-8 through C-12 show the variation in amplitude of

the tangential component of $E_1$ over the unrolled cone surface. The field along the

$\phi=0$ generator of the cone would be small (for $\beta$ small) increasing to a maximum near

$\pm 90^o$ and becoming small again for $180^o$. As $\beta$ increases toward $90^o$ the amplitude will

increase on the $\phi=0^o, 180^o$ surfaces and remain fairly constant on the surface near $\pm 90^o$.

Therefore, for large $\beta$ the amplitude is fairly constant with $\phi$.

The graphs in Figures C-13 through C-17 show that the amplitude variation of

the tangential component of $E_2$ is independent of $\beta$ which is clear from Figure C-6.

Figures C-18 through C-22 illustrate lines of constant phase within the illuminated

region of the cone. The fact that these lines are ellipses for $\beta=0$ to $80^o$, parabolas

for $\beta= 80^o$, and hyperbolas for $\beta= 90^o$, can be seen by observation of Figure C-7.
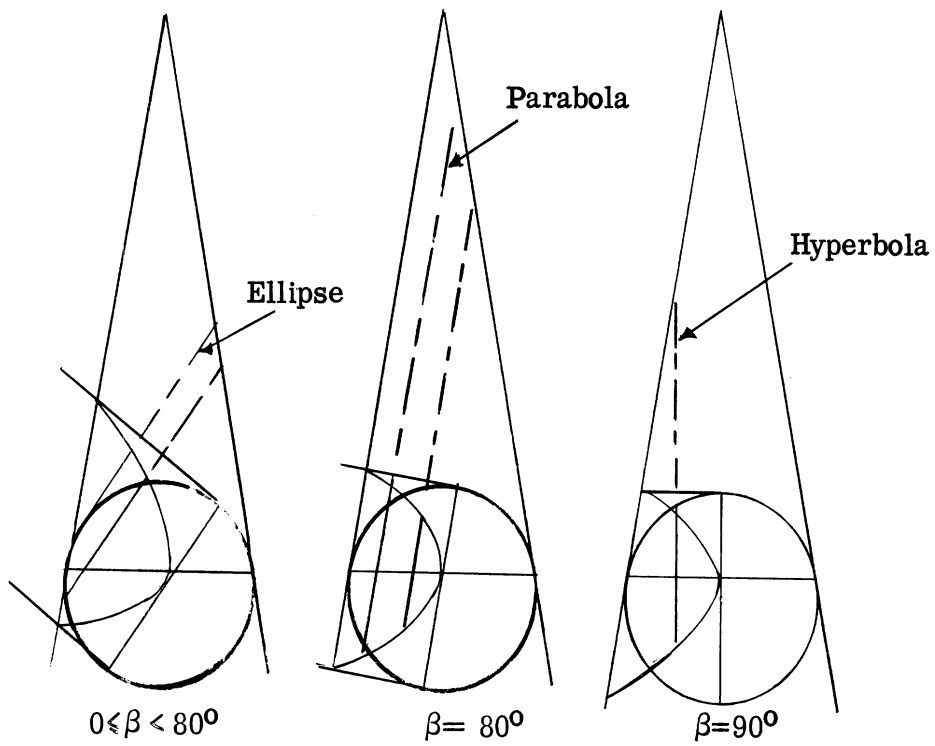
FIG. C-7

The direction of tangential $E_1$ is shown in Figures C-23 through C-27. It may be noted that, along the $\emptyset=0$ cone generator, as $E_1$ points more and more in the $\hat{n}(\emptyset=0)$ direction, the direction lines take a more acute change in direction. The direction lines would be reversed on either side of $\emptyset=0$ if the case $\beta=10^{\circ}$ had been calculated. In the case of $\beta=80^{\circ}$, the fact that the direction lines go along lines of constant r near $\emptyset=0^{\circ}$ is seen from the fact that $\vec{E_1}$ vector points along the cone near $\emptyset=0$; the dip near $90^{\circ}$ occurs since $\vec{E_1}$ is not tangent near $90^{\circ}$.

The direction of tangential $E_2$ is shown in Figure C-28; only in the case of $\beta=0^{\circ}$ is shown since $\hat{n} \times \vec{E_2}$ is independent of $\beta$.

The discussion of this appendix is illustrated through the application of the following parameter values:

$$\alpha = 10^{\circ}$$

$$a = 20"$$

$$\lambda = 3cm.$$

The results are presented in tabular form in Tables C.1 through C.3.

TABLE C.1: $|E|$ $(\alpha = 10^{\circ})$ Amplitude

| $\phi$ | $|E_1|$ | | | | | $|E_2|$ |
|---|---|---|---|---|---|---|
| | $\beta = 0^{\circ}$ | $\beta = 20^{\circ}$ | $\beta = 40^{\circ}$ | $\beta = 60^{\circ}$ | $\beta = 80^{\circ}$ | |
| $0^{\circ}$ | 0.17363 | 0.500 | 0.766 | 0.940 | 1.000 | 1.000 |
| $10^{\circ}$ | | 0.524 | 0.776 | 0.942 | 1.000 | 0.985 |
| $20^{\circ}$ | 0.37893 | 0.586 | 0.802 | 0.950 | 1.000 | 0.942 |
| $30^{\circ}$ | | 0.670 | 0.841 | 0.961 | 1.000 | 0.870 |
| $40^{\circ}$ | 0.65641 | 0.760 | 0.885 | 0.974 | 0.999 | 0.774 |
| $50^{\circ}$ | | 0.845 | 0.928 | 0.986 | 0.998 | 0.656 |
| $60^{\circ}$ | 0.87037 | 0.915 | 0.964 | 0.995 | 0.996 | 0.522 |
| $70^{\circ}$ | | 0.966 | 0.989 | 1.000 | 0.994 | 0.379 |
| $80^{\circ}$ | 0.98527 | 0.995 | 1.000 | 0.998 | 0.990 | 0.244 |
| $90^{\circ}$ | | 0.998 | 0.994 | 0.989 | 0.985 | 0.174 |
| $100^{\circ}$ | 0.98527 | 0.975 | 0.970 | 0.972 | 0.980 | 0.244 |
| $110^{\circ}$ | | 0.927 | 0.929 | 0.948 | 0.973 | 0.379 |
| $120^{\circ}$ | 0.87037 | 0.853 | 0.872 | 0.918 | 0.967 | 0.522 |
| $130^{\circ}$ | | 0.756 | 0.803 | 0.884 | 0.960 | 0.656 |
| $140^{\circ}$ | 0.65641 | 0.640 | 0.724 | 0.850 | 0.953 | 0.774 |
| $150^{\circ}$ | | | | | | 0.870 |
| $160^{\circ}$ | 0.37893 | | values not needed | | | 0.942 |
| $170^{\circ}$ | | | | | | 0.985 |
| $180^{\circ}$ | 0.17363 | | | | | 1.000 |

## TABLE C.2:
### Boundary of Illuminated Region and Phase on Boundary:

$\beta = 20^{\circ}$

| r in cm. | $\phi$ | Phase | $\lambda$ Period for the given $\phi$, in cm. |
|---|---|---|---|
| 98.9 | $0^{\circ}$ | 63.26066 $(2\pi)$ | 3.464 |
| 100 | $16^{\circ}$ 33' | 62.805 $(2\pi)$ | 3.454 |
| 125 | $58^{\circ}$ 2' | 54.488 $(2\pi)$ | 3.354 |
| 150 | $76^{\circ}$ 50' | 46.151 $(2\pi)$ | 3.289 |
| 175 | $89^{\circ}$ 6' | 37.813 $(2\pi)$ | 3.245 |
| 200 | $98^{\circ}$ 15' | 29.475 $(2\pi)$ | 3.212 |
| 225 | $105^{\circ}$ 30' | 21.138 $(2\pi)$ | 3.187 |
| 250 | $111^{\circ}$ 29' | 12.8 $(2\pi)$ | 3.167 |
| 275 | $116^{\circ}$ 32' | 4.463 $(2\pi)$ | 3.1515 |
| 288.38 | $118^{\circ}$ 58' $= \phi$ max | 0 | |
| 300 | $37^{\circ}$ 48' | 3.875 $(2\pi)$ | 3.415 |
| 302.9 | $0^{\circ}$ | | |

$\beta = 40^{\circ}$

| r in cm. | $\phi$ | Phase | $\lambda$ Period for the given $\phi$, in cm. |
|---|---|---|---|
| 179.9 | $0^{\circ}$ | 36.3488 $(2\pi)$ | 4.6672 |
| 200 | $49^{\circ}$ 37' | 29.475 $(2\pi)$ | 4.479 |
| 225 | $64^{\circ}$ 38' | 21.138 $(2\pi)$ | 4.246 |
| 250 | $80^{\circ}$ 23' | 12.8 $(2\pi)$ | 4.077 |
| 275 | $92^{\circ}$ 46' | 4.463 $(2\pi)$ | 4.005 |
| 288.38 | $102^{\circ}$ 08' $= \phi$ max | 0 | |
| 300 | $62^{\circ}$ 12' | 3.875 $(2\pi)$ | 4.291 |
| 313 | $0^{\circ}$ | | |

TABLE C.2:
Boundary of Illuminated Region and Phase on Boundary:
(Continued)

$\beta = 60^\circ$

| r in cm. | $\phi$ | Phase | $\mathscr{L}$ Period for the given $\phi$, in cm. |
|---|---|---|---|
| 216.4 | $0^\circ$ | 24.207 $(2\pi)$ | 8.74 |
| 225 | $34^\circ$ 53' | 21.138 $(2\pi)$ | 8.129 |
| 250 | $66^\circ$ 22' | 12.8 $(2\pi)$ | 6.9405 |
| 275 | $86^\circ$ 42' | 4.463 $(2\pi)$ | 6.202 |
| 288.38 | $95^\circ$ 50' = $\phi$ max | 0 $(2\pi)$ | |
| 300 | $73^\circ$ 21' | 3.875 $(2\pi)$ | 6.676 |
| 325 | $0^\circ$ | 12.212 $(2\pi)$ | |

$\beta = 80^\circ$

| r in cm. | $\phi$ | Phase | $\mathscr{L}$ Period for the given $\phi$, in cm. |
|---|---|---|---|
| 238.2 | $0^\circ$ | ka = 16.95 $(2\pi)$ | |
| 250 | $44^\circ$ 54' | 12.8 $(2\pi)$ | 60.105 |
| 275 | $78^\circ$ 17' | 4.463 $(2\pi)$ | 22.018 |
| 288.38 | $91^\circ$ 47' ($\phi$ max) | 0 | |
| 300 | $76^\circ$ 23' 30" | 3.875 $(2\pi)$ | 22.94 |
| 325 | $41^\circ$ 56' | 12.21 $(2\pi)$ | 68.09 |
| 340.2 | $0^\circ$ | | |

TABLE C.3: Direction of $\vec{E}$ ($\alpha = 10°$)

| $\phi$ | $\theta_1$ | | | | | $\theta_2$ |
| --- | --- | --- | --- | --- | --- | --- |
| | $\beta = 0°$ | $\beta = 20°$ | $\beta = 40°$ | $\beta = 60°$ | $\beta = 80°$ | |
| 0° | 90° | 90° | 90° | 90° | 90° | 0° |
| 10° | | 71.8° | 80.1° | 84.7° | 88.3° | 178.2° |
| 20° | 25.5° | 56.7° | 70.9° | 79.6° | 86.6° | 176.4° |
| 30° | | 45.5° | 62.9° | 74.9° | 85.0° | 174.3° |
| 40° | 11.7° | 37.4° | 56.2° | 70.7° | 83.6° | 171.7° |
| 50° | | 31.5° | 50.8° | 67.1° | 82.3° | 168.3° |
| 60° | 5.7° | 27.2° | 46.5° | 64.2° | 81.3° | 161.3° |
| 70° | | 24.0° | 43.3° | 62.0° | 80.5° | 154.5° |
| 80° | 1.8° | 21.5° | 41.0° | 60.4° | 80.1° | 135.5° |
| 90° | | 19.7° | 39.6° | 59.6° | 79.8° | 90° |
| 100° | - 1.8° | 18.4° | 39.0° | 59.6° | 79.9° | 44.5° |
| 110° | | 17.7° | 39.2° | 60.3° | 80.3° | 25.5° |
| 120° | - 1.8° | 17.4° | 40.5° | 61.9° | 81.0° | 16.7° |
| 130° | | | | | | 11.7° |
| 140° | -11.7° | | | | | 8.3° |
| 150° | | values not needed | | | | 5.7° |
| 160° | -25.5° | | | | | 3.6° |
| 170° | | | | | | 1.8° |
| 180° | -90° | | | | | 0° |

50

r

100

150

200

250

300

350
-180

-160

-140

-120

-100

-80
-60

-40

-20

0

20

40

60

80

100

120

140

160

180

$\emptyset$ in degrees
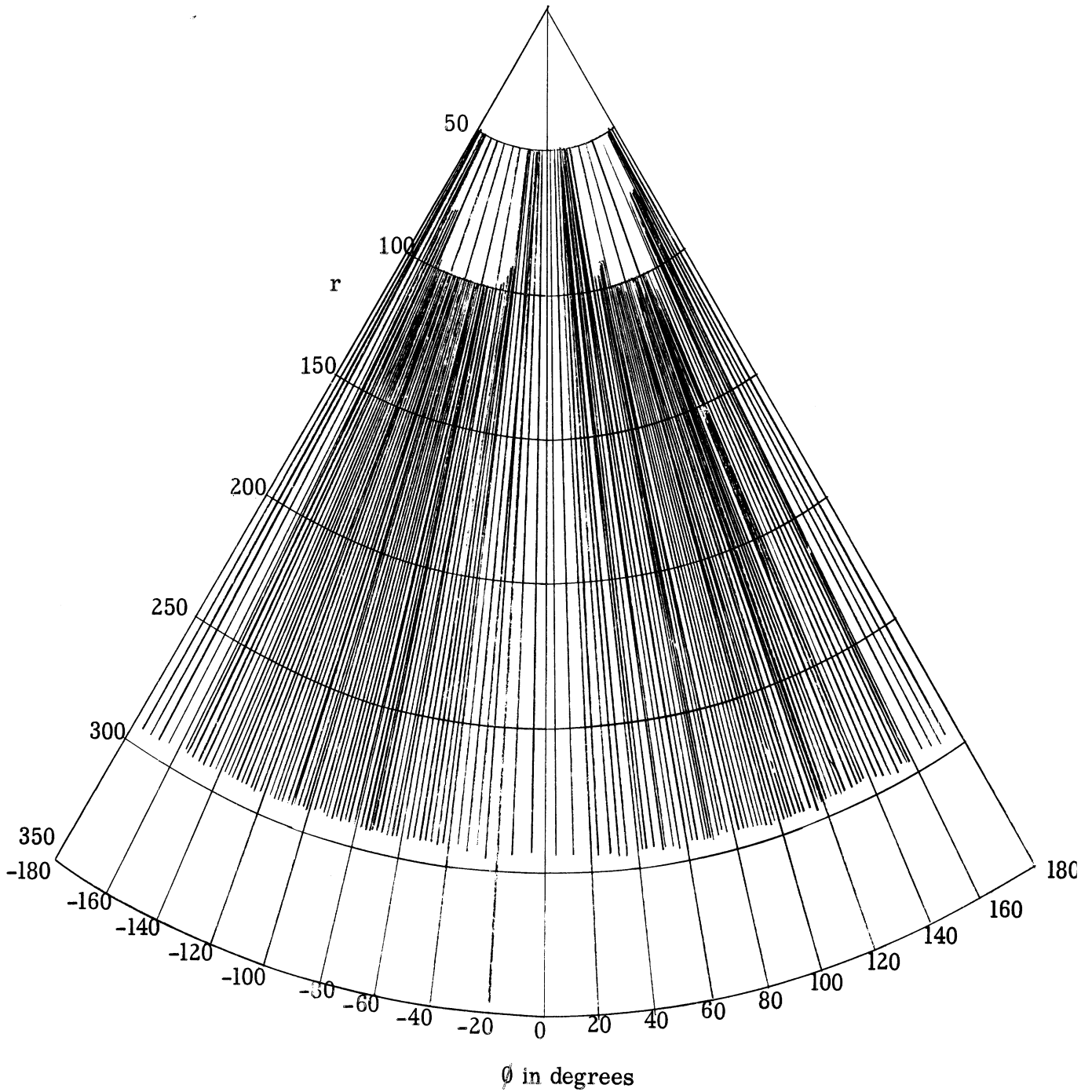
FIG. C-8  AMPLITUDE OF $E_1$ ON UNROLLED CONE SURFACE
FOR $\beta = 0^{\circ}$

$\emptyset$ in degrees
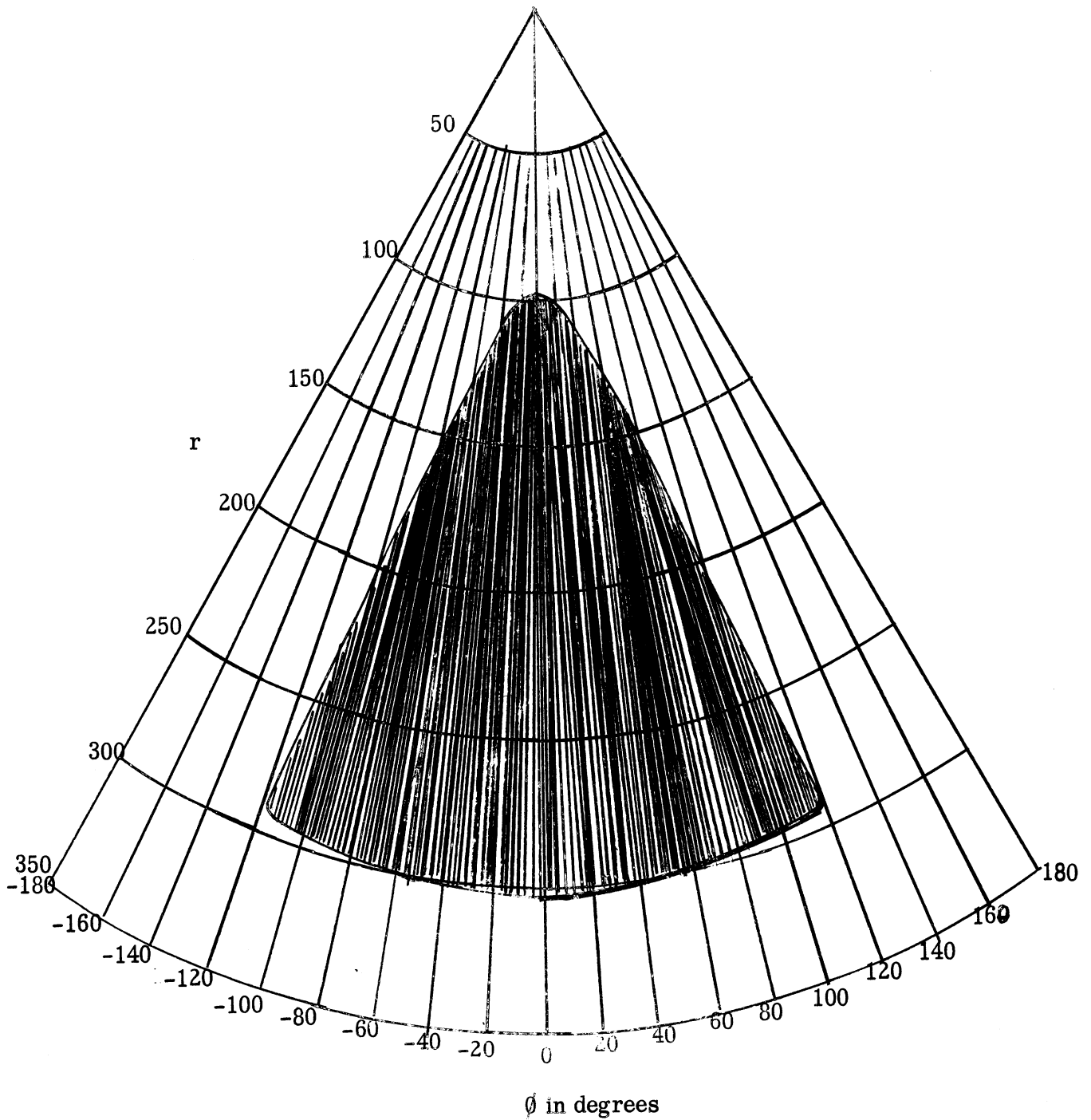
FIG. C-9 AMPLITUDE OF $E_1$ ON UNROLLED CONE
SURFACE FOR $\beta = 20°$

$\theta$ in degrees
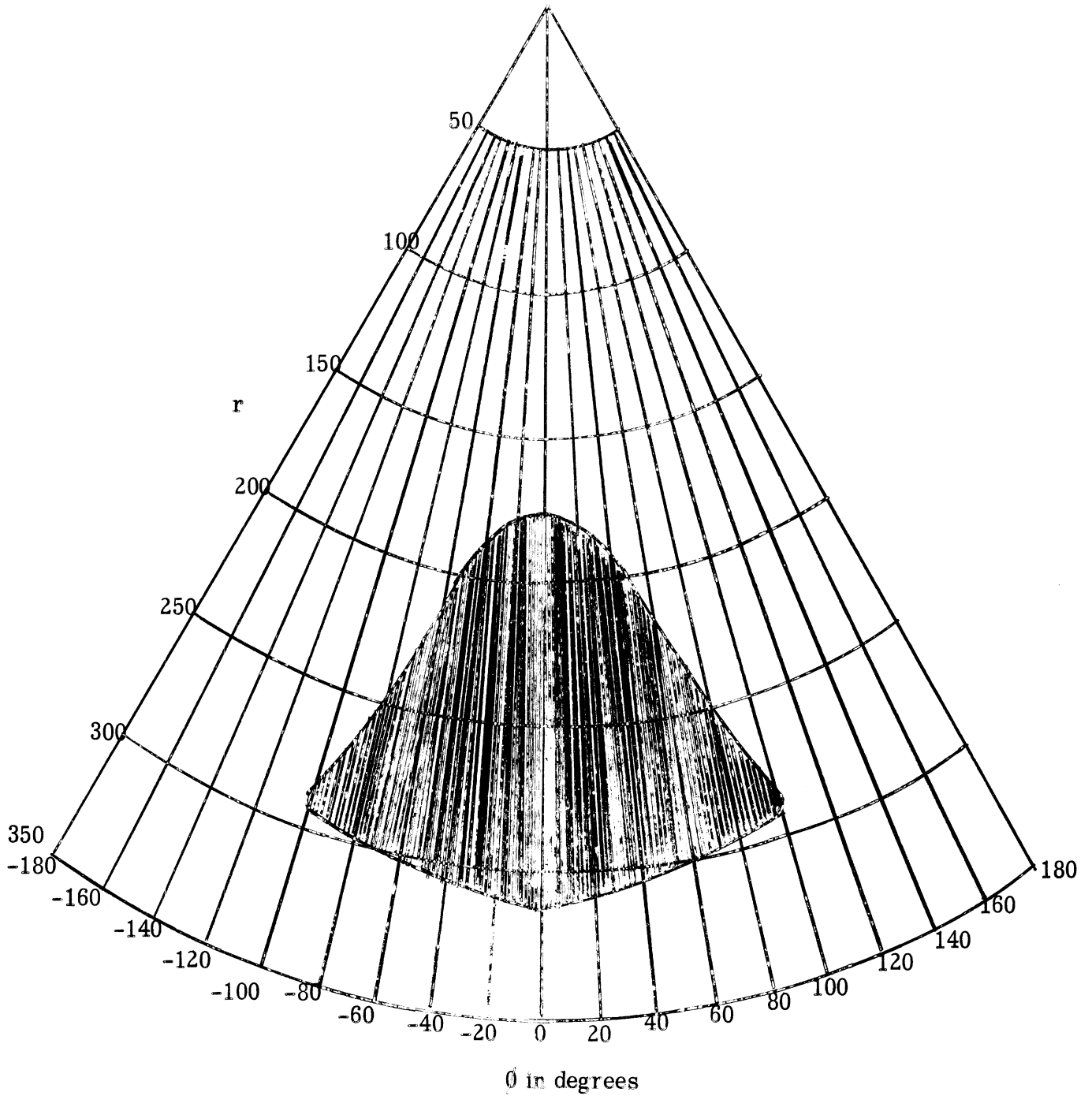
FIG. C-10  AMPLITUDE OF $E_t$ ON UNROLLED CONE SURFACE
FOR $\beta = 40°$
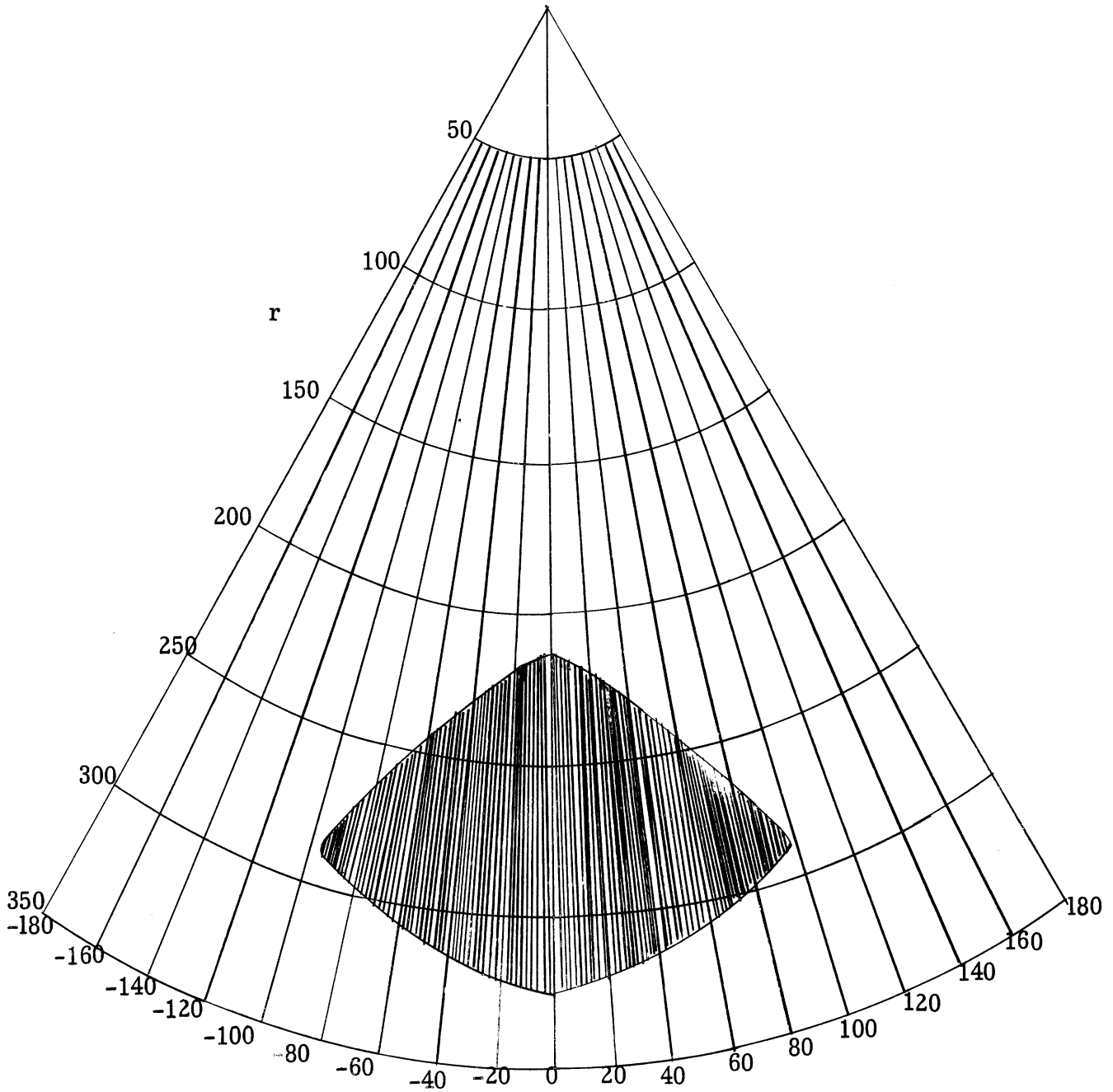
FIG. C-11   AMPLITUDE OF $E_1$ ON UNROLLED CONE
SURFACE FOR $\beta = 80°$
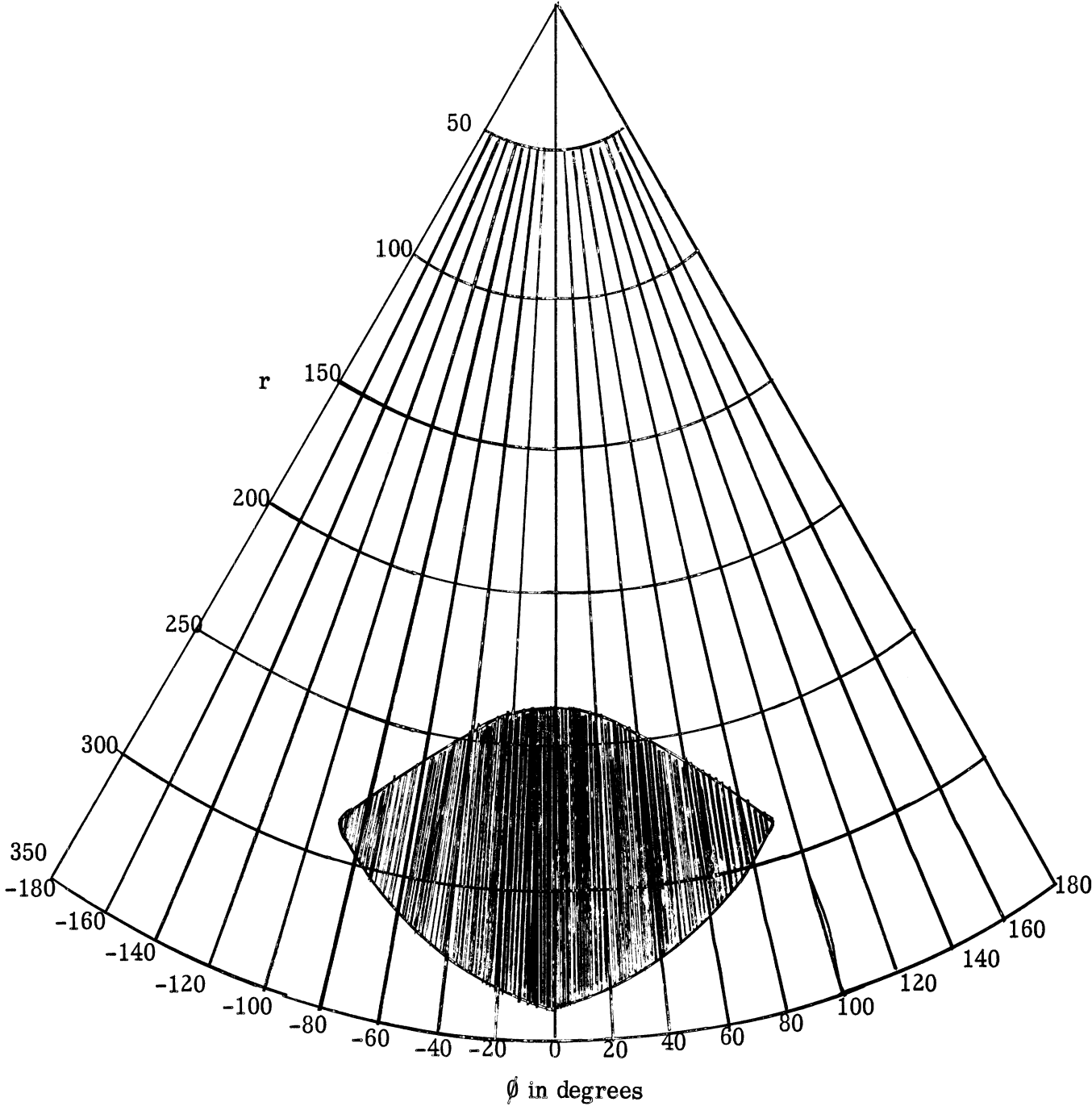
FIG. C-12    AMPLITUDE OF $E_1$ ON UNROLLED CONE
SURFACE FOR $\beta = 80^{\circ}$
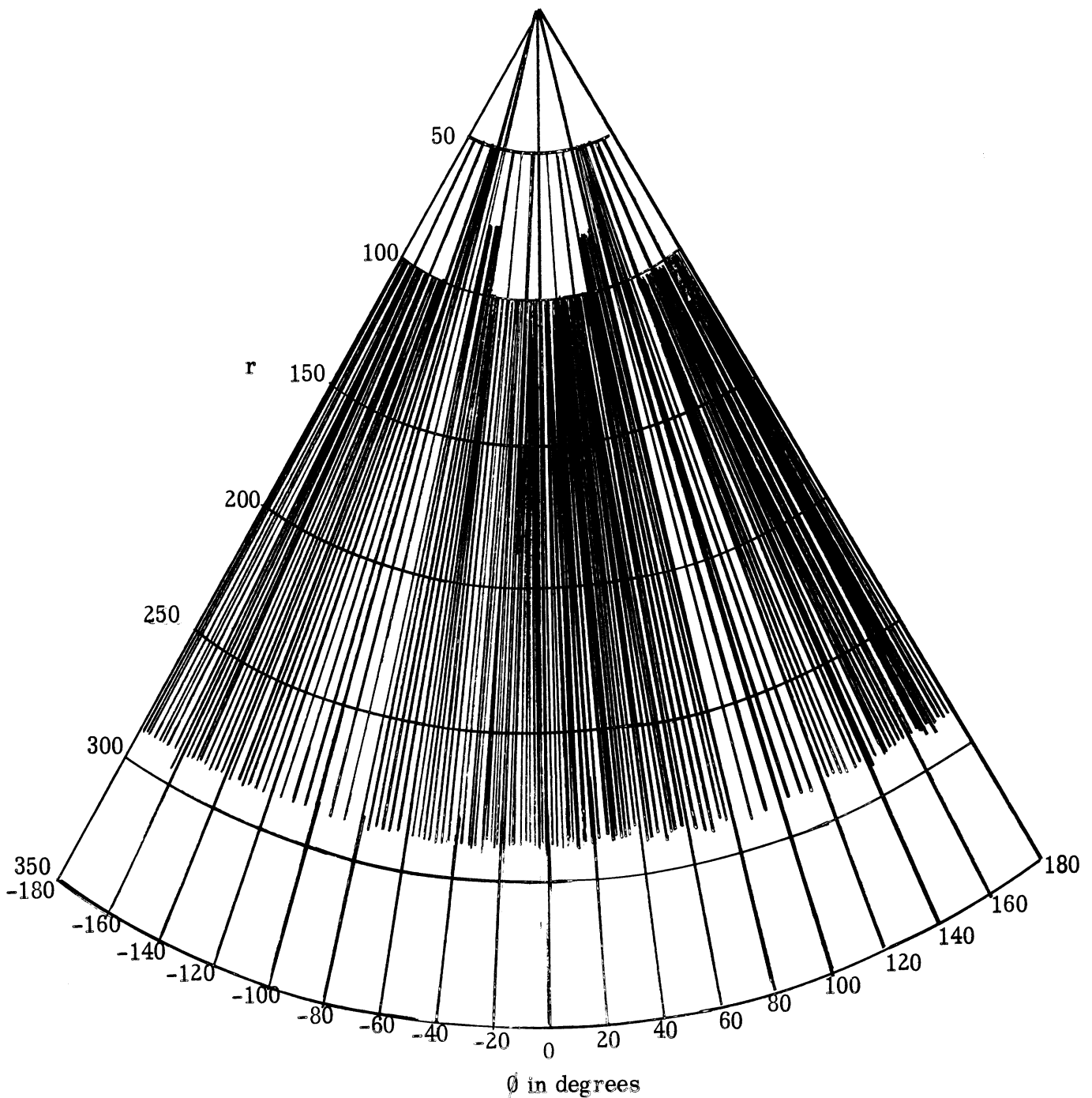
FIG. C-13    AMPLITUDE OF $E_2$ ON UNROLLED CONE
SURFACE FOR $\beta = 0^\circ$

($|E_2|$ is not $\beta$-dependent therefore only the envelope of the
intersection changes with $\beta$ .)
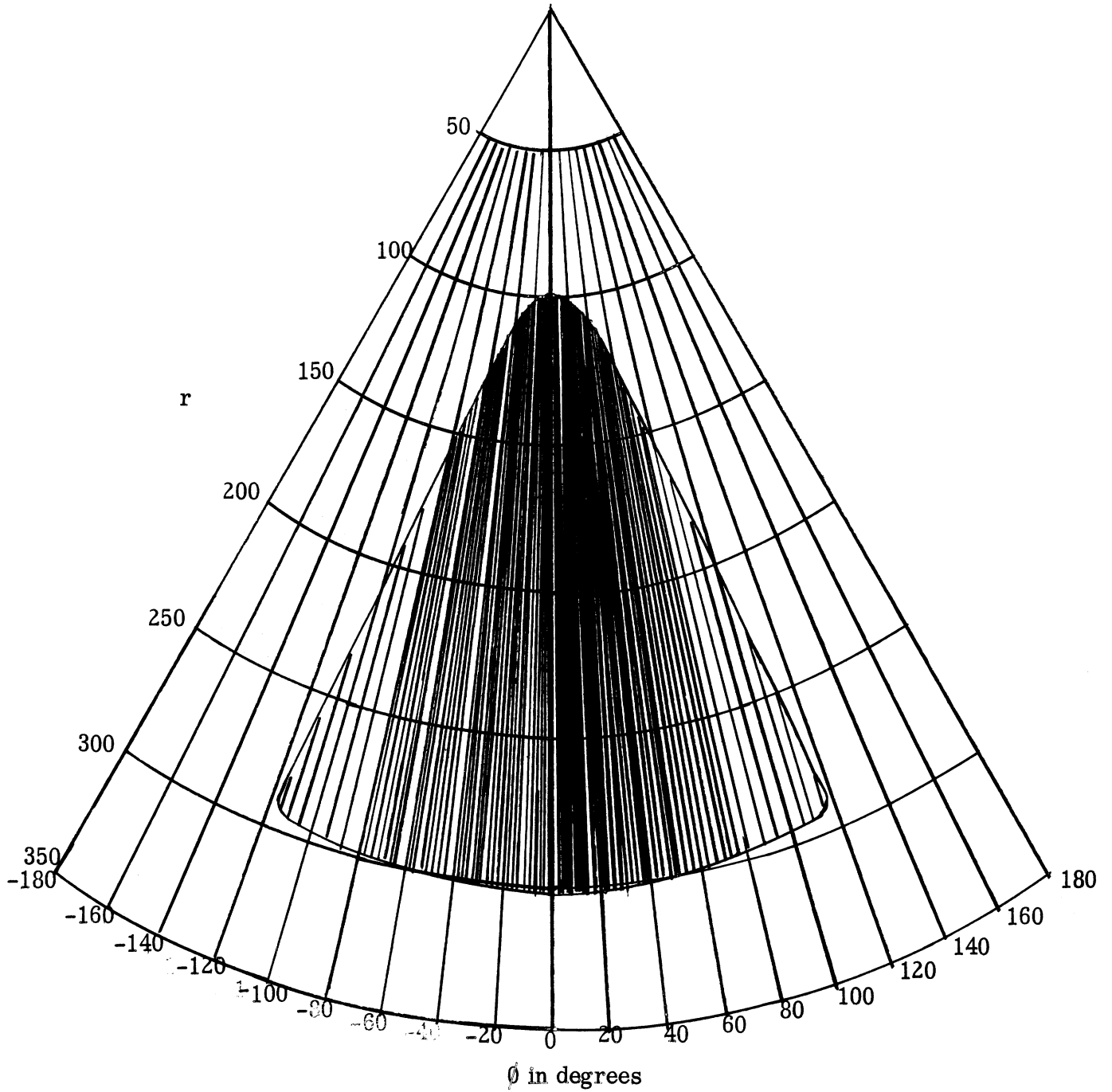
FIG. C-14 AMPLITUDE OF $E_2$ ON UNROLLED CONE
SURFACE FOR $\beta = 20^{\circ}$

( $|E_2|$ is not $\beta$-dependent therefore only the envelope of
the intersection changes with $\beta$. )
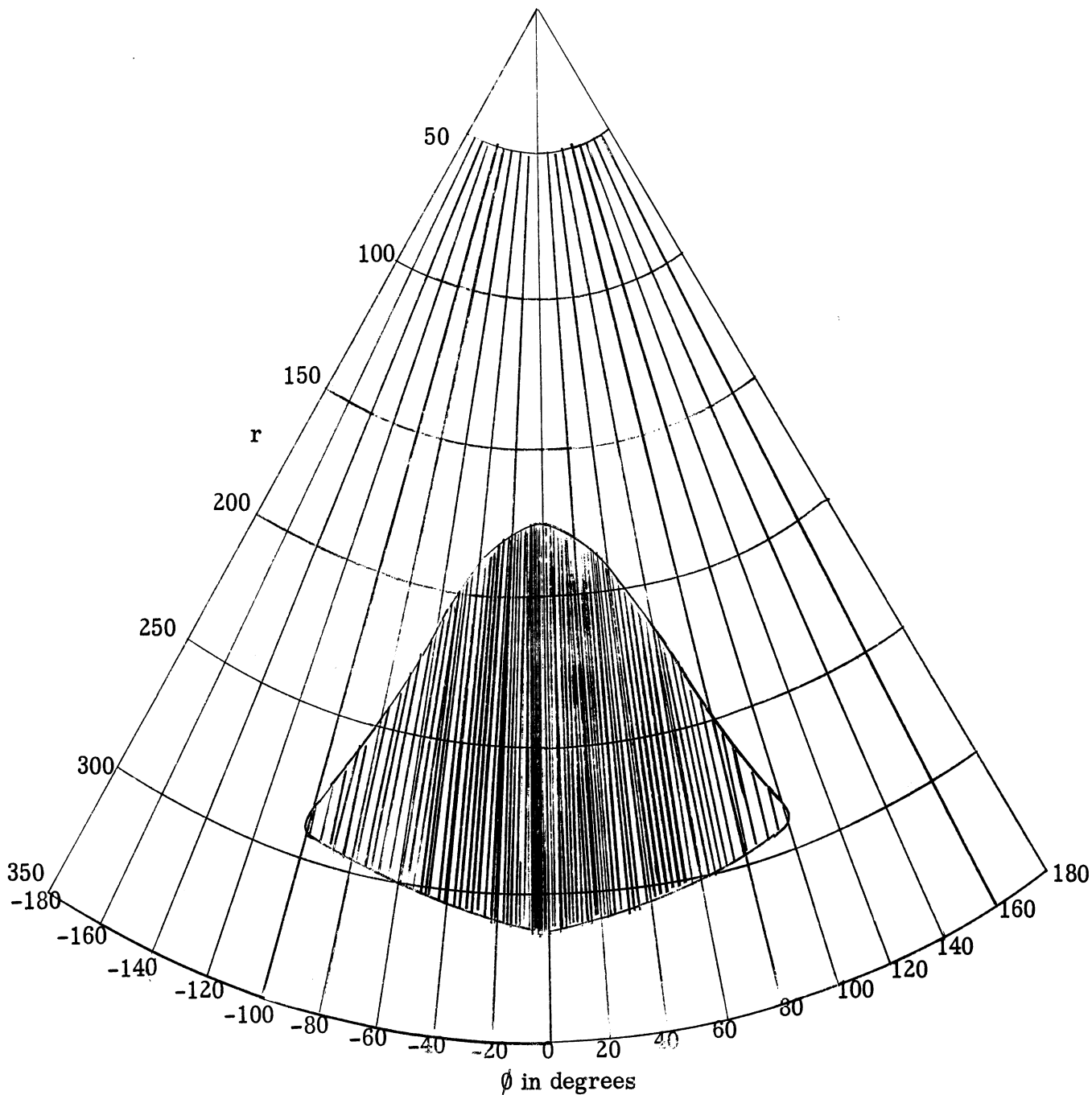
FIG. C-15   AMPLITUDE OF $E_2$ ON UNROLLED CONE
SURFACE FOR $\beta = 40^{\circ}$

( $|E_2|$ is not $\beta$-dependent therefore only the envelope of
the intersection changes with $\beta$. )
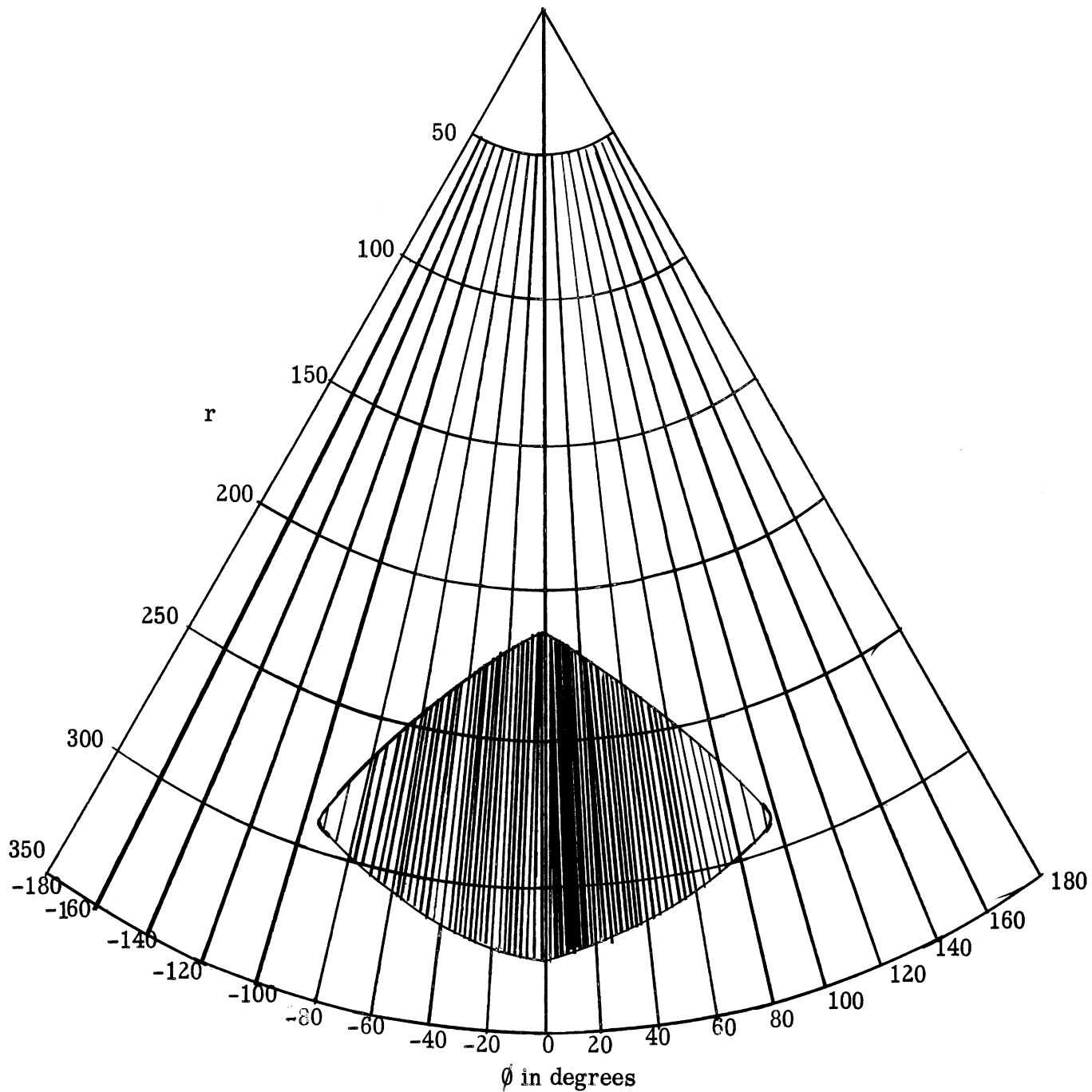
FIG. C-16  AMPLITUDE OF $E_2$ ON UNROLLED CONE
SURFACE FOR $\beta = 60^o$

($|E_2|$ is not $\beta$-dependent therefore only the envelope of
the intersection changes with $\beta$.)
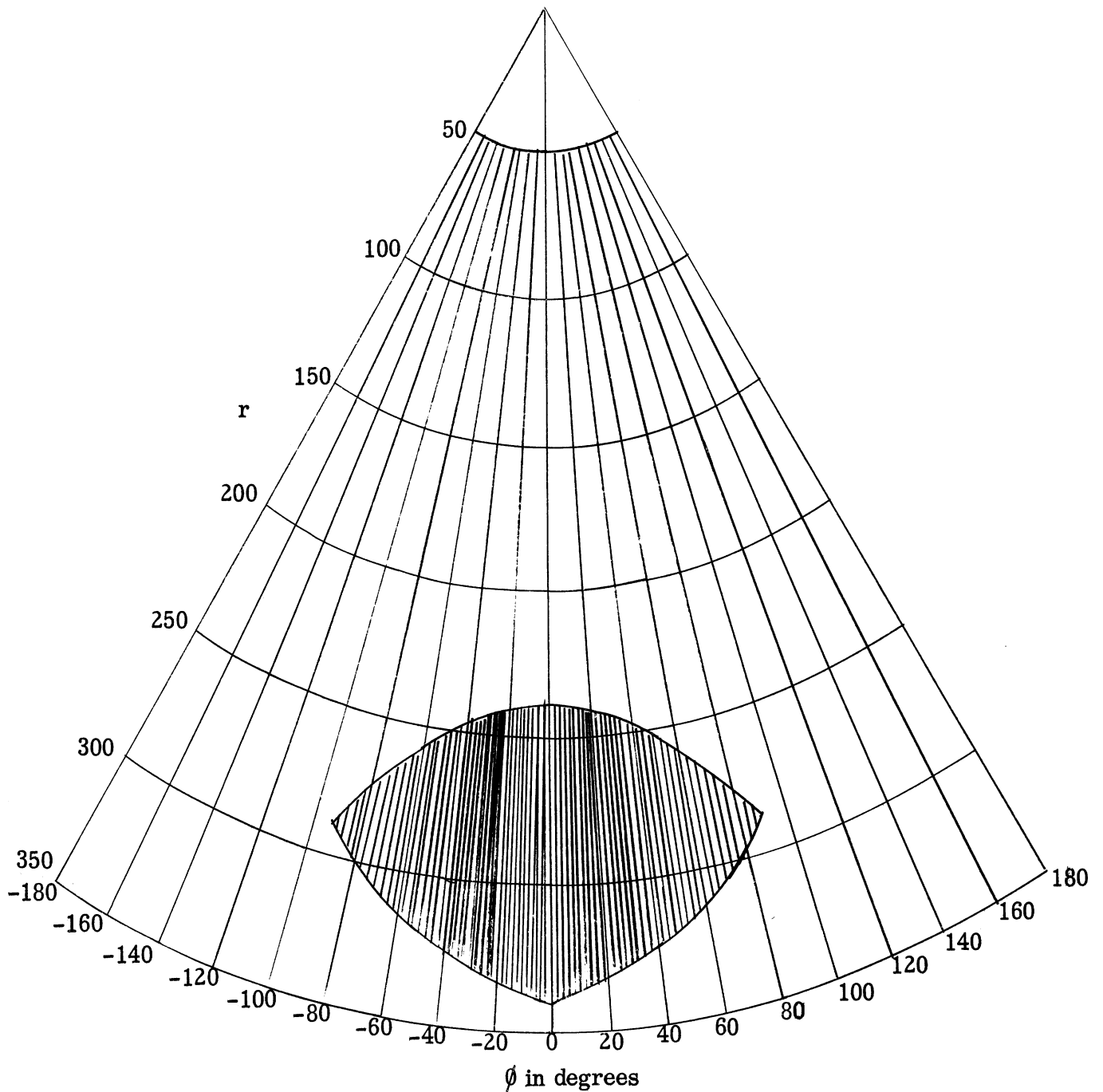
FIG. C-17 AMPLITUDE OF $E_2$ ON UNROLLED CONE
SURFACE FOR $\beta = 80^\circ$

($|E_2|$ is not $\beta$-dependent therefore only the envelope of
the intersection changes with $\beta$.)
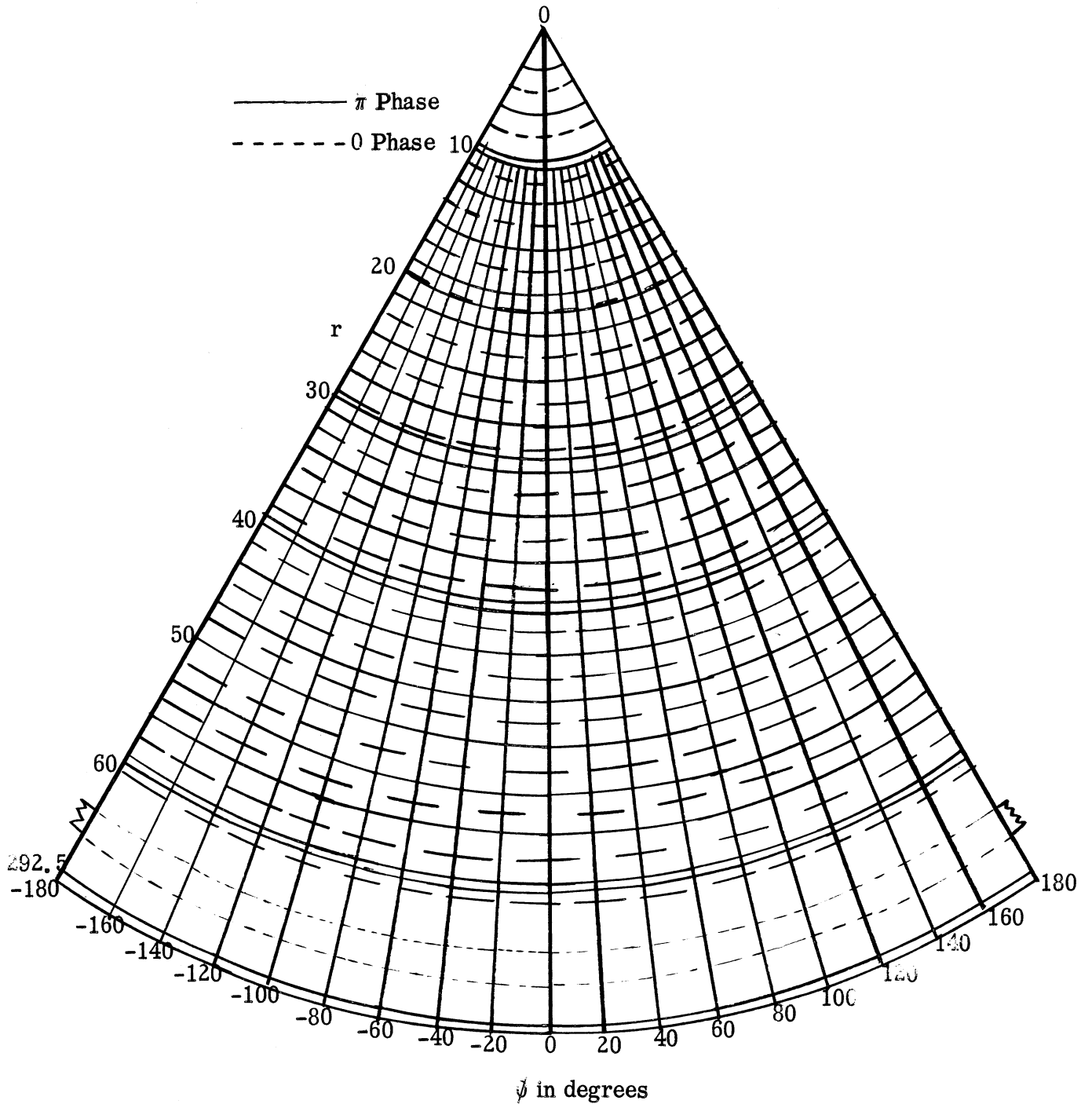
FIG. C-18  PHASE OF E ON UNROLLED CONE SURFACE
FOR $\beta = 0°$
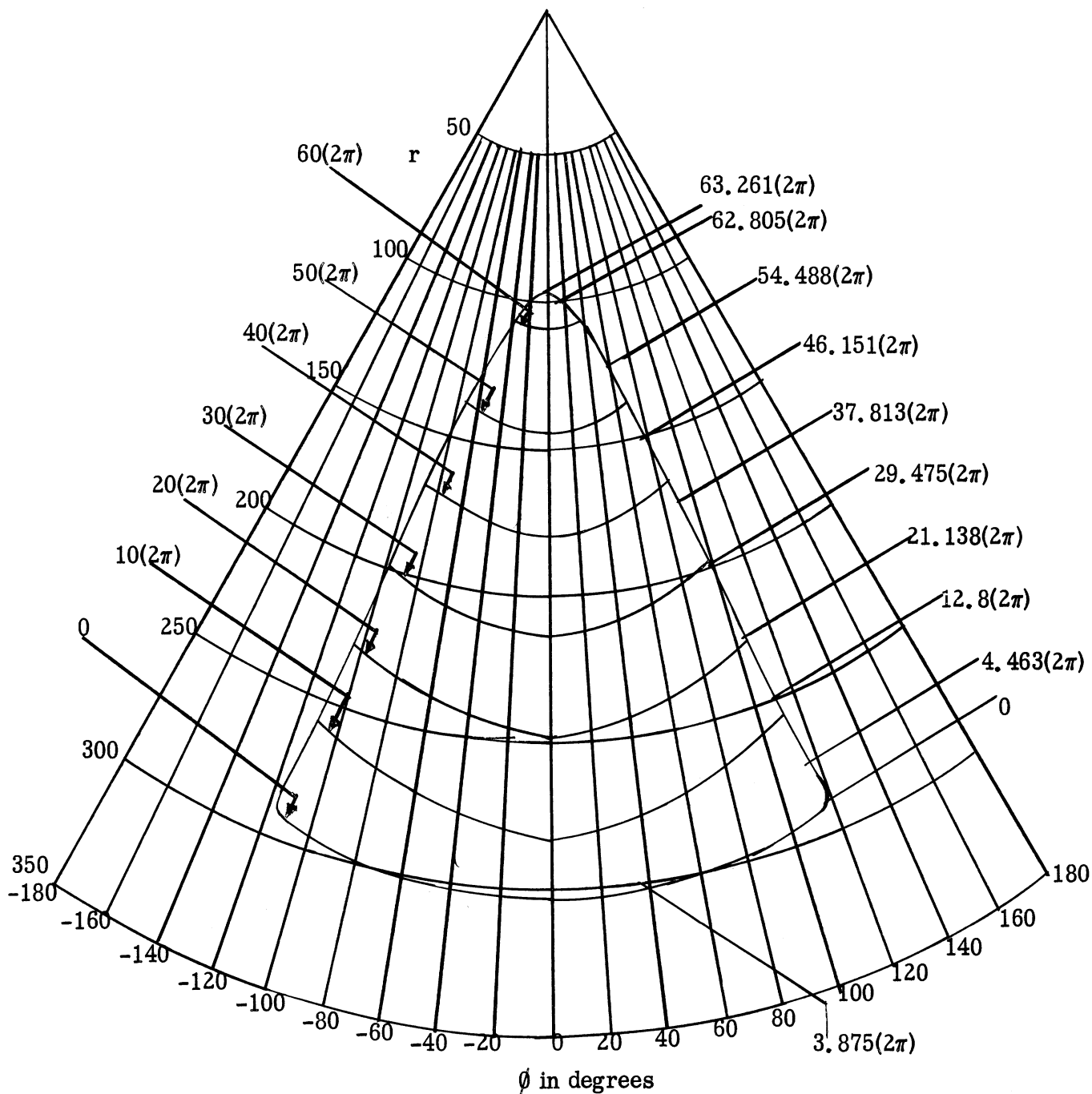
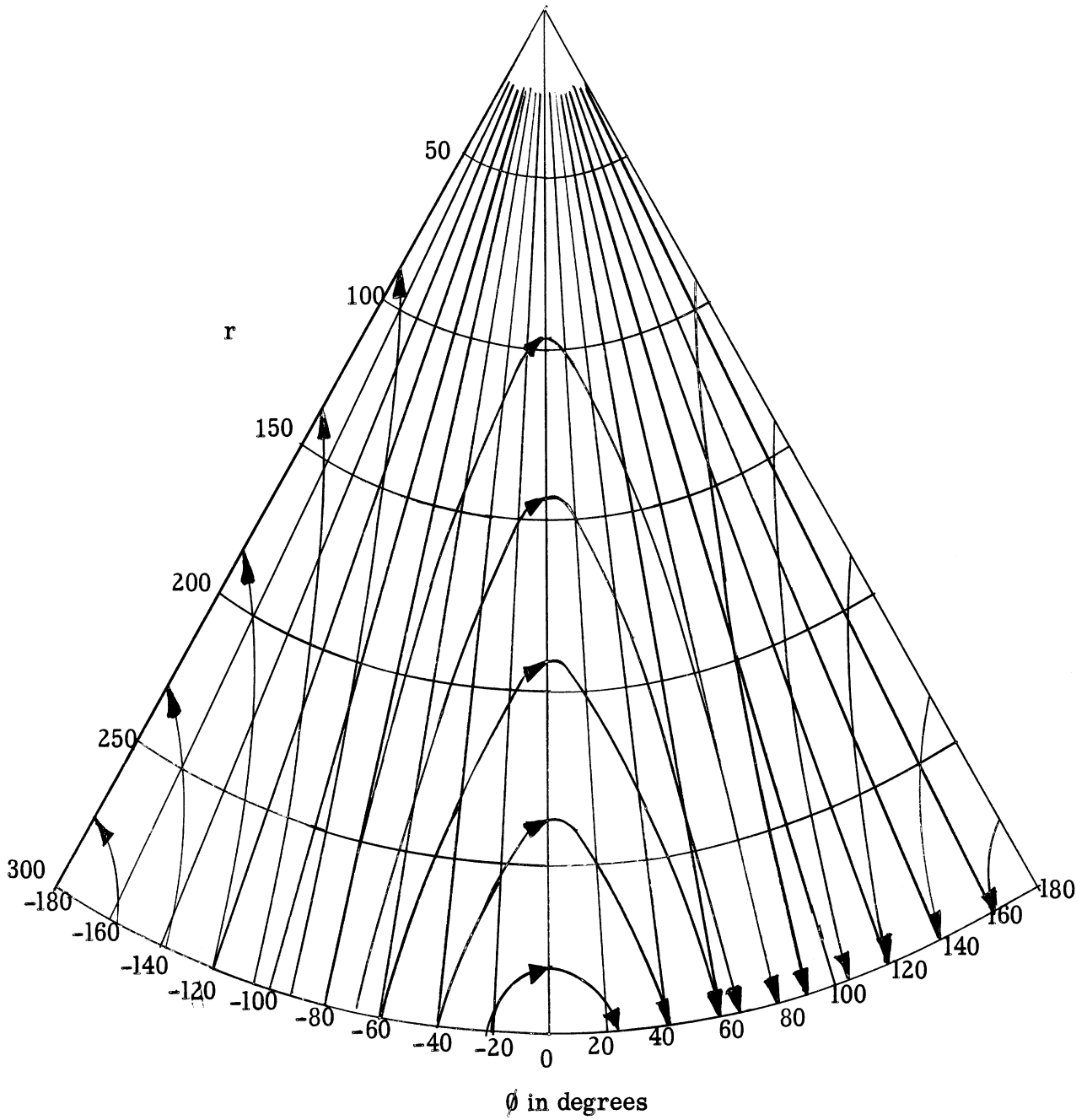FIG. C-19  PHASE OF E ON UNROLLED CONE SURFACE
FOR $\beta = 20^\circ$
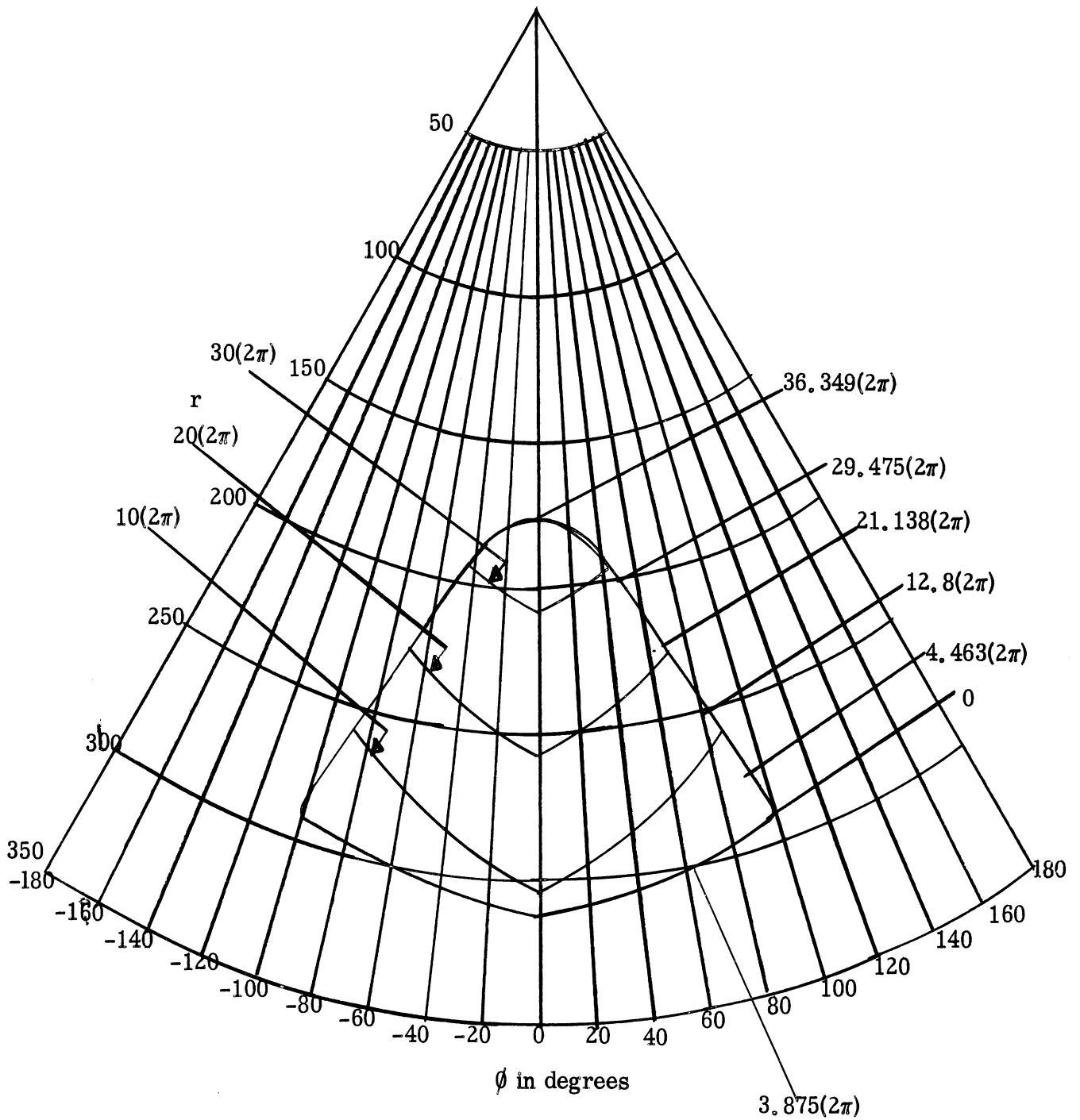
FIG. C-20    PHASE OF E ON UNROLLED CONE SURFACE
FOR $\beta = 40°$
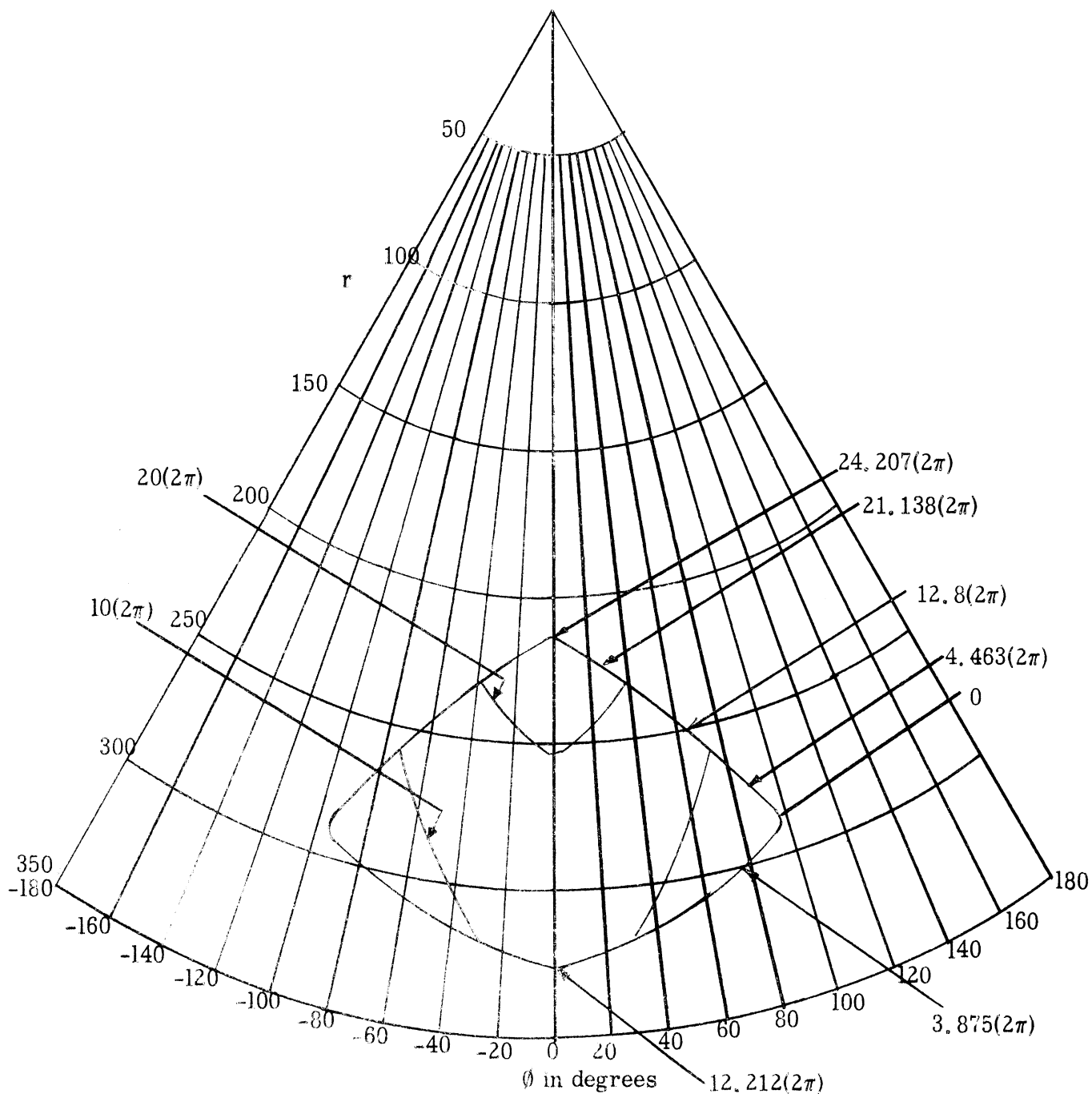
FIG. C-21    PHASE OF E ON UNROLLED CONE SURFACE
FOR $\beta = 60^\circ$
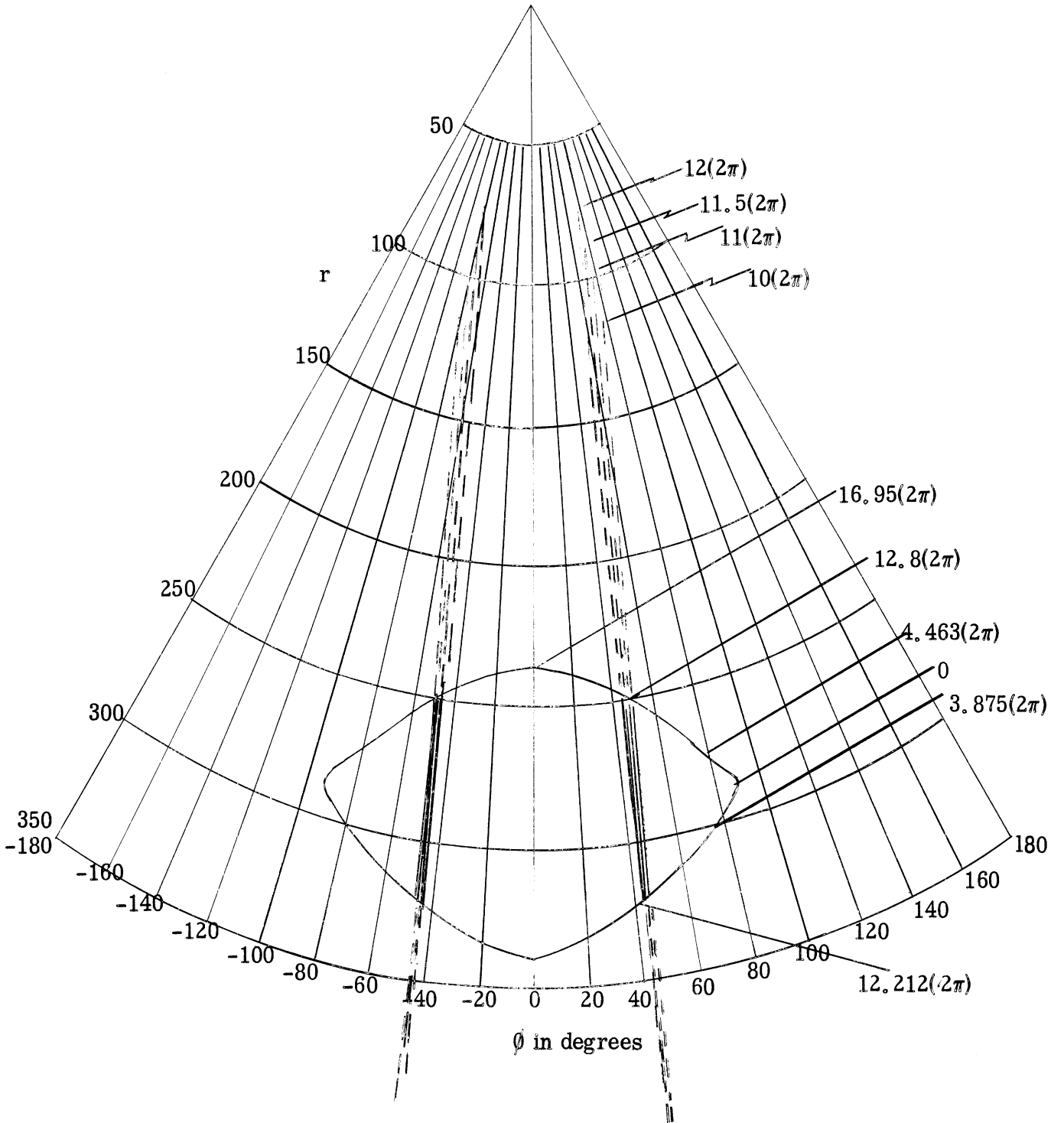
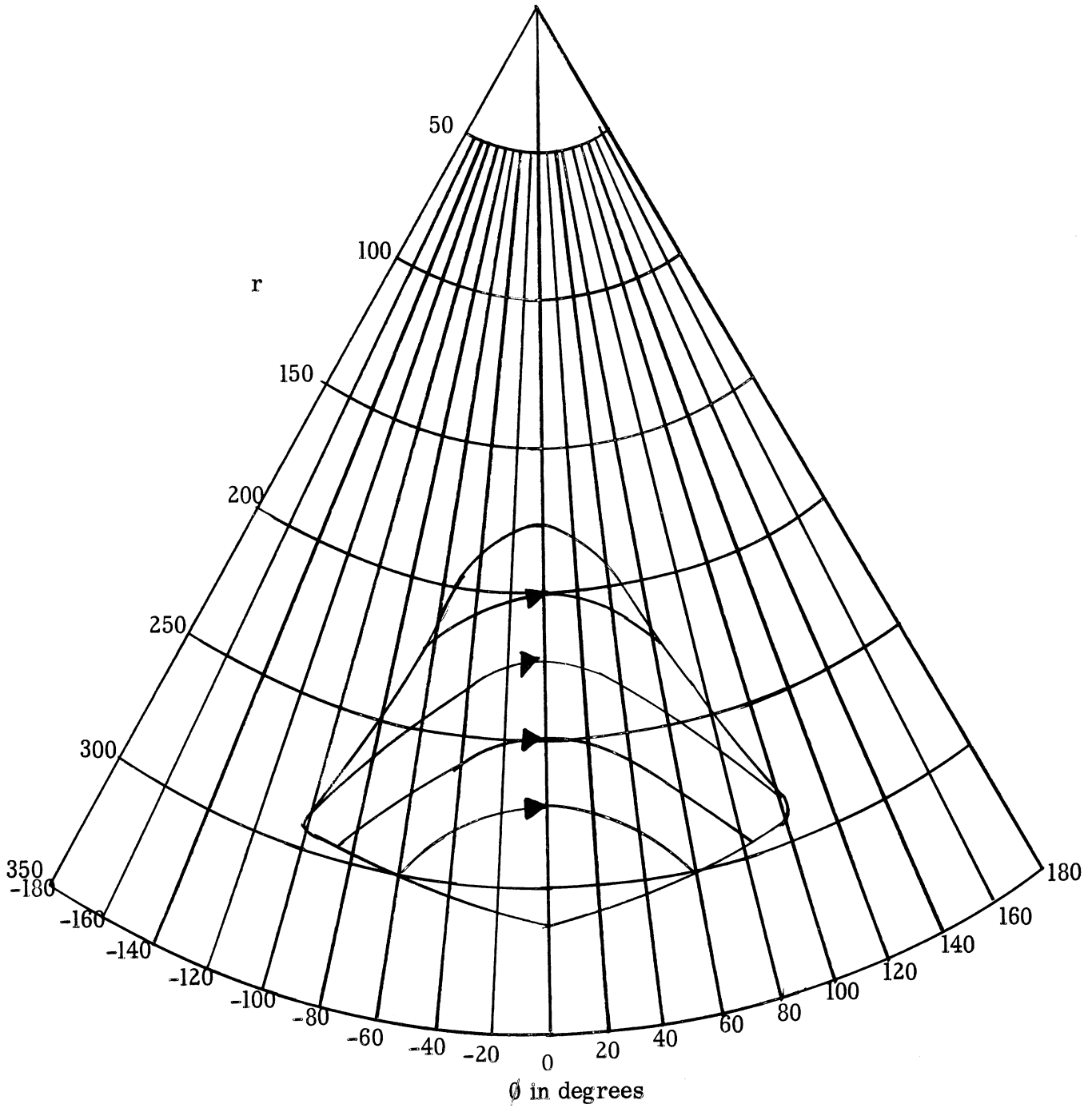FIG. C-22    PHASE OF E ON UNROLLED CONE SURFACE
FOR $\beta = 80°$

FIG. C-23 DIRECTION OF $\hat{n} \times \vec{E}_1$ ON UNROLLED CONE SURFACE FOR $\beta = 0°$
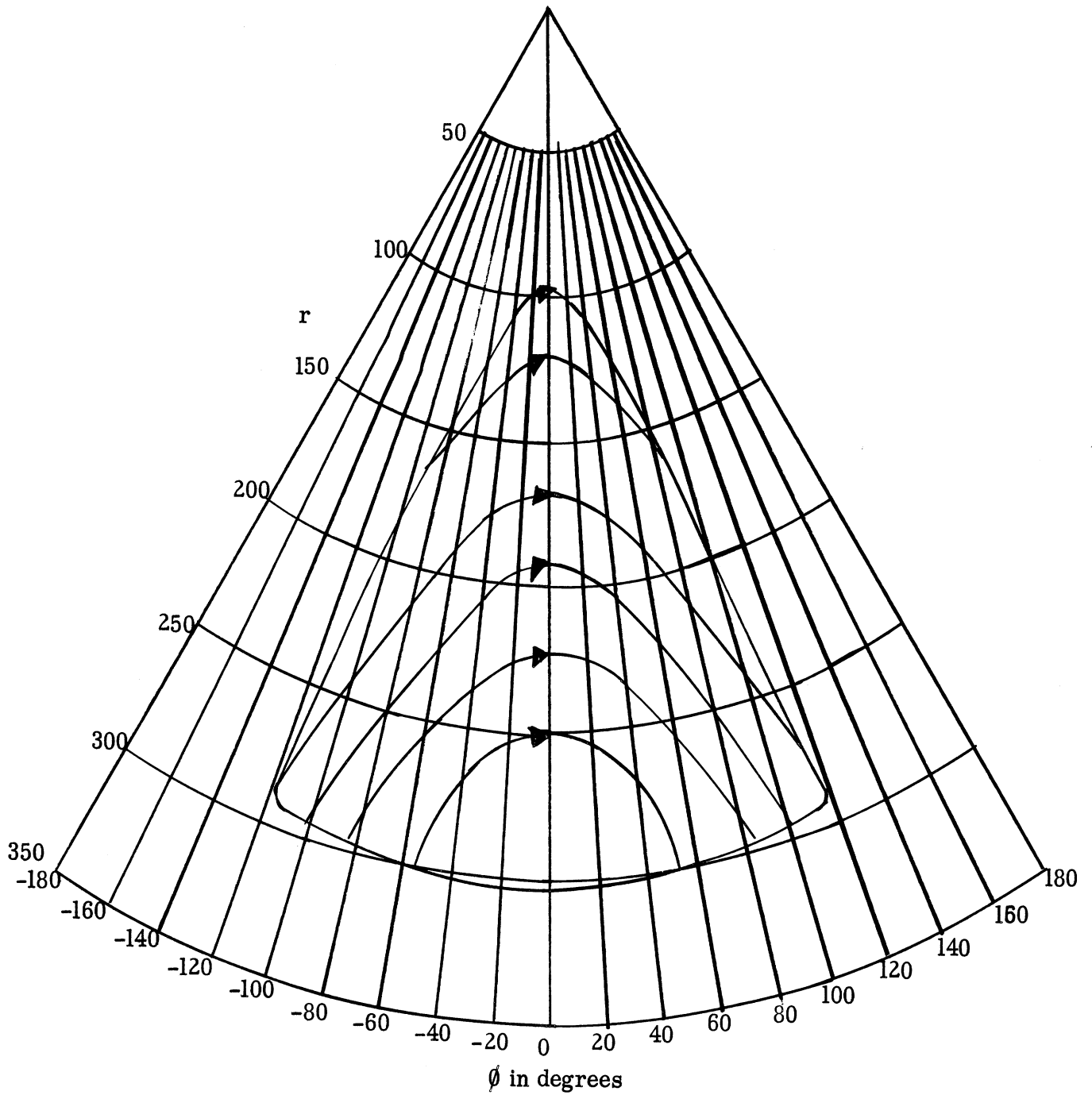
FIG. C-24 DIRECTION OF $\hat{n} \times \vec{E}_1$ ON UNROLLED CONE SURFACE FOR $\beta = 20°$

FIG. C-25  DIRECTION OF $\hat{n} \times \vec{E}_1$ ON UNROLLED CONE
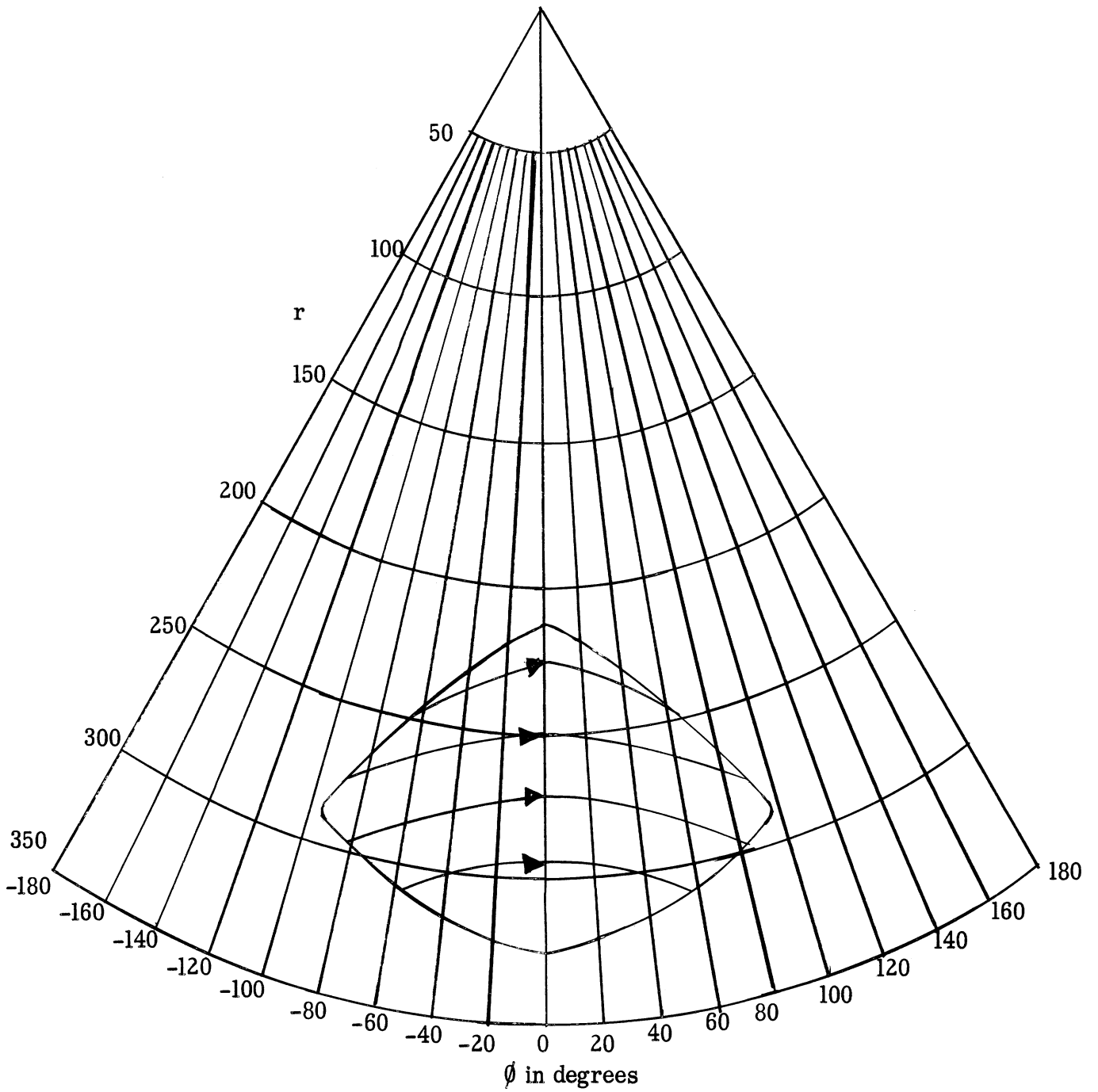SURFACE FOR $\beta = 40^\circ$

FIG. C-26  DIRECTION OF $\hat{n} \times \vec{E_1}$ ON UNROLLED CONE
SURFACE FOR $\beta = 60°$

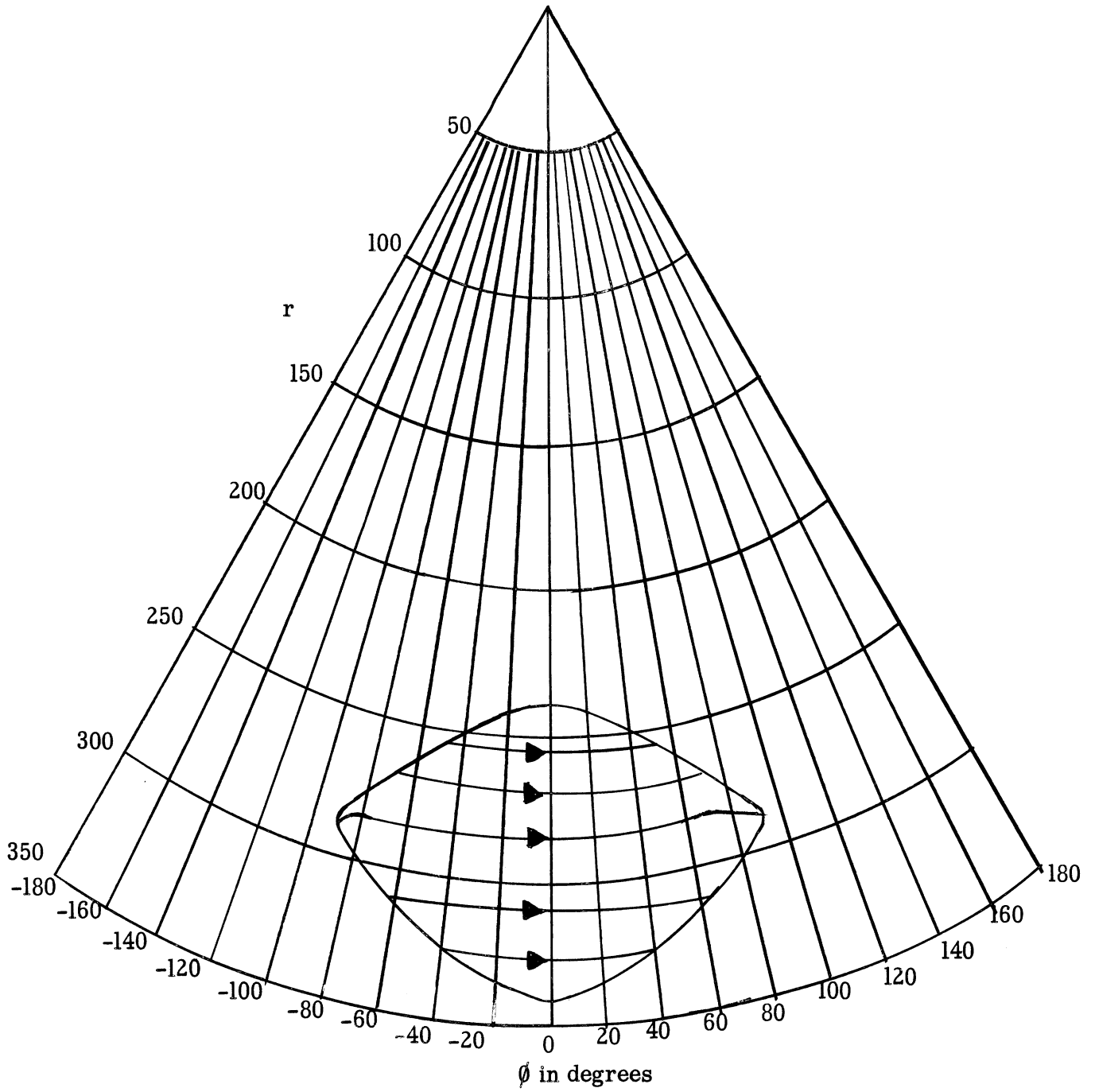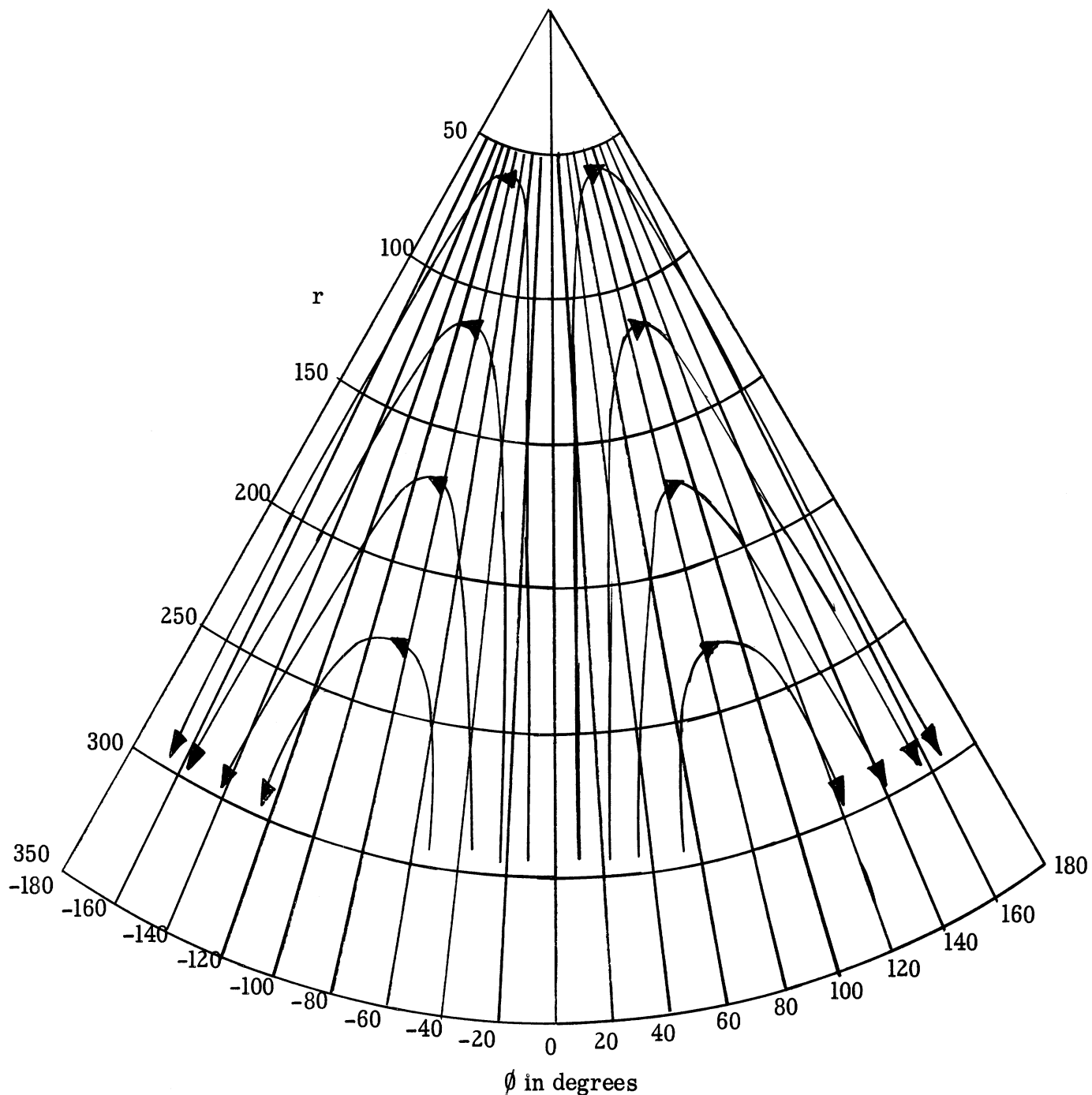FIG. C-27 DIRECTION OF $\hat{n} \times \vec{E}_1$ ON UNROLLED CONE
SURFACE FOR $\beta = 80°$

FIG. C-29 DIRECTION OF $\hat{n} \times \vec{E}_2$ ON UNROLLED CONE
SURFACE FOR $\beta = 0^o$

($\hat{n} \times \vec{E}_2$ is independent of $\beta$, only the envelope of the inter-
section curve changes with $\beta$.)

REFERENCES

1.  V. A. Fock, Journal of Physics, X, 399(1946).

2.  N. A. Logan, "The Role of Fock Functions in the Theory of Diffraction by Convex Surfaces", Air Force Cambridge Research Center, Paper presented at the URSI Meeting, May 22 - 25 1957, in Washington, D. C.

3.  J. B. Keller, "Diffraction by a Convex Cylinder", Transactions of the Institute of Radio Engineers, Vol. AP-4, 312(1956).

4.  R. F. Goodrich, "Studies in Radar Cross Sections XXVI - Fock Theory Applied to an Infinite Cone", The University of Michigan, Report No. 2591-3-T (January 1958).

5.  P. E. Mayes and W. D. James, "Pattern Synthesis With Small Radiating Slots in a Prescribed Conducting Surface", The University of Illinois, Prepared under Subcontract with The University of Michigan, Purchase Order 154216 (1957).

6.  L. B. Felsen, "Field Solutions for a Class of Corrugated Wedge and Cone Surfaces", Polytechnic Institute of Brooklyn, Microwave Research Institute, Memorandum No. 32 (19 July 1957).

7.  C. N. Campopiano, "Summary of Asymptotic Expansions for Bessel Functions", Polytechnic Institute of Brooklyn, Microwave Research Institute, Report No. R-582-57, PIB-502 (28 May 1957).

8.  L. B. Felsen, "Radiation Patterns of Leaky and Surface Wave Distributions on a Wedge", Polytechnic Institute of Brooklyn, Microwave Research Institute, Memorandum No. 33 (23 September 1957).

9.  L. B. Felsen, "Radiation of Sound From a Vibrating Wedge", Polytechnic Institute of Brooklyn, Microwave Research Institute, Report No. R-613-57, PIB-541 (11 October 1957).

10. C. N. Campopiano and L. B. Felsen, "Radiation Patterns of Two-Dimensional Leaky and Surface Wave Distributions on a Semi-Infinite Cone", Polytechnic Institute of Brooklyn, Microwave Research Institute, Memorandum No. 35 (18 November 1957).

11. K. M. Siegel, H. A. Alperin, R. R. Bonkowski, J. W. Crispin, Jr., A. L. Maffett, C. E. Schensted and I. V. Schensted, "Studies in Radar Cross Sections VIII - Theoretical Cross Sections as a Function of Separation Angle Between Transmitter and Receiver at Small Wavelengths", The University of Michigan, Report No. UMM-115 (October 1953).

REFERENCES
(cont'd)

12. Wolfgang Grobner and Nikolaus Hofreiter, "Integraltafel, Erster Teil, Unbestimmte Integrale", Springer-Verlag (1949).

13. K. M. Siegel, H. A. Alperin, J. W. Crispin, Jr., H. E. Hunter, R. E. Kleinman, W. C. Orthwein and C. E. Schensted, "Studies in Radar Cross Sections IV - Comparison Between Theory and Experiment of the Cross Section of a Cone", The University of Michigan, Report No. UMM-92 (February 1953).

14. L. B. Felsen, "Plane-Wave Scattering by Small-Angle Cones", Transactions of the Institute of Radio Engineers, Professional Group on Antennas and Propagation, Vol. AP-5 (January 1957).

15. R. F. Goodrich, A. L. Maffett, N. E. Reitlinger, C. E. Schensted and K. M. Siegel, "Studies in Radar Cross Sections XXII - Elementary Slot Radiators", The University of Michigan, Report No. 2472-13-T (November 1956).

16. R. F. Goodrich, R. E. Kleinman, A. L. Maffett, N. E. Reitlinger, C. E. Schensted and K. M. Siegel, "Radiation and Scattering from Simple Shapes II", Presented at Congres International Circuits et Antennas Hyperfréquences, Paris, France, 21 - 28 October 1957.

17. Tables of Fock Functions, Air Force Cambridge Research Center, Antenna Laboratory (to be published).